2021

Metabolic Coordination of Stem Cell Fate Controls Tumor Initiation and Tissue Repair

Sanjeethan C. Baksh

METABOLIC COORDINATION OF STEM CELL FATE CONTROLS TUMOR INITIATION AND TISSUE REPAIR

A Thesis Presented to the Faculty of
The Rockefeller University
in Partial Fulfillment of the Requirements for
the degree of Doctor of Philosophy

by
Sanjeethan C. Baksh
June 2021

METABOLIC COORIDNATION OF STEM CELL FATE CONTROLS TUMOR INITIATION AND TISSUE REPAIR

Sanjeethan C. Baksh, Ph.D.
The Rockefeller University 2021

Tissue stem cells balance fate decisions of self-renewal and differentiation to maintain homeostasis over the lifetime of an organism, as well as to repair tissues upon injury and wounding. Disrupting the balance between self-renewal and differentiation results in pathology: excessive self-renewal at the expense of differentiation is associated with tumor initiation, whereas failure to properly self-renew leads to stem cell exhaustion and aging. Stem cell fate is under tight regulation by the surrounding microenvironment, or niche, which includes neighboring cell types, signaling molecules, extracellular matrix, and nutrients. While the role of stromal cells and the signals they produce has been extensively studied with regards to control of stem cell fate, relatively little known is about how tissue stem cells integrate extracellular nutrient availability with fate decisions. Moreover, while intracellular metabolic pathways have been shown to regulate the balance of self-renewal and differentiation, it remains unknown whether or not endogenous metabolic pathways or nutrient availability predispose stem cells towards transformation or control their responses to tissue injury.

Here, I address these questions in epidermal stem cells (EpdSCs), which maintain integrity of the skin barrier over an organism's life. EpdSCs are a cell of origin for squamous cell carcinomas (SCCs), amongst the most common and threatening malignancies worldwide. Additionally, EpdSCs of the interfollicular epidermis (IFE) and hair follicle (HF) respond to injuries in the skin barrier to repair the breach. First focusing on tumor initiation, I find oncogenic EpdSCs are serine auxotrophs, whose growth and self-renewal require abundant exogenous serine. When extracellular serine is limited *in vitro* and *in vivo,* EpdSCs activate *de novo* serine synthesis,

which in turn produces the metabolite α-ketoglutarate (αKG). αKG stimulates terminal differentiation via activation of αKG-dependent dioxygenases that remove the repressive histone modification H3K27me3, which otherwise promotes EpdSC self-renewal. Accordingly, serine starvation or enforced αKG production antagonizes SCC initiation and growth. Conversely, blocking serine synthesis or repressing αKG-driven demethylation facilitates malignant progression *in vivo*.

Finally, I extend these findings to stem cell responses to tissue injury. In the epidermis, abrasion of the IFE activates HFSCs to repair the breach, which is associated with transient hyperproliferation, migration and activation of a plasticity program termed lineage infidelity wherein HFSCs undergo a fate switch to become IFE-SCs, fueling regeneration of a non-cognate tissue. I find that environmental serine restriction accelerates HFSC-mediated wound repair, which I link specifically to acceleration of stem cell plasticity and acquisition of IFE fate. Altogether, these findings reveal that extracellular serine is a critical determinant of EpdSC fate and provide insight into how nutrient availability is integrated with stem cell fate decisions during tumor initiation and tissue repair.

For my parents, who every day teach me what love and sacrifice mean.

ACKNOWLEDGMENTS

First and foremost, thank you to my co-mentors Dr. Elaine Fuchs and Dr. Lydia Finley. Both Elaine and Lydia have shaped me into the scientist I am today in different ways. Elaine has provided incomparable resources, and the flexibility to explore my interests and follow the science wherever it may lead. Elaine has a magnetic passion for science, which is what initially drew me to her lab, and she continues to be the most excited person in our group about the trajectory of our projects. Her ability to leap from immunology to metabolism to cancer to chromatin, all while remaining the world's foremost expert in epithelial stem cells of the skin, is remarkable. Lydia has been a constant source of support and intellectual input at every stage of my project. She has cultivated my ability to formulate questions and design creative experiments to tackle them and forced me to challenge my own interpretations of my data. Lydia is without a doubt the most brilliant person I have ever met in my life, but despite always being the smartest person in the room she has always treated her trainees with respect. She encourages our curiosity, welcomes our questions no matter how naïve, and her humility, scientific rigor, and insightfulness have been an inspiration to me over the years. Both Elaine and Lydia have challenged me to explore new and exciting questions. Their distinct styles of mentorship have complemented each other throughout my thesis, and I am incredibly grateful to have had the opportunity to train under such remarkable scientists.

Thank you to Dr. Paul Cohen and Dr. David Allis for serving on my thesis committee. Their insights and questions into my project over the years have been instrumental in cultivating my thoughts and shaping my approach to science. Thank you to my external examiner, Dr. Celeste Simon, for taking the time to participate in my defense.

I have also been fortunate to have outstanding collaborators and friends in both labs. While I am appreciative for the feedback from all members of my labs, in the Finley lab I am particularly grateful for my very close collaboration with Pavlina Todorova, who is the most careful and critical scientist I have ever had the pleasure of working with. She has never shied away from tackling difficult questions and problems throughout the course of our collaboration, and when she draws a conclusion, I know that I can trust it to be true. In the Fuchs lab, I am thankful for my friend and colleague Shiri Gur-Cohen, with whom I've had many long and insightful brainstorming sessions about our respective projects and who I've always been able to rely on for help with particularly difficult experiments. I will miss our frequent coffee breaks, which I will always associate with some of our best scientific ideas. The work on wound repair was performed in collaboration with Shiri, Jesse Novak (a new MD-PhD student in the Fuchs lab), Kevin Gonzales (a postdoctoral fellow in the Fuchs lab), and Ben Jackson (an MD-PhD student in the Finley lab). I am lucky to have overlapped with many other brilliant scientists in the Fuchs lab, including Stephanie Ellis, Melanie Laurin, Rachel Niec, Nicole Infarinato and Nicholas Gomez, all of whom over the years have provided critical feedback and insights into my project. Most importantly, I am fortunate to now count all of these colleagues as lifelong friends, who I will continue to rely on throughout my career. Many thanks are due as well to our incredible staff in the lab, especially June Racelis, Prashant Nasseir, Lynette Hidalgo, and Megan Sribour, who provide the support and infrastructure to keep our projects going.

The Rockefeller University is an amazing place to be a graduate student, and I am grateful to the staff of our university who keep it running. In particular, Svetlana Mazel, Stanka Semova and Songyan Han from the FCRC and Lavo Ramos-Espiritu at HTSRC have been at various times instrumental in the progress of my project. Thanks to members of the Rockefeller Dean's Office

for their guidance, and the custodial and food service staff for their passing smiles over the years. I am also particularly grateful for the incredible community I have found at the Tri-Institutional MD-PhD program. Thank you to Dr. Olaf Andersen, Dr. Ruth Gotian, Dr. Catharine Boothroyd, Renee Horton, Hanna Silvast, Dr. Ben Levitt and Dr. Mark Pecker for their personal and professional guidance and support over the years. We are incredibly lucky to have you all at the helm of our ship. I have also been fortunate to receive mentorship from Dr. Juliet Aizer over the course of my training, and I am so grateful for her kindness, support and open ears.

This thesis was written and presented during the midst of the COVID-19 pandemic. Although I did not anticipate my PhD ending via a virtual presentation, I am eternally grateful for the stability afforded to me by the Rockefeller University and the Tri-Institutional MD-PhD program during this remarkably uncertain time, as well as the countless sacrifices made by healthcare workers, grocery and food service workers, public transit employees, sanitation workers, and all the other essential employees who have kept society afloat. It was additionally written during the peak of a rebellion against centuries of institutionalized, state-sanctioned racism in America, most notably at the hands of police and the prison industrial complex. While writing this thesis, I often found myself distracted and frozen by the weight of the pain I felt for the families of George Floyd, Breonna Taylor, Tony McDade, and countless other Black people who have been brutalized by racism and capitalism in America. I am inspired by the many activists and organizers who have remained militant in their demands for a more just society, and I believe we all owe a great debt of gratitude to those who fight for justice, often at great personal cost. As I move forward in my career as a physician-scientist, I will remain steadfast in my dedication to racial justice within the fields of science and medicine.

Lastly, I owe an enormous debt of gratitude to my family and my friends, who have become my chosen family in New York. To Chelsea, Andy, Andrew, Neha, and Ceci: I am continuously humbled by your brilliance and love and can't imagine going through my graduate training without you all by my side. To my brothers Nik, Daniel and Dominick and sister-in-law Caitlin, thank you for always putting a smile on my face. And to my parents, who left everything they knew to make a better life for their children in America, I am in awe of your bravery and the sacrifices you've made for us. Thank you all for making my life bright and beautiful.

TABLE OF CONTENTS

LIST OF FIGURES

LIST OF TABLES

LIST OF ABBREVIATIONS

2HG	2-hydroxyglutarate
3PG	3-phosphoglycerate
AITL	Angioimmunoblastic T-cell lymphoma
AKB	alpha-ketobutyrate
ALKBH5	Alkane hydroxylase B homolog 5
AML	Acute myeloid leukemia
ASNS	Asparagine synhtetase
ATF4	Activating transcription factor 4
BCAA	Branched chain amino acid
BCAT	Branched chain amino acid transferase
BCC	Basal cell carcinoma
BRD4	Bromodomain-containing protein 4
C/EBPα	CCAAT-enhancer-binding protein alpha
CreER	Cre recombinase estrogen receptor fusion protein
CTCF	CCCTC-binding factor
d5-2HG	D-2-hydroxyglutaric-2,3,3,4,4-d5 acid
DCA	Dichloroacetate
DMBA	7,12-dimethylbenz[a]anthracene
dpw	days post wounding
EdU	5-Ethynyl-2′-deoxyuridine
EMT	Epithelial mesenchymal transition
EpdSC	Epidermal stem cell
ESC	Embryonic stem cell
EZH2	Enhancer of zeste homolog 2
FH	Fumarate hydratase
FTO	Fat mass and obesity associated gene
GC-MS	Gas chromatography-mass spectrometry
GFP	Green fluorescent protein
GOT	Glutamate-oxaloacetate transaminase
H2B-mRFP	Histone H2B-monomeric red fluorescent protein fusion
H3K27me3	Histone H3 lysine 27 trimethylation
H3K9me3	Histone H3 lysine 9 trimethylation
HF	Hair follicle
HFSC	Hair follicle stem cell
HG	Hair germ
HIF	Hypoxia inducible factor
HNF4α	Hepatocyte nuclear factor 4-alpha
HSC	Hematopoietic stem cell

IDH	Isocitrate dehydrogenase
IFE	Interfollicular epidermis
IKKβ	Inhibitor of nuclear factor kappa-B kinase subunit beta
IRES	Internal ribosome entry site
JMJD3	Jumonji domain-containing protein D3
K10	Keratin-10
K14	Keratin-14
KEAP1	Kelch-like ECH-associated protein 1
KLF5	Kruppel-like factor 5
LbNOX	*Lactobacillus brevix* nicotinamide adenine dinucleotide oxidase
LDH	Lactate dehydrogenase
m/z	Mass to charge ratio
m6A	N^6-methyladenosine
MDH	Malate dehydrogenase
mitoLbNOX	Mitochondrially localized Lactobacillus brevix nicotinamide adenine dinucleotide oxidase
mTORC1	Mammalian target of rapamycin, complex I
NAD+	Nicotinamide adenine dinucleotide, oxidized
NADH	Nicotinamide adenine dinucleotide, reduced
NEAA	Nonessential amino acid
NFκB	Nuclear factor of kappa light polypeptide gene enhancer in B-cells
NRF2	Nuclear factor erythroid 2-related factor 2
OGDH	2-oxoglutarate dehydrogenase
PC	Pyruvate carboxylase
PDH	Pyruvate dehydrogenase
PEG-ASNase	Pegylated Asparaginase
PHD	Prolyl hydroxylase
PHGDH	Phosphoglycerate dehydrogenase
PSAT	Phosphoserine aminotransferase
PSPH	Phosphoserine phosphatase
RTK	Receptor tyrosine kinase
SC	Stem cell
SCC	Squamous cell carcinoma
SCC-SC	Squamous cell carcinoma-stem cell
scRNA-seq	Single cell RNA-sequencing
SDH	Succinate dehydrogenase
Ser/Gly	Serine and glycine
SHMT	Serine hydroxymethyltransferase
SLC1A4	Solute carrier family 1 member 4
SLC1A5	Solute carrier family 1 member 5

SOX2	Sex determining region Y box 2
SOX9	Sex determining region Y box 9
SSP	Serine synthesis pathway
STAT3	Signal transducer and activator of transcription 3
TAD	Topological associated domain
TCA	Tricarboxylic acid
TET	Ten eleven translocation
TF	Transcription factor
TPA	12-O-tetradecanoylphorbol-13-acetate
tSC	Tumor stem cell
UTX	Ubiquitously transcribed tetratricopeptide repeat, X chromosome
WT	Wild type
YFP	Yellow fluorescent protein
αKG	alpha-ketoglutarate

CHAPTER ONE: INTRODUCTION

1.1 INTRODUCTION

Development and homeostasis of multicellular organisms depends on cells acquiring and maintaining the correct fate at the right place and time. Cell fate determination, wherein less differentiated cells progressively acquire specific fates and functions, is essential for proper embryogenesis and normal development. Even in postnatal life, proper cell fate determination is critical for maintenance of tissue homeostasis, which requires stem cells to balance self-renewal and differentiation. In both the embryo and postnatal tissues, cell fate determination depends both on inductive signals from the environment and the competence of cells to respond appropriately to these signals[1–3]. The landmark discovery of the Spemann-Mangold organizer demonstrated that a collection of embryonic cells is sufficient to re-pattern fate determination programs in amphibian embryos[4]. Early in development, factors secreted by the organizer can induce non-neural tissue to adopt a neural fate, but this plasticity is lost as development progresses. In postnatal life, inductive signals triggered by threats to tissue integrity can drive stem cells to mount proliferative programs to restore homeostasis[3]. Even differentiated cells can be coaxed to respond to inductive signals when needed: for example, upon injury to the intestinal stem cell pool, differentiated Paneth cells are able to de-differentiate into stem cells, facilitating intestinal repair[5]. These examples highlight how cell fate changes require precise environmental cues, which interact with cell-state specific factors, to shape appropriate cellular outcomes. Accordingly, dysregulation of either extracellular cues or their downstream intracellular responses compromise cell fate programs and results in diseases ranging from birth defects to cancer [2,3]. Consequently, understanding the molecular regulation of cell fate decisions is critically important for understanding the mechanistic basis of both normal physiology and disease states.

The transcriptional program of a cell is a key determinant of cell identity. The paramount importance of transcriptional programs to cell identity is perhaps best highlighted by the reprogramming of fully differentiated cells to pluripotent stem cells simply by expressing four key pluripotency transcription factors[6]. Thus, understanding the mechanisms that regulate a cell's transcriptional output is key to understanding cell fate decisions. Transcriptional changes can be facilitated by remodeling a cell's chromatin landscape, and a large body of work has focused on the role of chromatin regulation in cell fate decisions [1–3,7]. In particular, chemical modifications on DNA and histones provide a critical avenue for cells to control activation of gene expression programs. These chemical modifications are derived from intermediates of cellular metabolism, most notably S-adenosylmethionine and acetyl-CoA, which serve as the donors for methylation and acetylation modifications, respectively. Enzymes that remove these modifications often also require metabolites as critical co-substrates. Accordingly, fluctuations in the availability of key metabolites that modulate activity of chromatin-modifying enzymes are postulated to contribute to transcriptional regulation by shaping the chromatin landscape [8–10].

Intracellular metabolite levels are responsive to both cell-intrinsic metabolic pathway activity as well as extrinsic cues from the microenvironment, including growth factors and nutrient availability. Many inputs, including tissue lineage, proliferative status and nutrient availability, collectively determine the metabolic demands of individual cells[11,12]. Accordingly, recent studies highlight that cell-type specific metabolic demands influence cellular proliferation and fate in response to microenvironmental changes, including changes in key nutrients [13–15]. Emerging evidence additionally suggests that tissues experience distinct nutrient microenvironments, and that heterogeneity in extracellular nutrients can control cell fate by controlling the availability of metabolites that regulate the chromatin landscape [14,16–20]. In this manner, intracellular metabolites

are emerging as critical components of cell fate determination programs, capable of integrating extracellular nutrient status and intracellular biochemical demands to influence transcriptional networks and cell fate decisions.

Here, I review the proposed mechanisms by which select intracellular metabolites integrate environmental inputs to shape pathways determining lineage specific cell fates . I focus on metabolic intermediates of the tricarboxylic acid (TCA) cycle, a central regulatory hub of nutrient metabolism within cells. Multiple extracellular nutrients can feed into the TCA cycle, although in proliferating cells the major TCA cycle fuels are glucose and glutamine (Fig. 1.1a). Several intermediates of the TCA cycle, including α-ketoglutarate (αKG), succinate, and fumarate have been shown to regulate gene expression programs in various contexts [8,21]. Thus, the TCA cycle may integrate both extracellular nutrient availability and downstream transcriptional changes during cell fate changes. In particular, I discuss evidence that regulation of gene expression and cell fate by TCA cycle metabolites is context-dependent, with metabolites acting both upstream and downstream of lineage specific signaling and specification programs to shape cell fate. Finally, I discuss how nutrient availability creates permissive environments for cell fate outcomes by regulating intracellular metabolic pathways.

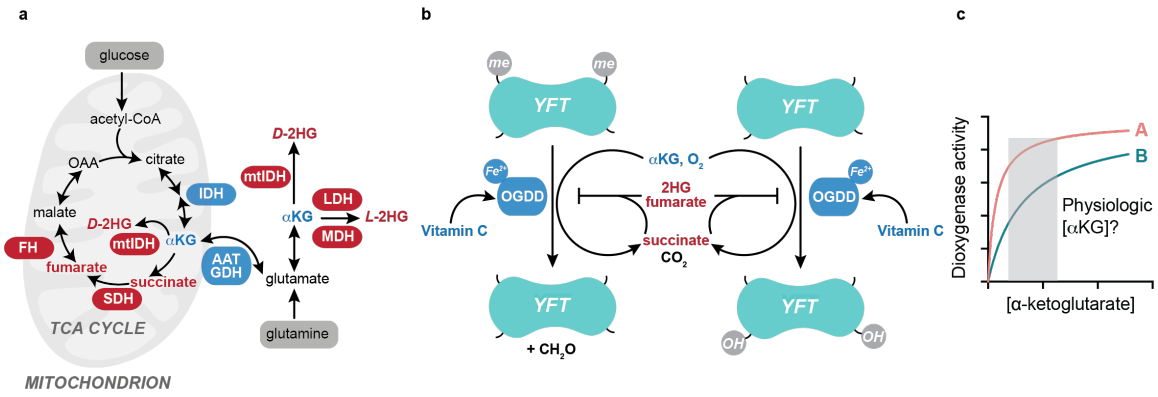

Fig. 1.1: Metabolic regulation of αKG-dependent dioxygenases. a, Schematic of key pathways involved in synthesis and break down of αKG, 2HG, fumarate and succinate. Enzymes directly involved in αKG metabolism are shown in blue, those involved in 2HG, fumarate and succinate metabolism are shown in red. **b,** Generalized schematic of αKG-dependent dioxygenase (also known as 2-oxoglutarate dependent dioxygenase or OGDD) action on your favorite target. Dioxygenases cataly ze net demethylation or hydroxylation reactions using αKG and molecular oxygen as co-substrates and producing succinate as a by-product. Vitamin C, oxygen and αKG have been shown to promote dioxygenase activity, whereas succinate, fumarate and 2HG have been shown to suppress their activity. **c,** Enzymatic assays provide potential insights into metabolic regulation of dioxygenase catalytic activity. In this example, dioxygenase B is expected to be sensitive to physiological fluctuations in αKG concentrations, whereas dioxygenase A will be less sensitive. However, it remains unclear what true physiological αKG concentrations are, given that dioxygenases may be sensitive to compartmentalized metabolite pools.

1.2 αKG-DEPENDENT DIOXYGENASES AS METABOLIC MEDIATORS OF CELL FATE CONTROL

Mechanistically, changes in TCA cycle metabolites are postulated to affect cell fate by regulating activity of α-ketoglutarate dependent dioxygenases [22,23]. The family of αKG-dependent dioxygneases comprises over 60 enzymes, including Jumonji C-domain lysine demethylases (JmjC-KDMs), which demethylate histones, Ten-Eleven Translocation (TET) DNA methylcytosine oxidases, and prolyl hydroxylases, which control collagen biogenesis and hypoxia-inducible factor (HIF) stability. TCA cycle intermediates serve both as critical co-substrates and competitive inhibitors of αKG-dependent dioxygenases: the enzymes consume αKG and

molecular oxygen as part of their reaction cycle, yielding succinate and carbon dioxide[8]. αKG-dependent dioxygenases are inhibited by other TCA cycle metabolites including succinate and fumarate, as well as the related metabolite 2-hydroxyglutarate (2HG), which can exist in cells as both a *D* and *L* enantiomer (Fig. 1.1b). Mutations in several of the enzymes that are involved in the production and breakdown of these metabolites, including isocitrate dehydrogenase (IDH1 and IDH2), succinate dehydrogenase (SDH), and fumarate hydratase (FH) have been shown to be drivers in cancer by disrupting normal cell fate decisions [21] (Fig. 1.1a). Even absent these mutations, however, intracellular abundances of αKG, succinate, fumarate and 2HG have been shown to regulate cell fate, including in stem cells, immune cells, and cancer cells [8,21].

The observation that TCA cycle metabolites can control αKG-dependent dioxygenases and cell fate raises major questions, including how a non-specific signal such as TCA cycle intermediate abundance can lead to a specific outcome in cell fate. One possibility is that the effect of a change in metabolite abundance is read out by a cell based on the relative affinity of dioxygenases for that metabolite. Briefly, the K_m of an enzyme for a particular substrate must be within the range of physiological fluctuations in concentration of that substrate in order for the enzyme's activity to be significantly affected by changes in substrate levels [8,10] (Figure 1.1c). *In vitro* enzymatic assays suggest that the K_m of αKG-dependent dioxygenases for αKG are in the low (~1-50) micromolar range, whereas the K_i and IC_{50} of succinate, fumarate, and 2HG are in the upper micromolar to low millimolar range [24]. Even within these ranges, however, there is evidence for differential effects of metabolites on dioxygenase activity [22,24,25]. For example, *in vitro* studies suggest that (*L*)- but not (*D*)-2HG inhibits prolyl hydroxylase function [22,25], and even closely-related dioxygenases can exhibit vastly different affinity for the same metabolite [24,26]. Thus, the response to a metabolite may be contingent upon the enzymatic properties of dioxygenases, and it

will be of major interest in the future to understand whether the expression patterns of dioxygenases with varying affinity for metabolites provides a biochemical rationale for specific outcomes driven by metabolic perturbations.

Nevertheless, there are several important limitations to cell-free systems in understanding metabolic control of cell fate. First, kinetic constants determined in simplified settings *in vitro* may not reflect enzyme behavior in a complex environment *in vivo*. Second, current approaches to measure metabolite concentrations provide information on whole cell or tissue abundances, while chromatin modifying αKG-dependent dioxygenases may be sensitive only to nucleo-cytosolic levels of metabolites, where substrates may be more (or less) limiting [27,28]. Suggestively, cancer associated IDH mutations (mtIDH), which convert αKG to 2HG, occur in both cytosolic IDH1 and mitochondrial IDH2, but mtIDH1 traditionally drives lower production of 2HG than mtIDH2. However, 2HG production by mtIDH1 is increased upon ectopic targeting to the mitochondria, potentially reflecting limited substrate availability in the cytosol [28]. Whether or not nucleo-cytosolic dioxygenases compete for a limited pool of αKG remains to be explored.

An additional challenge in understanding how changes in select TCA cycle metabolites may coordinately influence cell fate is the fact that multiple dioxygenase-sensitive marks are often affected by metabolic changes [29–32]. For example, succinate and fumarate accumulation in cancer cells is linked to HIF stabilization and hypermethylation of DNA as well as multiple histone lysine residues [31,33,34]. The ability of a single metabolite to influence multiple relevant pathways highlights the importance of these molecules but poses a challenge in understanding which changes represent biologically relevant, primary responses. For example, fumarate accumulation in *FH* deficient cells was thought to drive tumorigenesis in the kidney via inhibition of PHDs and subsequent stabilization of HIFs. However, double knockout of HIF1α and HIF2α did not prevent

FH-loss induced renal cyst formation, which was instead dependent on hyper-activation of NRF2 signaling driven not by fumarate-mediated inhibition of αKG-dependent dioxygenases but rather by direct covalent modification of reactive cysteines on KEAP1, a major negative regulator of NRF2 [35]. Indeed, many studies provide evidence that metabolites regulate cell fate decisions and dioxygenase-sensitive marks but remain correlative with regards to the precise mechanisms by which these effects are mediated.

The most rigorous approach to studying metabolic control of cell fate will involve both cell-free biochemical studies and genetic experiments in relevant *in vivo* systems. This combined approach recently revealed a critical role for molecular oxygen in muscle differentiation. αKG-dependent dioxygenases consume oxygen as part of their reaction cycle, and therefore may directly respond to hypoxia. The authors found that hypoxia impaired myogenic differentiation by inhibiting the αKG-dependent H3K27me3 demethylase UTX, which has a low *in vitro* oxygen affinity. Notably, the closely related H3K27me3 demethylase, JMJD3, has relatively high oxygen affinity and was not sensitive to hypoxia. Mutagenesis of key residues in UTX's catalytic domain to resemble that of JMJD3 was sufficient to increase oxygen affinity and restore differentiation in hypoxia[26]. It will be critical in the future to perform analogous experiments to manipulate sensitivity to fluctuations in TCA cycle metabolites so as to identify primary responders in cell fate decisions linked to these metabolites.

1.3 CANCER ASSOCIATED MUTATIONS HIJACK METABOLIC CONTROL OF CELL FATE

The identification of recurrent oncogenic mutations in metabolic enzymes sparked interest in the role of metabolites as drivers of cell fate decisions. Mutations in IDH1 and IDH2 lead to

accumulation of (*D*)-2HG, while mutations in SDH components and FH lead to accumulation of succinate and fumarate, respectively[31,36,37]. 2HG, succinate, and fumarate are collectively known as oncometabolites, competitively inhibit αKG-dependent dioxygenases, and are often suggested to exert similar functions in blocking stem cell differentiation [30,31,33,34,38].

In vitro differentiation of mesenchymal, hepatic, hematopoietic and neural progenitors are all suppressed by expression of mtIDH1/2 or 2HG treatment alone [22,30,39,40]. *In vivo*, expression of mtIDH in the brain, bone marrow and liver all lead to expansion of resident progenitor populations and suppression of terminal differentiation [39,41,42]. SDH-deficient paragangliomas arise in the oxygen sensing carotid bodies, a neural crest derived organ, and *Sdhd* loss is associated with carotid body hypertrophy and reduced differentiation [43,44]. Together, these studies suggest that inhibitory metabolites act by suppressing the competence of stem cells to respond to appropriate differentiation stimuli, such that stem cell division is skewed towards self-renewal.

In classic models of cell fate induction, cellular competence to respond to inductive signals for fate changes can be suppressed by direct inhibitors of that signaling pathway. For example, in the developing skin spatially restricted expression of Wnt inhibitors leads to distinct fate outcomes of Wnt-responsive and non-responsive cells[45,46]. By analogy, the pervasive observation that oncometabolites block differentiation across multiple lineages raises the possibility that αKG could be an inductive signal for adult stem cell differentiation. In support of this model, ascorbate, which promotes αKG-dependent dioxygenase function, drives hematopoietic stem cell (HSC) differentiation and suppresses leukemogenesis[47,48]. Exogenous αKG also promotes cytokine-induced HSC differentiation[49], and αKG is necessary and sufficient for effector T-cell differentiation[50,51]. Notably, the effects of αKG extend beyond tissues that are prone to transformation by oncometabolites. In both intestinal and epidermal stem cells, αKG is sufficient

for stem cell differentiation and suppressed tumor initiation and progression[14,52]. The effects of αKG extend to transformed cells: in pancreatic cancer cells, p53 restoration drives αKG-dependent differentiation, and αKG alone is sufficient to recapitulate the effects of p53[53]. When tested in these settings, succinate showed little effect except under conditions of αKG accumulation[14,53], consistent with αKG acting as an inductive signal and its antagonists establishing repressive thresholds for cell fate changes. In this manner, mutations in metabolic enzymes that lead to accumulation of 2HG, succinate and fumarate may be akin to mutations in key tissue specific signaling pathways that normally act to restrain stem cell self-renewal.

1.4 CANCER ASSOCIATED MUTATIONS SUGGEST LINEAGE SPECIFIC EFFECTS OF METABOLITES

Despite evidence that 2HG, succinate and fumarate act via similar mechanisms, mutations that drive accumulation of these oncometabolites occur in tumors of distinct lineages. For example, acute myeloid leukemia (AML) and gliomas harbor IDH but not SDH and FH mutations, whereas the opposite is true for renal cell carcinoma and neuroendocrine tumors[31,54,55]. The non-overlapping patterns of mutations suggest tissue-specific functions of these metabolites, despite their similar effects in biochemical assays. Thus, it is critical to understand how metabolites act in the context of the particular cohort of lineage specific signals and factors experienced by individual cells. Below, I discuss evidence that the response to a metabolite is lineage specific and in subsequent sections I review potential mechanisms by which lineage factors and environmental inputs might shape the cellular response to individual metabolites. Collectively, these studies raise two related but separate points: specific metabolites may be required for particular chromatin

changes and cell fate decisions, and different lineages may exhibit distinct responses and sensitivities to metabolites.

The potential for context-specific effects of metabolites has been best studied in hematopoiesis, which is fueled by HSCs. Consistent with an oncogenic function for 2HG, expression of mtIDH1/2 or treatment with (*D*)-2HG alone leads to increased proliferation and self-renewal of HSCs and other hematopoietic progenitors at the expense of proper differentiation *in vitro* and *in vivo*[23,38,41]. Accordingly, mtIDH2 cooperates with additional oncogenic hits to drive leukemogenesis in mice [56]. In contrast, both SDH and FH loss lead to impaired HSC maintenance and function. Moreover, FH loss suppressed, rather than supported, leukemic transformation [57,58].

One possible explanation for disparate effects of IDH, SDH and FH mutations is that SDH and FH are components of the core oxidative TCA cycle, whereas IDH1 and IDH2 are not. Thus, it may be that HSCs are unable to cope with TCA cycle truncation, which requires distinct metabolic adaptations [59]. A second potential reason for this discrepancy, however, is the unique effects of (*D*)-2HG versus succinate and fumarate on αKG-dependent dioxygenases. Whereas mtIDH1/2 inhibited both TET2-mediated DNA demethylation and JmjC-KDM-mediated histone demethylation, FH loss in HSCs only inhibited histone demethylation [38,41,58]. Fumarate additionally functions to modify reactive cysteine residues, and thus is likely to exert functions independent of αKG-dependent dioxygenases [35,60]. Altogether, these studies support distinct effects of succinate, fumarate and 2HG accumulation on HSC behavior.

In AML, multiple neomorphic mutations in IDH1 and IDH2 occur, all of which are sufficient to induce (*D*)-2HG and block hematopoietic differentiation [23,38,41]. As noted above, 2HG accumulation is thought to play a major role in suppressing HSC differentiation by antagonizing TET2 function. This notion has been bolstered by the observation that IDH1/2 mutations in AML

are mutually exclusive with TET2 mutations, and TET2 loss of function phenocopies mtIDH expression [23,38]. Even within the hematopoietic lineage, however, IDH mutations may exert distinct effects. For example, IDH mutations occur only at R172 of IDH2 in angioimmunoblastic T-cell lymphoma (AITL), where they co-occur with TET2 mutations. IDH2 R172 mutants produce significantly more 2HG than other mutants, and only IDH2 R172 mutant expression disrupts T-cell differentiation in mouse models[61]. These data suggest that 2HG dosage may have cell-type specific effects and that the same metabolite can exert distinct effects at different stages of a developmental trajectory. Thus, gaining an understanding of how metabolites cooperate with lineage specific transcription factors and signaling pathways may provide insight into why metabolites exhibit cell-type specific effects.

1.5 METABOLIC INTERACTION WITH LINEAGE SPECIFIC TRANSCRIPTION FACTORS

Studies highlighting the context-specific effects of oncometabolites indicate that metabolites will likely regulate cell fate decisions in a tissue-specific manner. Given the abundance of literature on the critical role transcription factors (TFs) and cell-type specific enhancer landscapes play in establishing and maintaining cell identity, it is likely that effects of metabolites will vary according to their ability to interact with lineage specific transcriptional machinery. In this section I discuss two potential mechanisms by which metabolites may regulate cell fate changes: first, I review evidence that metabolites can directly control TF abundance and expression; and second, I review data suggesting that metabolites regulate TF activity by globally modulating co-activator function. Since different cell fate changes are likely to rely on distinct TF

and co-activator cohorts, these data may provide an explanation for lineage specific effects of metabolites.

Limited evidence suggests that metabolites may act upstream of lineage TFs. In the liver, mutant IDH1 expression blunts progenitor differentiation into hepatocytes by silencing the master TF HNF4α[39]. In intestinal tumor organoids, αKG is sufficient to suppress activation of the master intestinal stem cell regulator β-catenin and induce differentiation[52]. Despite these observations and correlations with changes in DNA and histone methylation at TF promoters and target gene loci, the exact mechanisms by which metabolites affect expression of specific TFs are not well understood.

Appealing mechanisms by which metabolites could act upstream of master lineage regulators are via post-transcriptional and post-translational regulation of TF expression. The RNA demethylases FTO and ALKBH5, which demethylate N^6-methyladenosine (m6A), are αKG-dependent dioxygenases. m6A destabilizes transcripts and has been found to regulate expression of key TFs in embryonic stem cells (ESCs) and HSCs [62–64]. Moreover, it was recently shown that 2HG suppresses FTO activity in leukemia cells, leading to decreased expression of the lineage TF CCAAT enhancer binding protein α (C/EBPα), which enforces normal HSC quiescence and myeloid differentiation [65–67]. In this manner, direct metabolic regulation of key TF expression may enable specific cell fate outcomes.

Metabolites also exert post-translational control over TFs, as exemplified by the dominant role of αKG-dependent prolyl hydroxylation in the control of HIF1α stability [25,33]. Studies in macrophages recently uncovered the ability of αKG-dependent prolyl hydroxylases to regulate other TFs during cell fate decisions. These studies revealed that αKG is necessary for anti-inflammatory M2 polarization and sufficient to suppress pro-inflammatory M1 polarization. While

the effects of αKG on M2 polarization required the H3K27me3-demethylase JMJD3, αKG suppressed M1 polarization by inhibiting the master inflammatory TF NFκB via prolyl-hydroxylase-dependent modification of its activator IKKβ. Accordingly, a hydroxylation-dead IKKβ mutant rendered M1 polarization resistant to αKG [68]. Thus, exploring post-transcriptional and post-translational regulation of TFs by αKG-dependent hydroxylases may identify new layers of regulation by which metabolites can induce cell fate changes (Fig. 1.2a).

Transcription factors can regulate gene expression by recruiting co-activators and/or co-repressors to target loci [7]. Co-activators, including TETs and H3K27me3 demethylases JMJD3/UTX, require αKG as a co-substrate, raising the possibility that metabolites function in cell fate decisions by regulating TF function via potentiating or suppressing co-activator activity (Fig. 1.2b). This model has been best studied in mouse embryonic stem cells (ESCs). ESCs can be maintained *in vitro* in a heterogeneous state of metastable pluripotency or as a homogeneous population of cells in the naïve ground state of pluripotency via culture in specific media formulations. The naïve ground state of pluripotency is intrinsically associated with an accumulation of αKG at the expense of succinate, which is reflected by an increase in the αKG/succinate ratio, due to reduced αKG catabolism in the TCA cycle[13,29]. Notably, supplementing metastable ESCs with αKG is sufficient to facilitate TET and UTX/JMJD3-mediated DNA and histone demethylation, respectively, and increase pluripotent self-renewal[29].

The ground state of pluripotency is characterized by a robust TF network, whose action is facilitated in part by recruitment of TET1/2 to key pluripotency loci [69–71]. This robust transcriptional network enables naive, but not metastable, ESCs to maintain growth and pluripotency upon inhibition of the co-activator Brd4, which binds acetylated histones to activate transcription and is usually essential for maintenance of gene expression programs[72]. The ability

of pluripotency TFs to confer Brd4 independence and sustain self-renewal is sensitive to metabolic perturbations, since glutamine starvation – which depletes αKG – blunts expression of key pluripotency genes and ascorbate enhances self-renewal in the presence of Brd4 inhibitors [69]. Intriguingly, mtIDH AMLs are highly sensitive to Brd4 inhibition [56]. Whether or not this sensitivity is due to decreased ability of αKG-dependent dioxygenases to function downstream of master hematopoietic TFs upon 2HG accumulation remains to be explored but would be consistent with the data in ESCs.

Core pluripotency TFs are known to drive their own expression, creating a positive feedback loop, and can remain bound to target genes even upon induction of differentiation stimuli[73,74]. This enables ESCs to revert to pluripotency upon withdrawal of differentiation stimuli so long as these key TFs remain chromatin bound [74]. Thus, if αKG acts by promoting pluripotency TF function, loss of these TFs from chromatin late in differentiation would blunt the effects of αKG. Consistently, αKG can only sustain ESC pluripotency when provided early after a differentiation stimulus, when expression of pluripotency TFs remains high [75]. Differentiation is associated with a decrease in αKG that coincides with the loss of pluripotency TFs; conversely, overexpression of key pluripotency factors such as NANOG or activated STAT3 are sufficient to increase αKG, suggesting that αKG accumulation may be a component of the feed-forward loop of the pluripotency network [13,75].

Notably, αKG doesn't always enhance ESC self-renewal. In more committed pluripotent cells such as human ESCs and mouse post-implantation epiblast ESCs, however, αKG actually facilitated differentiation, which was antagonized by succinate [76,77]. The differential response to αKG may reflect either the more committed state of human and mouse epiblast ESCs or the particular differentiation stimuli used in each condition. Alternatively, αKG may exert different

outcomes as a result of distinct requirements for self-renewal vs. differentiation in different cell states, either due to different cohorts of TFs or different required changes in chromatin to achieve a cell state change. Notably, the naïve and more committed, primed states of pluripotency have dramatically different levels of DNA methylation [78], and thus may have different sensitivity to metabolic perturbations that favor demethylation. Given that αKG can influence both TF expression directly and function indirectly, metabolites are likely to play numerous roles in particular cell fate decisions, depending on the specific requirements of that cell state.

Recent evidence suggests that oncometabolites also can act by blunting co-activator action at lineage specific genes. For example, during muscle differentiation the master TF MyoD recruits H3K9me2/3 demethylases to target loci to promote expression. Accordingly, mtIDH1 expression suppresses MyoD-mediated differentiation, which is rescued by genetic inhibition of H3K9 methyltransferases. Whereas normal myogenic differentiation is accompanied by selective hypomethylation of H3K9 at myogenic targets, mtIDH1 expression drives global, apparently non-selective increases in H3K9me3 [79]. These results support a model wherein 2HG accumulation in myoblasts establishes a global chromatin landscape that is incompatible with differentiation due to inhibition of H3K9 demethylases, whereas locus specificity during differentiation is achieved by TF recruitment of co-activators. Consistently, work in neural, mesenchymal and hematopoietic cells shows that IDH mutations render stem cells unable to appropriately respond to differentiation stimuli, although the interaction between master TFs, co-activators and metabolites remain to be explored in these settings [23,30,38,40]. Thus, the ability of metabolites to regulate specific cell fate changes is likely due to the combinatorial effects on lineage specific factor expression and function, and gaining a detailed understanding of context-specific effects of metabolites will likely require integration of these multiple regulatory nodes.

Fig. 1.2. Potential mechanisms of metabolic control of cell fate. a, αKG-dependent dioxygenases can directly impact expression of key transcription factors (KTFs) both by regulating mRNA methylation and protein hydroxylation, both of which trigger target degradation. **b,** Metabolites can regulate TF function by influencing co-activator function, a subset of which are αKG-dependent dioxygenases. Transcription factors recruit co-activators such as TETs and KDMs to target loci in order to locally remodel chromatin. **c,** Metabolites can impact enhancer function and long range chromatin interactions by controlling CTCF binding to DNA, which is suppressed by DNA methylation. αKG enforces TAD architecture in cells by facilitating CTCF binding, whereas 2HG, succinate and fumarate disrupt TAD architecture. In the presence of CTCF, a cell-type specific active enhancer drives expression of your favorite gene-A (YFG-A), whereas YFG-B is suppressed. Upon loss of CTCF binding, however, TAD boundaries are disrupted and the active enhancer drives expression of YFG-B.

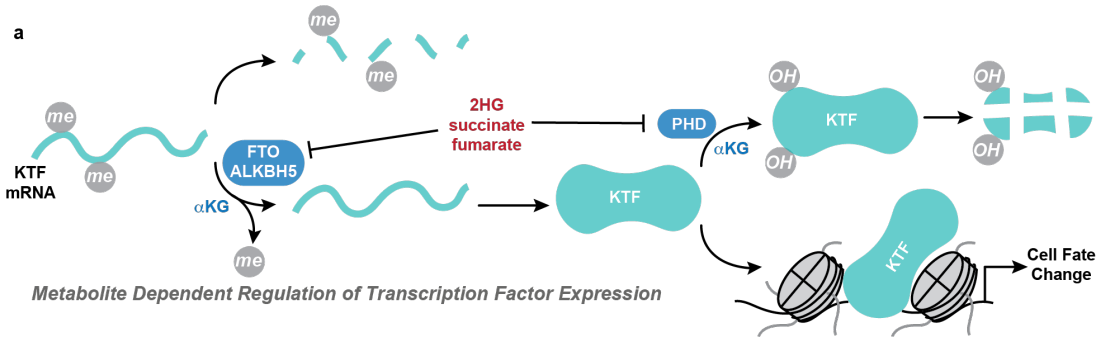

Metabolite Dependent Regulation of Transcription Factor Expression

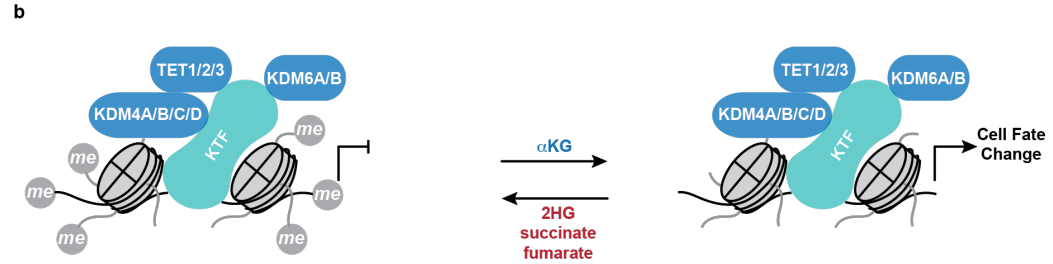

Metabolite Dependent Regulation of Co-activator Function

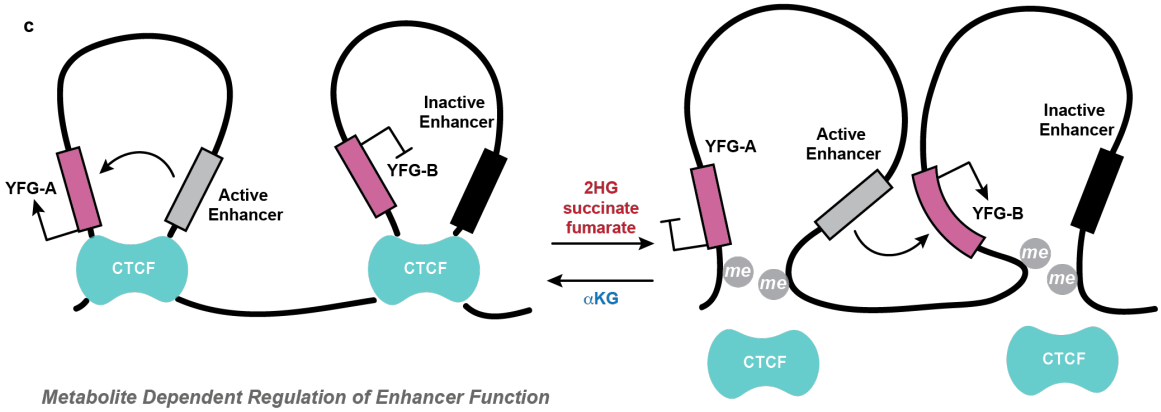

Metabolite Dependent Regulation of Enhancer Function

1.6 METABOLIC CONTROL OF LINEAGE SPECIFIC ENHANCERS

A key component of cell fate decisions involves TF-mediated establishment and binding of cell type specific enhancers [80]. Active enhancers are marked by acetylation of H3K27 and can be suppressed by H3K27me3 and DNA methylation [81]. Accordingly, metabolic regulation of αKG-dependent dioxygenases can directly regulate enhancers. For example, FH deficient renal cells exhibit increased DNA and H3K27 methylation at a putative enhancer for the microRNA cluster mIR-200. Fumarate-mediated enhancer methylation suppressed the anti-metastatic miR-200 cluster, activating the epithelial-mesenchymal transition (EMT). Interestingly, exogenous αKG reversed fumarate-induced EMT, suggesting that ongoing αKG-dependent dioxygenase activity may be required for maintenance of the epithelial phenotype [82].

Recent studies profiling three-dimensional chromatin landscapes and the ubiquitously expressed transcription factor CCCTC-binding factor (CTCF) have provided additional insights into the interactions between metabolites and enhancers. The genome is organized into discrete regulatory units called topologically associated domains (TADs), whose boundaries are established by CTCF binding [83]. Enhancers preferentially drive expression of genes within their own TADs; accordingly, CTCF loss increases inter-boundary interactions at the expense of intra-boundary interactions, thereby modifying enhancer-promoter contacts and altering gene expression[83]. DNA methylation is emerging as a critical barrier to CTCF binding and TAD regulation that is susceptible to metabolic perturbation [83]. In both mtIDH gliomas and SDH-deficient gastrointestinal stromal tumors, hypermethylation of CTCF binding sites is associated with increased interactions between key receptor tyrosine kinase (RTK) genes and constitutive lineage-specific enhancers normally outside of their domains, driving RTK expression. Deletion of key CTCF binding sites alone phenocopied the effects of mtIDH or SDH loss on RTK

expression [84,85]. Similarly, experiments performed in a human ESC model of glioma demonstrated that mtIDH suppressed differentiation by disrupting CTCF binding, leading to reduced interaction of the *SOX2* locus with an active enhancer [86]. Collectively, these studies demonstrate the potential of oncometabolites to influence enhancer activity towards target genes (Fig. 1.2c).

Intriguingly, CTCF is ubiquitously expressed, and many of its binding sites are shared between different cell types [87]. Therefore, metabolic regulation of CTCF *per se* is not sufficient to result in tissue specific effects; rather, the particular enhancer landscape of a cell will play a key role determining the transcriptional outcomes of altered CTCF binding. For example, αKG induces increases in CTCF binding at overlapping loci in ESCs and T-cells, but cell-type specific changes in gene expression. In T-cells, αKG supports effector T-cell differentiation by increasing interactions of IL-2 target genes with active T-cell enhancers. Although αKG also increases CTCF binding in the vicinity of key ESC genes in T-cells, these genes are not transcriptionally induced because they lack active enhancers in T-cells[50]. Altogether, these data support a model wherein αKG and its inhibitors contribute to cell fate regulation by controlling three-dimensional chromatin architecture, but specific cell fate outcomes are driven by the enhancer landscape of a cell. Most likely, all of these factors can converge enabling metabolites regulate cell fate changes by co-regulating chromatin architecture and TF function.

1.7 NUTRIENTS REGULATE αKG-DEPENDENT DIOXYGENASES

In vivo cell fate changes do not occur in isolation, but rather in a spatiotemporally defined manner that is under the control of a cell's microenvironmental milieu, or niche[3]. Many niche derived signals can induce changes in intracellular metabolism. For example, growth factor signaling acutely increases nutrient uptake, and stromal cells can provide metabolic support to

stem cells by directly providing nutrients[88,89]. Additionally, the nutrients supplied to a tissue may also influence cell fate by controlling intracellular metabolite abundance. Stem cells of multiple tissues, including those of the blood, brain and skin are in close proximity to the vasculature, suggesting that their nutrient microenvironment may be closely regulated via control of blood supply and drainage [90–92]. Given recent evidence that the extracellular nutrient milieu may vary in a tissue-specific manner [16,93], I discuss the possibility that nutrient availability within stem cell niches could contribute to cell fate decisions through αKG-dependent dioxygenases (Fig. 1.3).

Oxygen. How cells adapt to hypoxia has been thoroughly reviewed elsewhere [94], and here I highlight how αKG-dependent dioxygenases contribute to the cellular response to changes in oxygen availability. While all αKG-dependent dioxygenases consume oxygen, only a subset have sufficiently low affinity for oxygen to be limited by physiological levels of hypoxia [26]. However, hypoxic conditions, which induce intracellular acidification and high intracellular NADH/NAD+ favor promiscuous reduction of αKG to (*L*)-2HG by lactate dehydrogenase and malate dehydrogenase [95,96]. This rise in (*L*)-2HG, which inhibits most αKG-dependent dioxygenases more potently than (*D*)-2HG, is necessary and sufficient for hypoxic hypermethylation of histones in certain contexts [97]. Collectively, these findings suggest that hypoxia may block αKG-dependent dioxygenase activity through multiple mechanisms.

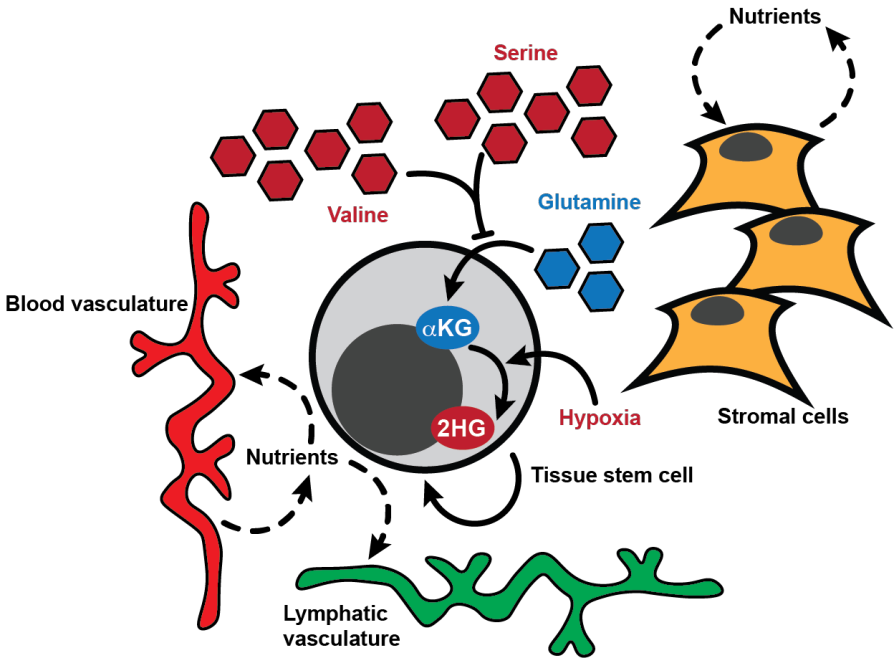

Fig. 1.3. Niche regulation of αKG-dependent dioxygenases. Summary of potential regulators within the stem cell niche of stem cell dioxygenase activity. αKG is largely derived from glutamine, whereas serine and valine have been shown to suppress intracellular αKG levels. Hypoxia directly antagonizes dioxygenase activity and facilitates production of 2HG from αKG. Finally, the role of niche cells in αKG-dependent dioxygenase activity has yet to be explored but is a potential regulator, as many stem cells reside in proximity to the vasculature and stromal cells may provide nutrients to stem cells and/or compete with stem cells for nutrients within the niche.

Intriguingly, many stem cells including neural and hematopoietic stem cells reside in hypoxic niches and can be regulated by HIF1α signaling [98–103]. Notably, malignant ependymomas, derived from hypoxic fetal neural precursors, require hypoxia to proliferate due to metabolic requirements to maintain histone methylation and acetylation [104]. Whether or not metabolic responses to hypoxia also contribute to normal stem cell behavior remains an open question. In particular, hypoxia-induced 2HG could create a non-permissive environment for differentiation, thereby coupling hypoxic niches to homeostatic stem cell self-renewal. While the majority of HSCs reside in hypoxic peri-sinusoidal niches, some studies report a small percentage of progenitors in well-oxygenated peri-arteriolar regions [105,106]. Whether these HSCs are functionally

distinct in their ability to differentiate remains to be seen, but an intriguing possibility is that 2HG levels would decline upon migration to better perfused niches, enabling differentiation. In this model, IDH1/2 mutations would effectively uncouple HSC differentiation from niche regulation via constitutive 2HG production. Studying the role of oncometabolites and αKG in tissue stem cells experiencing physiological hypoxia will be an interesting area of research in the future.

Amino acids. In most proliferating cells *in vitro*, glutamine is the major contributor to the carbon backbone of the TCA cycle. Glutamine is first deamidated to glutamate, which is then deaminated to αKG via transaminase reactions or glutamate dehydrogenase. Accordingly, manipulating extracellular glutamine levels has been shown to regulate TCA cycle metabolites, cell fate, and proliferation [21,107]. As discussed earlier, reduced catabolism of glutamine-derived αKG in the TCA cycle enables naïve mouse ESCs to maintain an elevated αKG/succinate ratio and to proliferate in the absence of glutamine [13,29]. Accordingly, glutamine has two distinct roles in regulating ESC fate. Transient glutamine withdrawal selects for ESCs with enhanced self-renewal due to death of more committed cells. However, because glutamine is the major source of αKG, prolonged glutamine starvation decreases ESC self-renewal. Re-supplementation of glutamine after a transient withdrawal therefore enables naïve ESCs to recover expression of key pluripotency markers [13].

Glutamine is also a key regulator of αKG abundance and cell fate in adult tissues. In macrophages, glutamine starvation blunts M2 polarization and favors a pro-inflammatory phenotype, which can be reversed by αKG supplementation [68]. Similarly, glutamine starvation in T-cells prevents effector differentiation, which can be restored via αKG treatment. Glutamine starved or (*L*)-2HG treated T-cells adopt a memory T-cell fate, a subset of which may have stem cell properties [50,51,108]. Similarly, glutamine starvation enhances stemness of intestinal organoids

harboring pre-malignant oncogenic mutations and increases tumor initiating capacity [52]. While these studies relied on *in vitro* glutamine starvation, heterogeneity in glutamine availability may also be an important determinant of cell fate *in vivo*. For example, glutamine deficiency in melanoma cores *in vivo* is sufficient to blunt cancer cell differentiation due to αKG depletion, and increasing dietary glutamine is sufficient to increase αKG levels and impair tumorigenesis [109,110]. Altogether, these data are consistent with glutamine availability creating a permissive environment for cell fate determination by enabling αKG accumulation. Thus, anti-cancer therapies aimed at suppressing glutamine uptake and catabolism may inadvertently select for the most aggressive stem cells in a tumor.

Conversion of glutamate to αKG is largely accomplished by transaminase enzymes in proliferating cells, which reversibly donate the amine nitrogen of glutamate to a ketoacid in order to synthesize a non-essential amino acid (NEAA) and αKG [107]. Emerging evidence suggests that which particular transaminases predominantly contribute to αKG may vary in a tissue-specific manner. In IDH wild-type AML, catabolism of the branched chain amino acids (BCAA) valine, leucine and isoleucine by branched chain aminotransferase 1 (BCAT1) restricts intracellular αKG levels, leading to DNA hypermethylation and HIF1α stabilization. Notably, BCAT1 loss blunts AML stem cell growth and induces myeloid differentiation [111]. Interestingly, normal HSCs are reliant on valine for their maintenance for unknown reasons [112]. BCAAs are essential and therefore their uptake is required by all cells for protein synthesis, but BCAT activity may be cell-type specific [113]. It is therefore intriguing to consider that valine supports HSC self-renewal by restricting intracellular αKG.

In other tissues, serine synthesis represents a notable source of nucleocytosolic αKG production via phosphoserine aminotransferase (PSAT1) activity. In breast cancer,

hyperactivation of the serine synthesis pathway maintains hypoxic breast cancer cell survival and supports αKG production for TCA cycle anaplerosis [114,115]. In this thesis, I show that in the murine epidermis, *in vivo* restriction of serine and its immediate downstream metabolite glycine triggers *de novo* serine synthesis activation in epidermal stem cells and accumulation of αKG, which is necessary and sufficient to drive stem cell differentiation, H3K27me3 demethylation, and tumor suppression [14]. Intriguingly, dietary serine and glycine restriction has proven effective in delaying tumorigenesis in other models as well, and it will be of interest to understand whether or not αKG-dependent stem cell differentiation plays a role in these systems[116,117]. Collectively, these studies demonstrate that dietary manipulation of extracellular nutrient availability is sufficient to regulate stem cell fate in part by controlling intracellular αKG levels.

1.8. CONCLUSIONS

Proper development and adult tissue function requires careful control over cell fate programs. Collectively, the above studies suggest that metabolites act as both inductive signals and regulators of competence during cell fate determination, and thus disruption of tissue specific pathways that maintain TCA cycle homeostasis promotes pathology, most notably by enforcing progenitor self-renewal and driving tumorigenesis. Metabolite abundances—determined by environmental nutrient availability and cell-type specific genetic programs—can collaborate closely with lineage specific transcriptional programs to regulate cell fate. Evidence across multiple tissues suggest a model wherein αKG acts as an inducer of cell fate changes, while succinate, fumarate and 2HG largely restrict competence to appropriately execute cell fate programs. Accordingly, nutrients that fuel intracellular αKG pools create permissive environments for cell fate decisions, and mutations that drive oncometabolite accumulation prevent αKG-

mediated cell decisions. The roles of specific oncometabolites in lineage-specific cancers warrants investigation into the role of αKG during development and differentiation of their normal tissue counterparts. More broadly, whether the tissue specific profiles of cancer-associated mutations in chromatin modifying enzymes such as TETs and DNA and histone methyltransferases likewise predict metabolite-responsive nodes co-opted by tumors will be an important area of future investigation.

Future studies should be aimed at better dissecting the roles of specific dioxygenases in responses to metabolites and the cell-type specific roles of metabolites within native tissue microenvironments. In particular, whether or not the availability of endogenous nutrients fluctuates sufficiently to modulate intracellular metabolite abundances and cell fate outcomes remains to be explored. Finally, although many studies support the role of metabolic changes regulating cell fate decisions, relatively few studies address whether or not basal metabolism supports the maintenance of cell-type specific gene expression outputs and accordingly, the maintenance of cell identity. For example, do transcription factors require a basal level of αKG to sustain cell identity once a cell's chromatin landscape is established, or do changes in αKG pools only enable dynamic reprogramming of gene expression? Improved technologies to enable measurement of extracellular, subcellular and cell-type specific metabolite abundances *in vivo*, coupled with genetic experiments to modulate dioxygenase sensitivity to metabolites, will facilitate our ability to gain a deeper understanding of the physiological and pathological roles of metabolites in controlling cell fate.

In this thesis I explore the role of nutrient availability and αKG-dependent dioxygenases in epithelial stem cells of the skin epidermis. The skin houses an abundant reservoir of stem cells which maintain distinct tissues within the organ. These include the stem cells of the interfollicular

epidermis (IFE), which maintain the skin barrier that is essential for maintaining organismal water and electrolyte balance while protecting us from external infectious and noxious agents, and those of the hair follicle (HF) which regenerate the hair coat of mammals.

Epithelial stem cells of the skin give rise to malignancies include squamous cell carcinomas (SCCs) and basal cell carcinomas (BCCs) and are additionally required for wound repair[3]. While many foundational studies have identified the core signaling and transcriptional machinery involved in skin stem cell homeostasis and pathology[118], the metabolic determinants of stem cell behavior in the skin remain largely unexplored. In particular, while recent studies have highlighted the importance of metabolic pathways such as glucose uptake and glycolysis in supporting skin stem cell proliferation[119,120], little is known about whether or not particular metabolites regulate stem cell identity or the balance of fate decisions in the skin. I explore the role of nutrient availability in regulating stem cell fate during SCC initiation as well as epidermal growth and differentiation. These studies establish extracellular nutrient availability as determinants of epidermal stem cell fate via control of αKG-dependent dioxygenases.

CHAPTER 2

EXTRACELLULAR SERINE CONTROLS EPIDERMAL STEM CELL FATE AND TUMOR INITIATION

2.1. INTRODUCTION

Stem cells (SCs) maintain tissue homeostasis by balancing self-renewal and differentiation[3]. With age, SCs can acquire cancer-associated mutations and clonally expand in the context of a grossly normal tissue[121–125]. How SCs contend with pre-malignant oncogenic mutations, and the mechanisms that ultimately drive a subset of progenitors to initiate neoplasms, remain largely unknown. The answers become increasingly important given evidence that SCs, but not terminally differentiated cells, are a major root of malignancy[126–129], and that driving SC differentiation is a potent tumor suppressive mechanism[130–133]. Thus, identifying factors that regulate oncogenic SC fate is critical to delineating the mechanisms that drive tumor initiation.

The innermost (basal) layer of mammalian epidermis houses an abundant reservoir of SCs responsible for maintaining the skin barrier. Acquisition of oncogenic mutations predisposes epidermal stem cells (EpdSCs) to initiate benign tumors, which progress to squamous cell carcinomas (SCCs), among the most common cancers worldwide[3]. As such, the epidermis is an excellent model to understand the mechanisms regulating pre-malignant SC behavior.

During SCC pre-malignancy, epigenetic and/or genetic mechanisms lead to induction of the transcription factor SOX2, which is necessary for tumor initiation and progression[134–136]. Ectopic activation of SOX2 in EpdSCs induces a stress response involving global protein synthesis repression and selective translation of oncogenic transcripts[135,137]. Since protein synthesis is intimately tied to amino acid availability[138], this prompts the intriguing but unexplored hypothesis that SCs may adapt to oncogenic stress by altering their metabolism.

Increasing evidence suggests that metabolites can regulate SC proliferation, self-renewal and differentiation[13,21,29,119,139]. Additionally, metabolic reprogramming supports bioenergetic and anabolic reactions that are necessary for proliferation[21], rendering tumor progression sensitive to

nutrient availability[116,117,140]. However, it remains unknown whether oncogenic lesions rewire endogenous metabolic programs in SCs, and if so, how this contributes to tumor initiation. Here, I assessed the consequences of oncogenic stress to EpdSC metabolism and discovered that metabolic reprogramming suppresses differentiation programs that otherwise antagonize tumorigenesis. These results hold promise for therapeutic avenues targeting oncogenic SCs.

2.2. RESULTS

2.2.1. Pre-malignant SC growth is dependent upon extracellular serine.

Sustained SOX2 expression in EpdSCs induced pre-tumorigenic lesions marked by hyperproliferation, expansion of $K14^+$ progenitors, and induction of the tumor stem cell (tSC) marker CD44 (Fig 2.1a). To explore the metabolism of pre-malignant EpdSCs prior to the onset of hyperproliferation, I crossed *R26-LSL-Sox2-IRES-eGFP*$^{fl/fl}$ and *Krt14-Cre*$^{+/wt}$ mice to generate littermate wild-type (WT) and $SOX2^+$ animals, where *Sox2* was induced developmentally in $K14^+$ epidermal progenitors[135,141] (Fig. 2.1b). At postnatal day 4 (P4) and in primary culture, $SOX2^+$ and WT EpdSCs proliferated comparably (Fig. 2.1b,c), enabling us to identify metabolic changes associated with pre-malignancy independently of hyperproliferation.

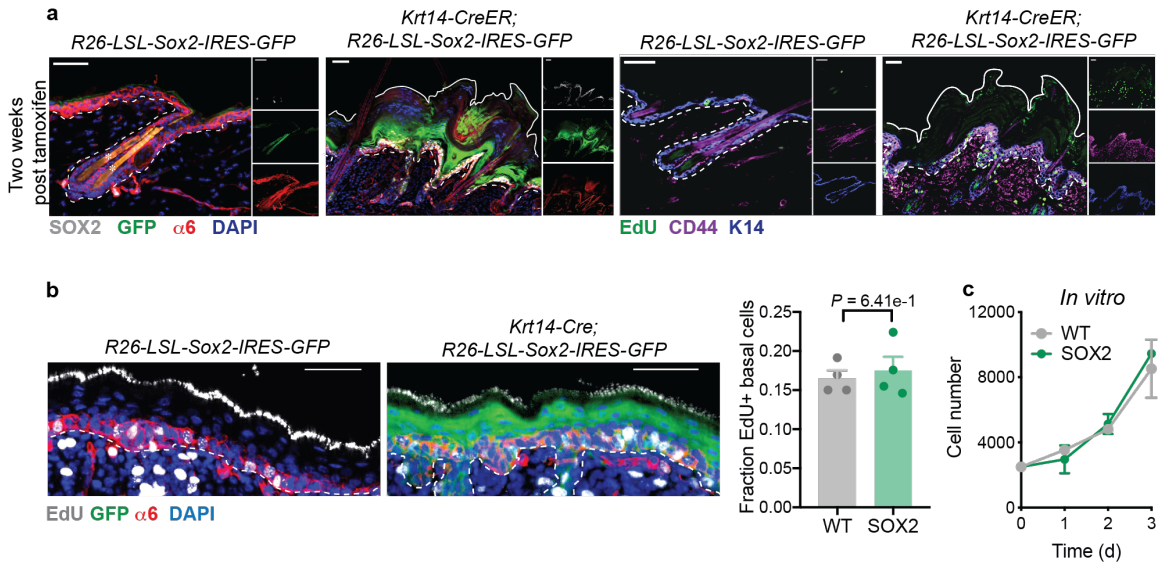

Figure 2.1. **SOX2 induction as a model of pre-malignancy in epidermal stem cells. a,** Representative immunofluorescence of progenitor markers α6 and K14, tumor SC markers CD44 and SOX2, and EdU incorporation in P65 WT and SOX2^{+} mice two weeks after tamoxifen administration. **b,** EdU incorporation into integrin-α6^{+} EpdSCs in P4 WT and SOX2^{+} mice. **c,** Growth of independently derived WT-1,2,3 and SOX2^{+}-1,2,3 EpdSC cultures.

Like SCC-SCs, SOX2^{+} EpdSCs decrease protein synthesis relative to WT EpdSCs[135,137]. Since amino acids provide the majority of cellular biomass[142], I asked whether pre-malignant EpdSCs have altered amino acid requirements. Gas chromatography-mass spectrometry (GC-MS) of medium from primary cultures revealed that essential amino acids were consumed at similar rates between WT and SOX2^{+} EpdSCs (Fig. 2.2a). Of the non-essential amino acids, only glutamine, tyrosine and serine were appreciably consumed, consistent with reports in cancer cells[142]. Of these, only serine was differentially consumed (Fig. 2.2a,b).

Unexpectedly, despite reduced translation[135], SOX2^{+} cells consumed more serine than WT cells. Glycine, which can be interconverted with serine by serine hydroxymethyltransferases (SHMT1/2), was not appreciably consumed (Fig. 2.2b). These results suggested that SOX2^{+} progenitors deviated from WT EpdSCs in serine metabolism. Culturing EpdSCs with uniformly

^{13}C-labeled serine confirmed that SOX2^{+} cells derived a larger portion of intracellular serine from extracellular sources (Fig. 2.2c).

I next analyzed the consequences of withdrawing extracellular serine from the culture medium. To minimize possible confounding effects arising from converting glycine to serine under starvation conditions, I also removed glycine. When deprived of exogenous serine and glycine (Ser/Gly), SOX2^{+} cells did not maintain intracellular serine pools as well as WT EpdSCs and their proliferation halted (Fig. 2.2d,e). By contrast, WT EpdSCs proliferated normally. Ser/Gly dependence was independent of the oncogene used to induce pre-malignancy, as HRas^{G12V}-expressing EpdSCs also required exogenous Ser/Gly to proliferate (Fig. 2.2f). These data indicate that oncogenic EpdSCs rely upon exogenous Ser/Gly to sustain proliferation.

The proliferative block of pre-malignant EpdSCs upon Ser/Gly deprivation was surprising, given that both can be synthesized *de novo*[143]. To determine whether synthesis of one or both amino acids was defective in SOX2^{+} cells, I depleted each individually. Consistent with minimal net consumption of glycine (Fig. 2.2b), glycine deprivation did not affect proliferation. By contrast, serine starvation alone inhibited SOX2^{+} proliferation comparably to combined Ser/Gly deprivation (Fig. 2.2g). Thus, pre-malignant EpdSCs are functional serine auxotrophs that rely upon obtaining serine from extracellular sources to proliferate. To avoid potential confounding effects of serine deprivation alone, I starved cells of both Ser/Gly in subsequent experiments.

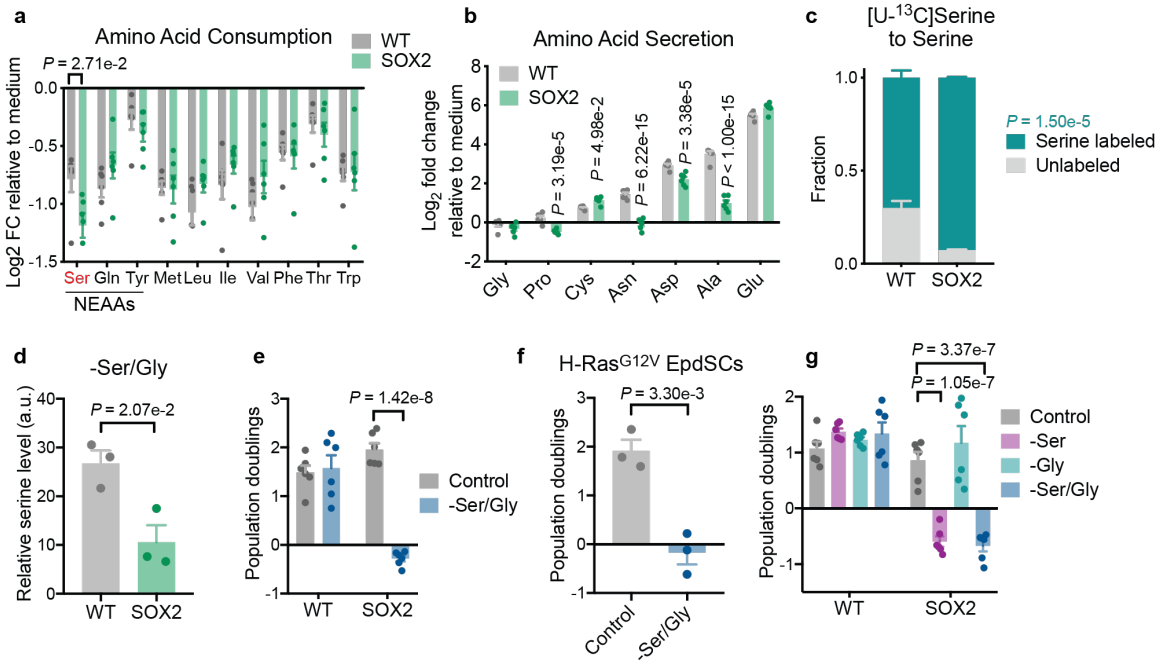

Fig 2.2. Pre-malignant EpdSCs are serine auxotrophs. a, b, Gas chromatography-mass spectrometry (GC-MS) of conditioned medium relative to control medium NEAA indicates non-essential amino acids that are consumed. **c,** 4 hour fractional labeling of intracellular serine from [U-^{13}C]serine. **d,** GC-MS of intracellular serine pools following 16 hours of ser/gly starvation. **e, f,** Growth during 48 hours of ser/gly starvation. **g,** Growth during 48 hours in indicated medium.

In addition to extracellular consumption, cells can derive serine either from SHMT1/2, or from the serine synthesis pathway (SSP), wherein glucose-derived 3-phosphoglycerate (3PG) is converted to serine through the sequential enzymes phosphoglycerate dehydrogenase (PHGDH), phosphoserine transaminase (PSAT1) and phosphoserine phosphatase (PSPH) (Fig. 2.3a). SOX2^{+} and WT cells exhibited comparable SHMT1/2 expression and Ser/Gly interconversion (Fig. 2.3b,c). Similarly, SOX2^{+} cells exhibited no defect in SSP enzyme expression upon Ser/Gly deprivation. However, labeling with [U-^{13}C]glucose revealed reduced glucose-derived serine synthesis in SOX2^{+} EpdSCs (Fig. 2.3d). Upon Ser/Gly starvation, WT cells derived the majority of their intracellular serine from glucose, while SOX2^{+} cells failed to do so (Fig. 2.3e). Thus, pre-malignant EpdSCs suppress glucose-dependent serine synthesis.

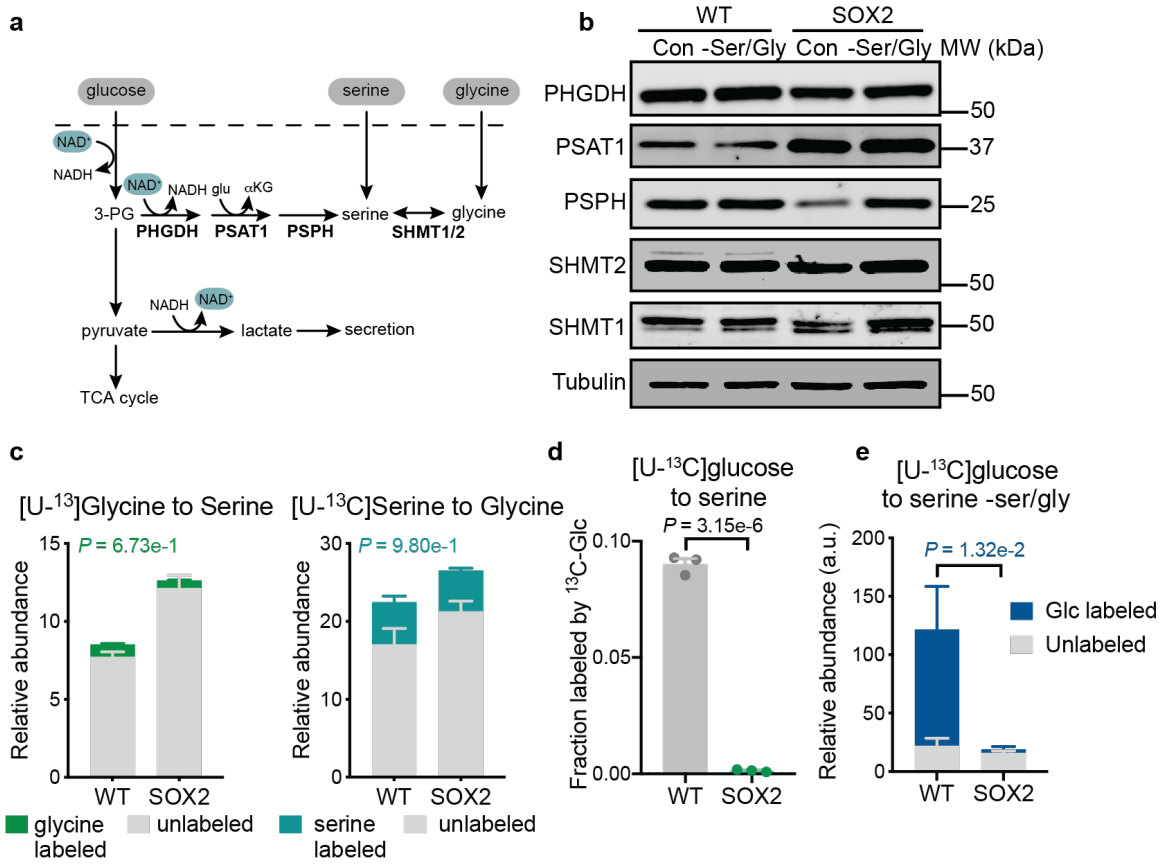

Fig. 2.3. Pre-malignant EpdSCs suppress glucose-derived serine synthesis. a, Schematic of intracellular serine sources. **b,** Western blot for enzymes that catalyze serine synthesis from either glucose or glycine following 24 hours of ser/gly starvation. **c,** 4 hour labeling of serine from glycine (left) or glycine from serine (right). **d,** 4 hour fractional labeling of serine from glucose. **e,** 4 hour labeling of serine from glucose following 16 hours of ser/gly starvation.

2.2.2 Limited cytosolic NAD+ regeneration drives serine auxotrophy

I next assessed why SOX2^{+} cells did not employ the SSP. Downstream of the serine precursor 3PG, the glycolytic end-product pyruvate can either be shunted to lactate or enter mitochondria to fuel the tricarboxylic acid (TCA) cycle. Pyruvate enters the TCA cycle either through pyruvate dehydrogenase (PDH) or pyruvate carboxylase (PC) to fuel citrate production (Fig. 2.4a).

Isotope tracing revealed that SOX2$^+$ cells increased glucose-derived citrate synthesis through both PDH and PC (Fig. 2.4b), indicating that pre-malignant EpdSCs were not generally defective in glucose metabolism. SOX2$^+$ cells demonstrated increased expression of pyruvate carboxylase (*Pcx*) and pyruvate dehydrogenase E1β (*Pdhb*) transcripts, suggesting a coordinated program favoring mitochondrial pyruvate consumption (Fig. 2.4c). I therefore asked whether increasing mitochondrial pyruvate metabolism conferred serine auxotrophy. Increasing pyruvate oxidation in WT EpdSCs with dichloroacetate (DCA)[144] induced serine auxotrophy (Fig. 2.4d). Conversely, blocking mitochondrial pyruvate import using UK-5099[145] conferred resistance to serine starvation (Fig. 2.4e). These results suggest that elevated mitochondrial pyruvate utilization can induce dependence on exogenous serine.

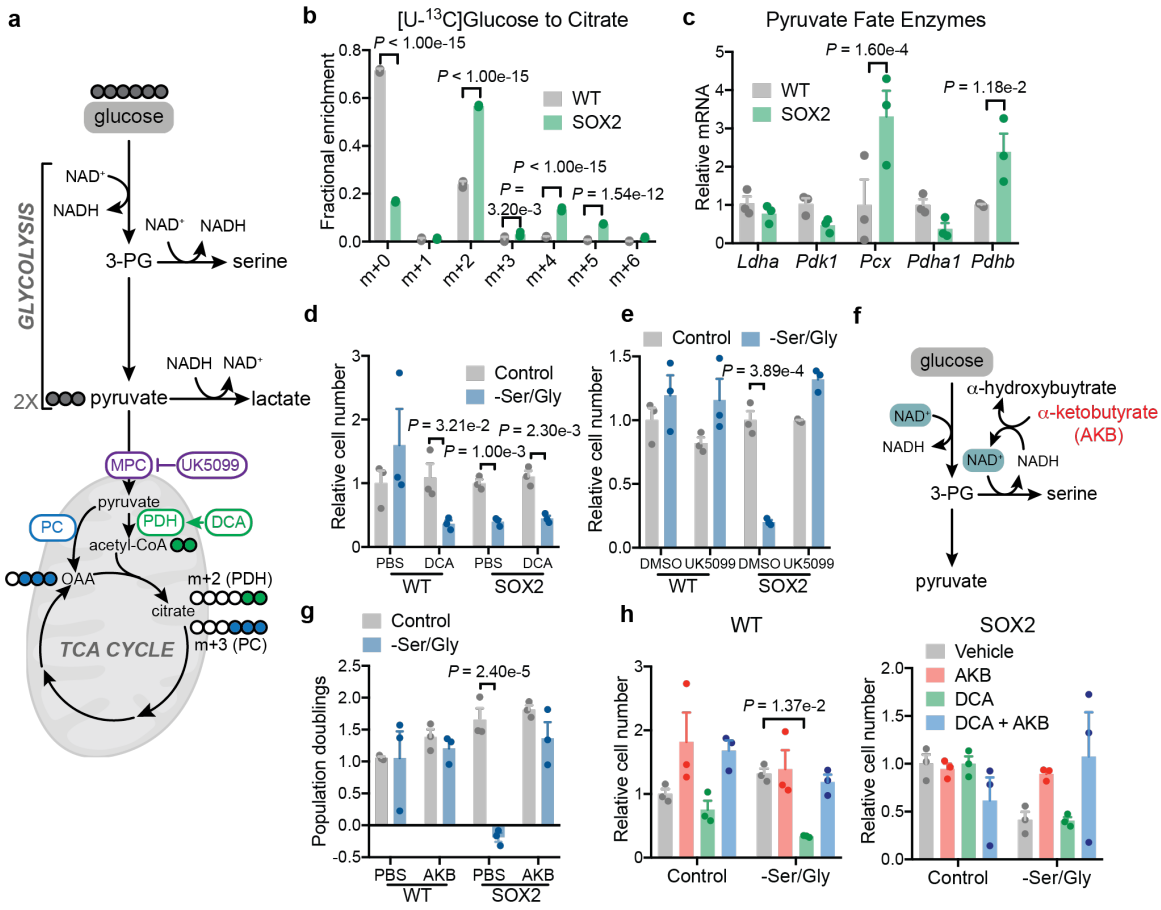

Fig. 2.4. Glucose oxidation drives serine auxotrophy. a, Schematic of glucose metabolism in glycolysis and the TCA cycle as well as associated inhibitors. **b,** 4 hour fractional labeling of citrate isotopologues from glucose. m+0 represents citrate that was not labeled by glucose, m+2 and m+3 represent PDH and PC derived citrate, respectively. Higher order (m+4, m+5, m+6) represent subsequent turns around the TCA cycle. **c,** qPCR for key pyruvate fate enzymes. **d-e,** Cell count following 48 hours of culture in indicated conditions. **f,** Mechanisms of action of AKB. **g,** Growth of cells during 48 hours of culture in indicated conditions. **h,** Cell count following 48 hours of culture in indicated conditions.

Once imported into mitochondria, pyruvate is no longer a substrate for cytosolic lactate dehydrogenase, which reduces pyruvate to lactate to regenerate oxidized NAD+ required for glycolysis. As NAD+ is also a cofactor for the rate-limiting SSP enzyme PHGDH[146], I hypothesized that enhanced mitochondrial pyruvate metabolism of SOX2$^+$ cells limits cytosolic NAD+ regeneration, thereby impairing the SSP. Consistent with this hypothesis, α-ketobutyrate (AKB), an alternative LDH substrate that enables NAD+ regeneration[147] rescued serine

auxotrophy in both $SOX2^+$ and DCA-exposed WT cells (Fig. 2.4f-h). Furthermore, the pyruvate/lactate ratio, which varies in concert specifically with the cytosolic NAD+/NADH ratio[148,149], was lower in $SOX2^+$ cells compared to WT cells (Fig. 2.5a,b). Supplementing pyruvate to increase the NAD+/NADH ratio[147,150] supported increased lactate secretion and rescued serine auxotrophy in $SOX2^+$ cells (Fig. 2.5c-e). Conversely, lowering the NAD+/NADH ratio with lactate supplementation induced auxotrophy in WT EpdSCs (Fig. 2.5e).

Genetic interventions to manipulate the NAD+/NADH ratio produced similar results. Expression of LbNOX, a bacterial NADH oxidase[148], increased the whole-cell NAD+/NADH ratio, increased [U-^{13}C]glucose labeling of serine, and rescued serine auxotrophy of both $SOX2^+$ cells and lactate-treated WT cells (Fig. 2.5f-j). Collectively, these findings indicate that cytosolic NAD+ regeneration controls serine biosynthesis in EpdSCs.

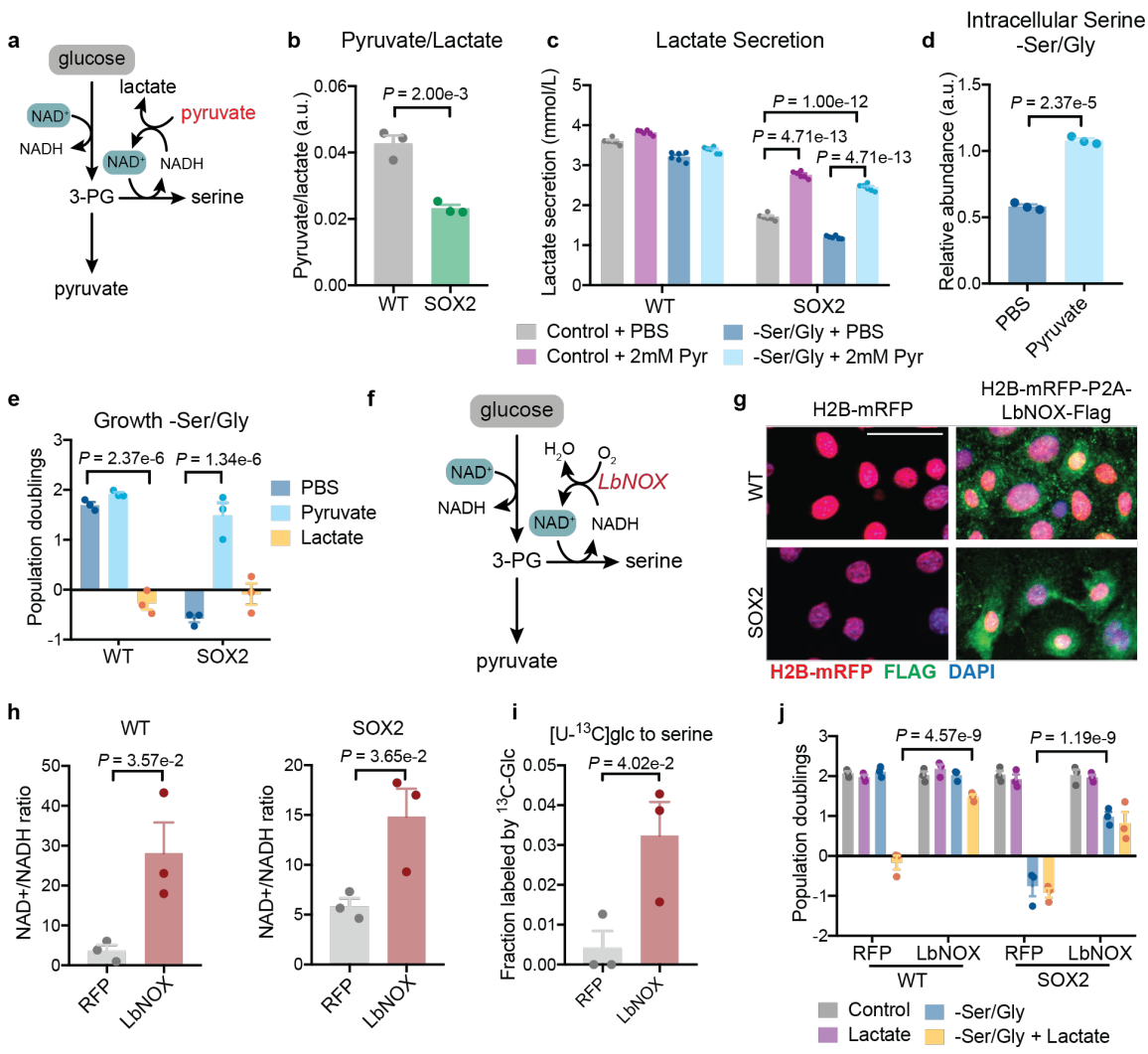

Fig. 2.5 Cytosolic NAD+ Regeneration Dictates Serine Auxotrophy. a, Schematic of pyruvate mechanism of action. **b,** GC-MS quantifaction of the pyruvate/lactate ratio. **c,** Lactate secretion during 24 hours of culture in indicated medium. **d,** Intracellular serine pools in SOX2^{+} cells following 16 hours in indicated medium. **e,** Growth during 48 hours of culture in indicated medium. **f,** Mechanism of action of LbNOX. **g,** Immunofluorescence validating expression of LbNOX. **h,** Quantification of whole cell NAD+/NADH ratio. **i,** 4 hour fractional labeling of serine in SOX2^{+} cells following 16 hours of ser/gly starvation. **j,** Growth during 48 hours of culture in indicated medium.

2.2.3. Serine restriction induces differentiation of wild-type EpdSCs

My findings thus far demonstrate that serine auxotrophy distinguishes pre-malignant EpdSCs from their normal counterparts. To understand how serine availability affects EpdSC function *in vivo*, I assessed the effects of dietary Ser/Gly withdrawal[116,117] on EpdSC growth and

differentiation, which must be balanced to maintain homeostasis. I placed pregnant mice on a Ser/Gly-free diet (Fig. 2.6a) and analyzed littermate WT and $SOX2^+$ animals at P0. The diet neither induced apoptosis in either genotype, nor affected WT EpdSC proliferation; in contrast, Ser/Gly restriction impaired $SOX2^+$ EpdSC proliferation (Fig. 2.6b,c). This effect was likely cell autonomous, as culturing EpdSCs with low levels of Ser/Gly to mimic dietary restriction specifically slowed growth of $SOX2^+$ EpdSCs (Fig. 2.6d). Reduced proliferation of $SOX2^+$ EpdSCs in low Ser/Gly conditions was accompanied by a failure to induce the SSP and sustain intracellular serine pools (Fig. 2.6e,f). Similar to my *in vitro* findings, $SOX2^+$ EpdSC proliferation *in vivo* was rescued by enhancing NAD+ regeneration via *in utero* transduction of epidermal progenitors[151] with LbNOX (Fig. 2.6g).

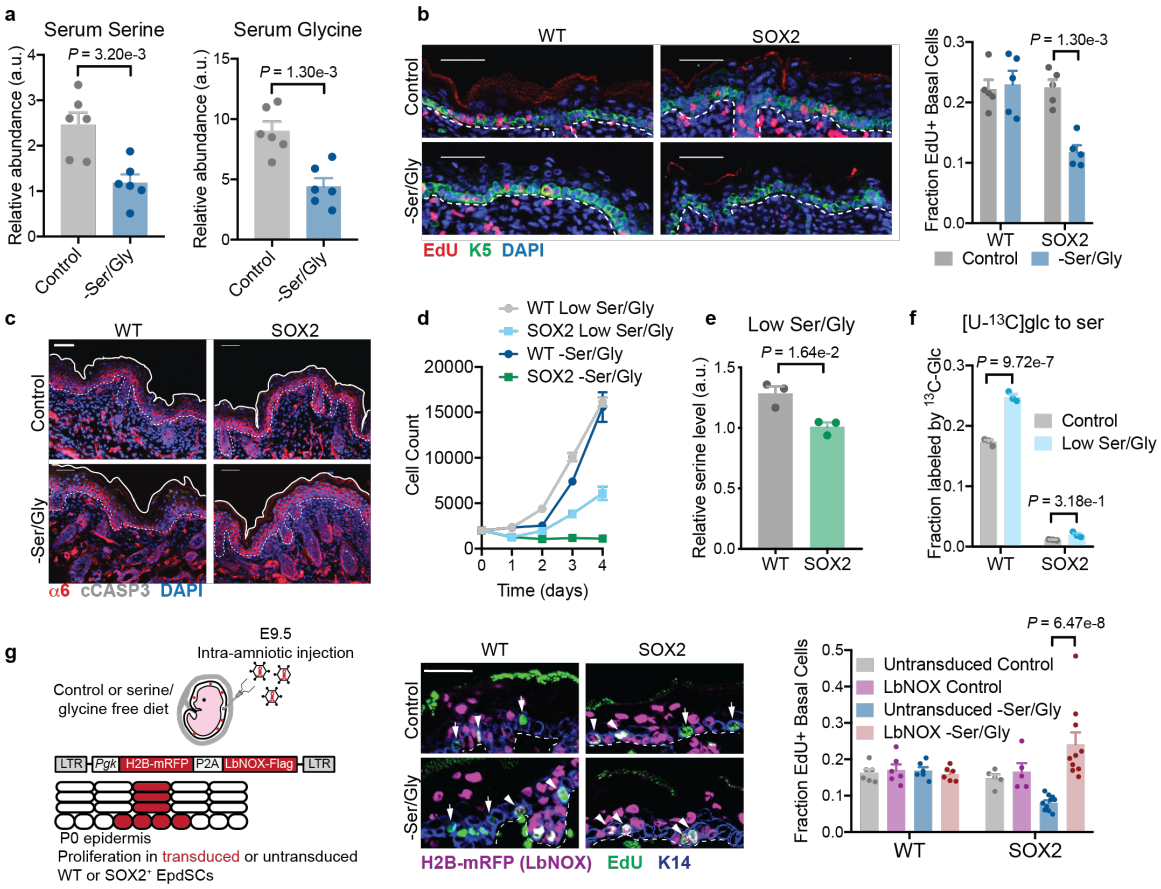

Fig. 2.6 Pre-malignant EpdSCs are *in vivo* serine auxotrophs. a, Serum serine and glycine levels of female mice maintained on a control or ser/gly free diet for 2 weeks. **b,** EdU incorporation in P0 mice on a control or ser/gly free diet. **c,** Immunofluorescence of cleaved caspase 3 in P0 mice on a control or ser/gly free diet. **d-f,** *In vitro* growth (**d**), intracellular serine pools (**e**) and 4 hr fractional labeling of serine from glucose (**f**) upon 50% reduction of extracellular ser/gly levels. **g,** Schematic (left) and analysis (right) of EdU incorporation in EpdSCs of mice transduced with LbNOX, comparing transduced and untransduced EpdSC proliferation in the same mice.

Notably, despite maintaining proliferation (Fig. 2.6), WT epidermis on a Ser/Gly-free diet displayed marked thickening of the differentiating layers, typified by expression of Involucrin and Keratin-10 (K10) (Fig. 2.7a). Epidermal differentiation is driven by asymmetric cell divisions of basal stem cells, in which the division axis of EpdSCs is perpendicular to the basement membrane, such that one daughter cell leaves the basal layer to generate a suprabasal cell committed to terminal differentiation[152]. Consistent with increased differentiation, epidermal thickening in WT

mice on a ser/gly free diet was accompanied by an increase in EpdSCs dividing perpendicularly to the basement membrane (Fig. 2.7b). To directly assess whether extracellular Ser/Gly starvation prompted EpdSCs to differentiate prematurely, I utilized a transgenic reporter mouse wherein the *Krt10* promoter drives H2B-mRFP, thereby marking induction of a terminal differentiation program[153]. Strikingly, Ser/Gly restriction significantly increased the proportion of prematurely-differentiated *Krt10*-H2B-mRFP^{+} EpdSCs (Fig. 2.7c). By contrast, SOX2^{+} EpdSCs maintained planar cell divisions and showed no increase in differentiation (Fig. 2.7b,c).

To determine whether the effect of Ser/Gly depletion on differentiation was cell-autonomous, I measured SC (*Krt14* and *Krt5*) and differentiation (*Lor* and *Flg*) gene expression *in vitro*. Consistent with our *in vivo* results, Ser/Gly depletion repressed *Krt14/K5* and increased *Lor/Flg* expression specifically in WT EpdSCs (Fig. 2.7d). Partial Ser/Gly restriction and serine starvation alone yielded similar results (Fig. 2.7e,f). Collectively, these data suggest that Ser/Gly availability regulates the balance between EpdSC growth and differentiation, and that oncogenic EpdSCs are resistant to Ser/Gly deprivation-induced differentiation.

Fig 2.7 Serine starvation drives WT EpdSC differentiation. a, Thickness of terminally differentiated cell layers of P0 mice. **b,** Representative classes (left) and quantification (right) of cell division angles of P0 mice based on the angle of the midbody marker Survivin relative to the basement membrane. SB = suprabasal. **c,** Quantification of the differentiation reporter *Krt10-H2B-mRFP* in P0 mice. **d,** qPCR of key stem cell and differentiation genes following 24 hours of ser/gly starvation *in vitro*. **e-f,** Immunofluorescence (**e**) and quantification (**f**) of the stem cell marker K14 following 24 hours of culture in indicated condition. **g,** Immunofluorescence and quantification of the stem cell marker following 24 hours of culture in indicated condition.

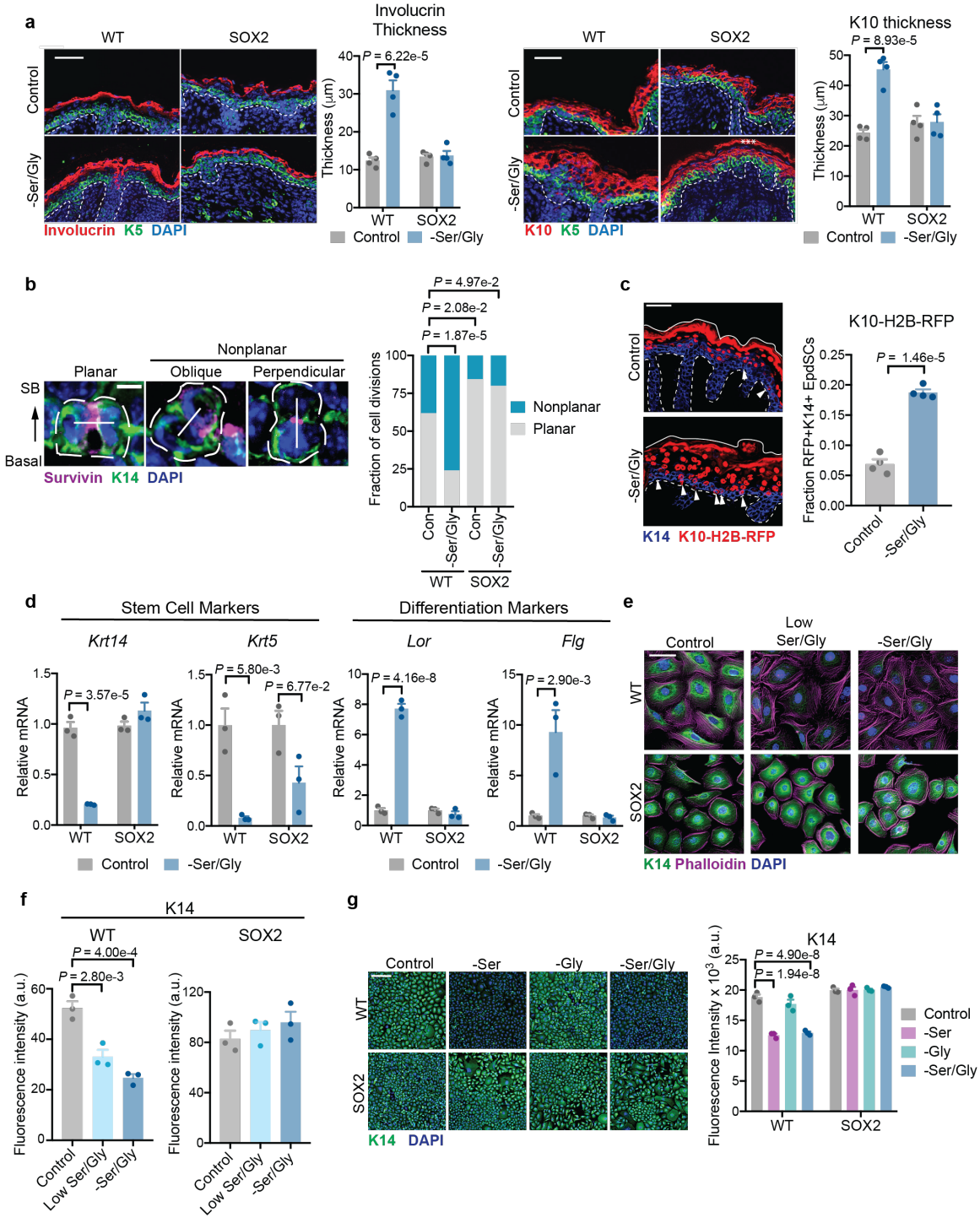
a
WT
SOX2
Control
-Ser/Gly
Involucrin K5 DAPI
Involucrin Thickness
P = 6.22e-5
Thickness (μm)
WT
SOX2
Control
-Ser/Gly
K10 K5 DAPI
K10 thickness
P = 8.93e-5
b
Nonplanar
Planar
Oblique
Perpendicular
SB
Basal
Survivin K14 DAPI
P = 4.97e-2
P = 2.08e-2
P = 1.87e-5
Fraction of cell divisions
Nonplanar
Planar
Con
-Ser/Gly
c
Control
-Ser/Gly
K14 K10-H2B-RFP
K10-H2B-RFP
P = 1.46e-5
Fraction RFP+K14+ EpdSCs
d
Stem Cell Markers
Differentiation Markers
Krt14
Krt5
Lor
Flg
Relative mRNA
P = 3.57e-5
P = 5.80e-3
P = 6.77e-2
P = 4.16e-8
P = 2.90e-3
e
Control
Low Ser/Gly
-Ser/Gly
WT
SOX2
K14 Phalloidin DAPI
f
K14
WT
SOX2
P = 4.00e-4
P = 2.80e-3
Fluorescence intensity (a.u.)
Control
Low Ser/Gly
-Ser/Gly
g
Control
-Ser
-Gly
-Ser/Gly
K14 DAPI
K14
P = 4.90e-8
P = 1.94e-8
Fluorescence Intensity x 10³ (a.u.)

2.2.4. *De novo* serine synthesis in EpdSCs promotes α-ketoglutarate-dependent differentiation

A priori, differentiation could be due to either serine depletion *per se* or induction of the SSP via one of its byproducts, NADH or α-ketoglutarate (αKG) (Fig. 2.8a). To uncouple these possibilities, I knocked down *Phgdh*, the first SSP enzyme. *Phgdh* suppression blocked precocious differentiation induced by serine restriction, suggesting that SSP flux, rather than serine depletion, drives epidermal differentiation (Fig. 2.8b-e).

I next asked which byproduct of the SSP promoted precocious differentiation. NADH seemed unlikely, as interventions that favor NADH oxidation (either AKB or UK5099), promoted, rather than inhibited, differentiation (Fig. 2.8f). By contrast, exogenous cell-permeable αKG was sufficient to induce differentiation in both WT and $SOX2^+$ EpdSCs (Fig. 2.9a). Moreover, αKG restored differentiation in *Phgdh*-deficient WT EpdSCs, underscoring its ability to trigger the consequences of SSP activation (Fig. 2.8d,e).

Indeed, Ser/Gly starvation of WT EpdSCs led to accumulation of αKG (Fig. 2.9b). Importantly, *Phgdh* silencing blunted αKG accumulation following Ser/Gly restriction (Fig. 2.9c). Many reactions can generate αKG from glutamine[107]. Based on calculations of serine and glutamine uptake in WT EpdSCs, I estimated that approximately 10% of consumed glutamine is used to sustain serine synthesis during Ser/Gly deprivation (Appendix Table 2.1-2.2).

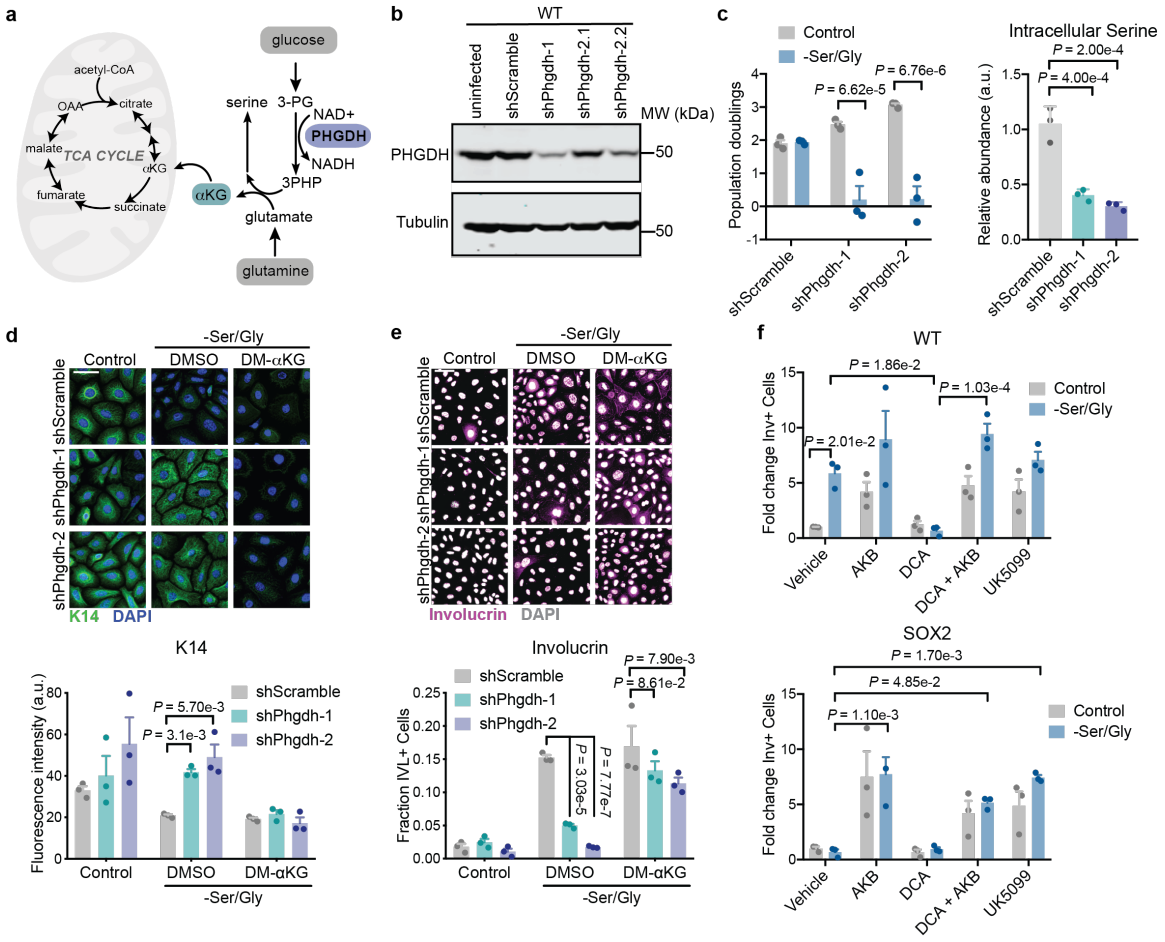

Fig 2.8 Glucose-derived serine synthesis drives αKG dependent differentiation. a, Schematic of serine biosynthesis and its by-products. **b,** Western blot validating knockdown of PHGDH in WT EpdSCs expressing either shScramble or sh*Phgdh* hairpins. sh*Phgdh*-1 and sh*Phgdh*-2.2 were used for subsequent experiments. **c,** Validation of sh*Phgdh* lines via proliferation (left) and GC-MS of intracellular serine pools (right) upon ser/gly starvation. **d,** Immunofluorescence (top) and quantification (bottom) of the stem cell marker K14 cultured in indicated conditions for 24 hours. **e,** Immunofluorescence (top) and quantification (bottom) of the differentiation marker Involucrin in indicated conditions for 24 hours. **f,** Quantification of Involucrin staining in WT (top) or SOX2^{+} (bottom) EpdSCs following culture in indicated conditions for 24 hours.

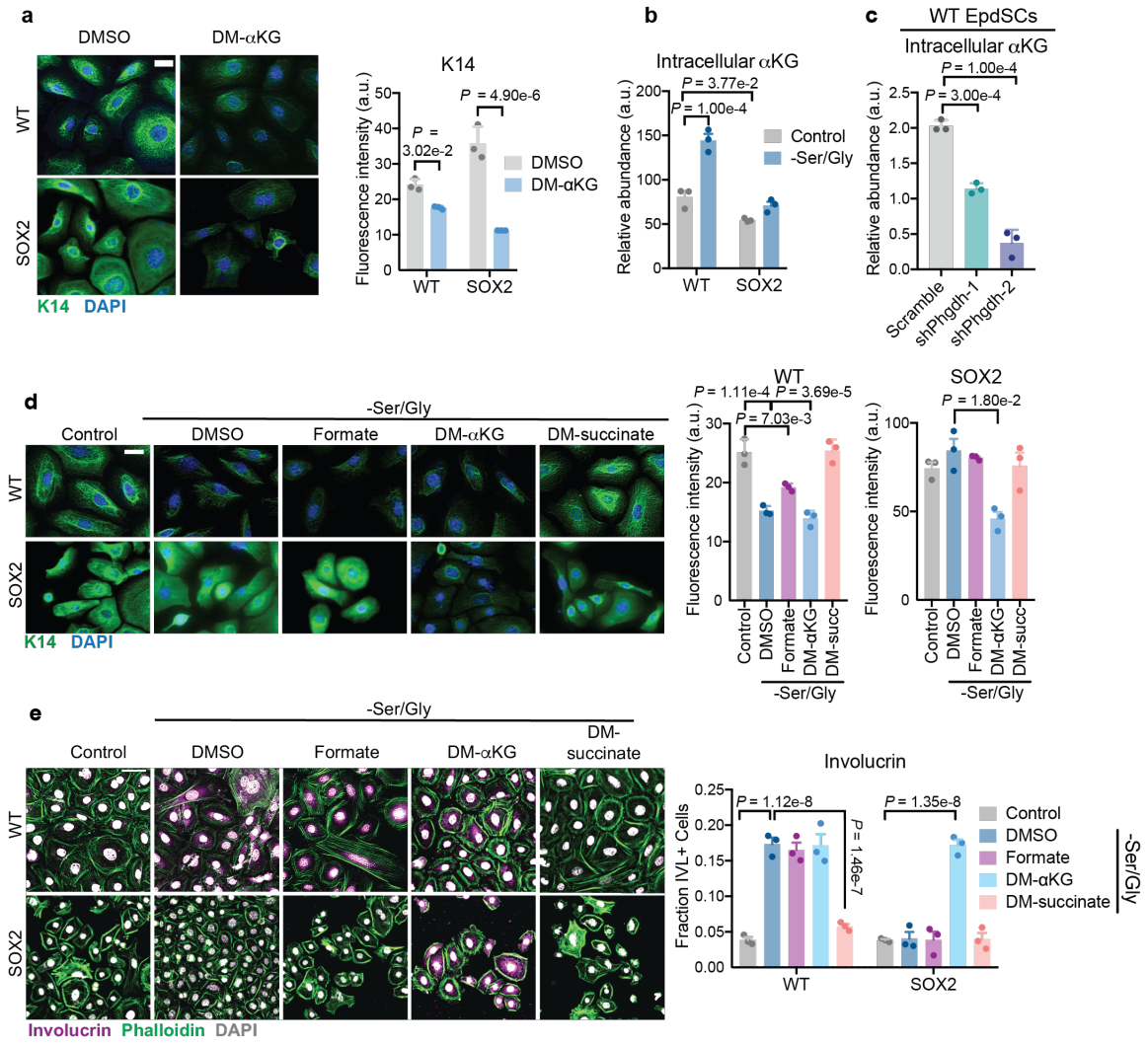

Fig 2.9 αKG is necessary and sufficient for ser/gly starvation induced differentiation. a, Immunofluorescence of K14 expression in cells cultured with dimethyl (DM)-αKG for 24 hours. **b-c**, GC-MS of intracellular αKG following 16 hours of culture. **d-e**, Immunofluorescence and analysis of K14 (**d**) or Involucrin (**e**) in cells cultured with 1 mM of the one carbon donor formate, 4 mM DM-αKG, or 4 mM DM-succinate for 24 hours.

Interestingly, αKG also affected SOX2$^+$ EpdSCs (Fig. 2.9a), indicating that they are not generally defective for differentiation. SOX2$^+$ EpdSCs exhibited reduced levels of αKG under both control and -Ser/Gly conditions (Fig. 2.9b), consistent with impaired SSP activity. Therefore, I asked whether rescuing αKG levels in these cells could restore differentiation. Indeed, αKG reversed the differentiation block of Ser/Gly-starved SOX2$^+$ EpdSCs (Fig. 2.9d,e). The ability of

αKG to restore differentiation was not merely due to its role as an anaplerotic substrate for the TCA cycle downstream of the SSP[154], since cell-permeable succinate, another TCA cycle intermediated, did not induce differentiation (Fig. 2.9d,e).

In addition to serving as a substrate for the TCA cycle, αKG is also a co-substrate for a large family of dioxygenases that consume αKG and produce succinate as part of their reaction cycle[8]. Succinate, a competitive inhibitor of these enzymes[8], was sufficient to block differentiation induced by Ser/Gly deprivation (Fig. 2.9d,e). Therefore, I hypothesized that Ser/Gly deprivation induced differentiation by activating αKG-dependent dioxygenases. Metabolic regulation of αKG-dependent dioxygenases, including the Jumonji-domain family of histone demethylases, has been implicated in chromatin regulation and cell fate decisions[8,21]. In the skin, trimethylation of histone 3 lysine 27 (H3K27me3) represses terminal differentiation gene expression. Accordingly, EpdSC differentiation is accelerated by conditional loss of *Ezh2,* an H3K27 methyltransferase, and inhibited by loss of the αKG-dependent H3K27me3 demethylase *JMJD3*[155,156].

Culturing EpdSCs with cell-permeable αKG revealed that H3K27me3 levels are sensitive to intracellular αKG levels (Fig. 2.10a). I therefore posited that serine biosynthesis might favor αKG-dependent H3K27me3 demethylation, and hence differentiation. Indeed when WT EpdSCs were starved for Ser/Gly or serine alone, H3K27me3 levels decreased (Fig. 2.10b-e). H3K27me3 loss was *Phgdh*-dependent, and αKG reversed the effects of *Phgdh* silencing (Fig. 2.10f).

Fig 2.10 Serine synthesis drives αKG-dependent histone demethylation. a, H3K27me3 levels in cells cultured with 4mM DM-αKG for 24 hours. **b,** H3K27me3 levels in EpdSCs of P0 mice. **c-d,** H3K27me3 levels in cells cultured for 24 hours in the indicated medium. **e,** H3K27me3 levels in shScramble or sh*Phgdh* WT EpdSCs cultured in the indicated medium with or without 4 mM DM-αKG for 24 hours. **f,** H3K27me3 levels in cells cultured in indicated medium with or without 1 mM formate, 4 mM DM-αKG, or 4 mM DM-succinate for 24 hours.

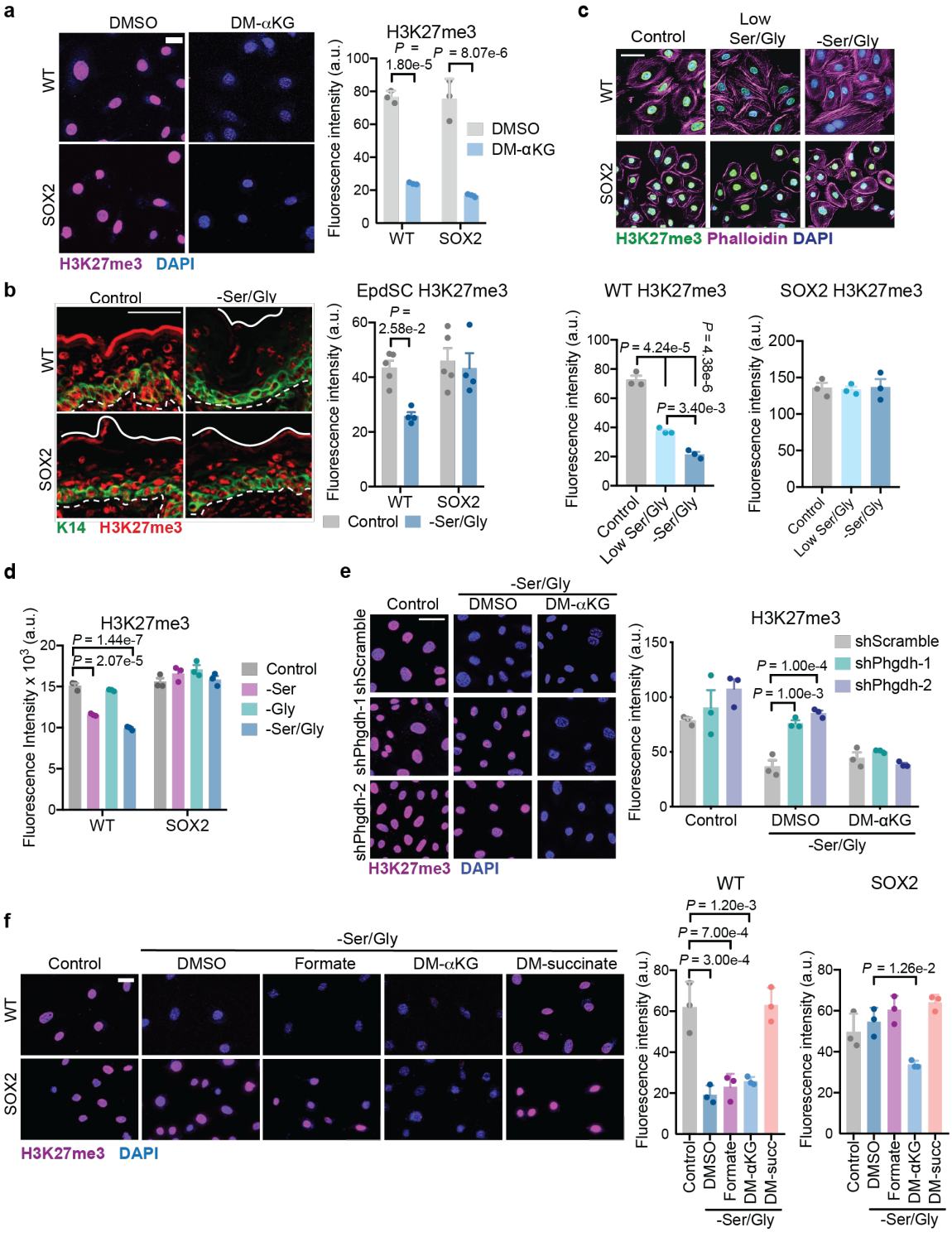
a
DMSO
DM-αKG
WT
SOX2
H3K27me3 DAPI
H3K27me3
P = 1.80e-5
P = 8.07e-6
Fluorescence intensity (a.u.)
DMSO
DM-αKG
WT
SOX2
c
Control
Low Ser/Gly
-Ser/Gly
H3K27me3 Phalloidin DAPI
b
Control
-Ser/Gly
K14 H3K27me3
EpdSC H3K27me3
P = 2.58e-2
Control
-Ser/Gly
WT H3K27me3
P = 4.24e-5
P = 4.38e-6
P = 3.40e-3
SOX2 H3K27me3
d
H3K27me3
P = 1.44e-7
P = 2.07e-5
Fluorescence Intensity x 10^3 (a.u.)
Control
-Ser
-Gly
-Ser/Gly
e
-Ser/Gly
Control
DMSO
DM-αKG
shScramble
shPhgdh-1
shPhgdh-2
H3K27me3 DAPI
H3K27me3
P = 1.00e-4
P = 1.00e-3
shScramble
shPhgdh-1
shPhgdh-2
f
-Ser/Gly
Control
DMSO
Formate
DM-αKG
DM-succinate
H3K27me3 DAPI
WT
SOX2
P = 1.20e-3
P = 7.00e-4
P = 3.00e-4
P = 1.26e-2
Control
DMSO
Formate
DM-αKG
DM-succ
-Ser/Gly

To directly test the role of H3K27me3 in differentiation induced by Ser/Gly starvation, I utilized inhibitors against JMJD3 (GSK-J4) and EZH2 (GSK-343) to block H3K27me3 demethlyation or methylation, respectively. GSK-J4 prevented H3K27me3 loss and differentiation induced by Ser/Gly starvation in WT EpdSCs. Conversely, GSK-343 suppressed H3K27me3 in both WT and $SOX2^+$ EpdSCs and promoted differentiation (Fig. 2.11).

Ser/Gly starvation can exert pleiotropic cellular effects, including depletion of one-carbon units that contribute to methylation reactions[157] and increased oxidative stress that can drive epidermal differentiation[117,158]. However, one-carbon units did not appear to be limiting, since supplying exogenous formate did not rescue H3K27me3 or differentiation (Fig. 2.9e,f, 2.10f). Likewise, while antioxidants blocked differentiation, consistent with known roles of ROS in differentiation[158], they neither affected H3K27me3 nor protected against differentiation upon EZH2 inhibition (Fig. 2.11). In contrast, cell-permeable αKG promoted H3K27me3 demethylation and differentiation in $SOX2^+$ cells, and cell-permeable succinate suppressed differentiation and H3K27me3 loss in WT EpdSCs (Fig. 2.9d,e, 2.10f)

Fig 2.11 Ser/Gly induced differentiation is driven by H3K27me3 demethylation. a, b, Immunofluorescence (**a**) and quantification (**b**) of H3K27me3 and K14 in cells cultured in indicated medium for 24 hours with the antioxidants esterified reduced glutathione (eGSH) or the vitamin E analog Trolox, the EZH2 inhibitor GSK343 or the JMJD3/UTX inhibitor GSKJ4. **c, d**, Immunuofluorescence (**c**) and quantification (**d**) of H3K27me3 and K14 in cells cultured for 24 hours in indicated medium with GSH, GSK343, or both.

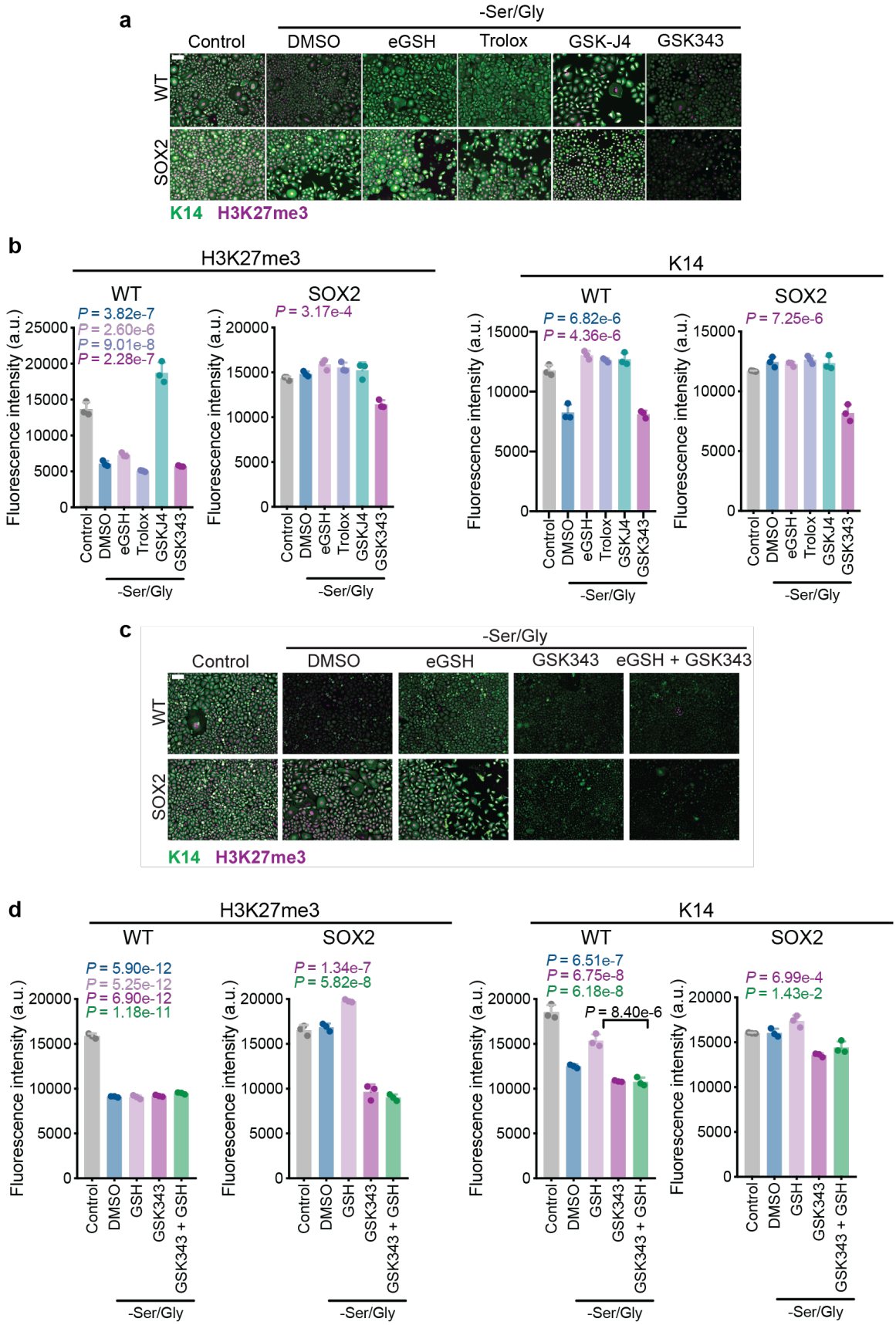
a
-Ser/Gly
Control
DMSO
eGSH
Trolox
GSK-J4
GSK343
WT
SOX2
K14 H3K27me3
b
H3K27me3
K14
WT
SOX2
Fluorescence intensity (a.u.)
P = 3.82e-7
P = 2.60e-6
P = 9.01e-8
P = 2.28e-7
P = 3.17e-4
P = 6.82e-6
P = 4.36e-6
P = 7.25e-6
Control
DMSO
eGSH
Trolox
GSKJ4
GSK343
-Ser/Gly
c
-Ser/Gly
Control
DMSO
eGSH
GSK343
eGSH + GSK343
WT
SOX2
K14 H3K27me3
d
H3K27me3
K14
WT
SOX2
Fluorescence intensity (a.u.)
P = 5.90e-12
P = 5.25e-12
P = 6.90e-12
P = 1.18e-11
P = 1.34e-7
P = 5.82e-8
P = 6.51e-7
P = 6.75e-8
P = 6.18e-8
P = 8.40e-6
P = 6.99e-4
P = 1.43e-2
Control
DMSO
GSH
GSK343
GSK343 + GSH
-Ser/Gly

Taken together, our data suggest that endogenous serine synthesis poises EpdSCs to differentiate by facilitating H3K27me3 demethylation, although additional αKG-dependent dioxygenases may contribute to epidermal differentiation. Moreover, SSP suppression enables pre-malignant EpdSCs to escape differentiation and enforce self-renewal.

2.2.5. Ser/Gly starvation impairs tumor initiation and growth

The finding that Ser/Gly starvation induced differentiation led us to posit that Ser/Gly deprivation might impair tumor initiation. To investigate this possibility, I placed mice on a Ser/Gly-free diet prior to administration of a classical chemical carcinogenesis protocol, in which mice are administered a single dose of 7,12-dimethylbenz[a]anthracene (DMBA) followed by twice weekly 12-O-tetradecanoylphorbol-13-acetate (TPA), that leads to initiation of EpdSC-derived benign papillomas and malignant SCCs[159] (Fig. 2.12a). Compared to a control diet, Ser/Gly starvation significantly impaired tumor initiation and reduced tumor burden (Fig. 2.12b). Similar results were obtained upon orthotopic injection of established SCCs into immunocompromised (*Nude*) mice (Fig. 2.12c).

Tumor growth under dietary Ser/Gly starvation requires enhanced SSP activity[17,116]. Based upon our data, I hypothesized that SSP activation might also

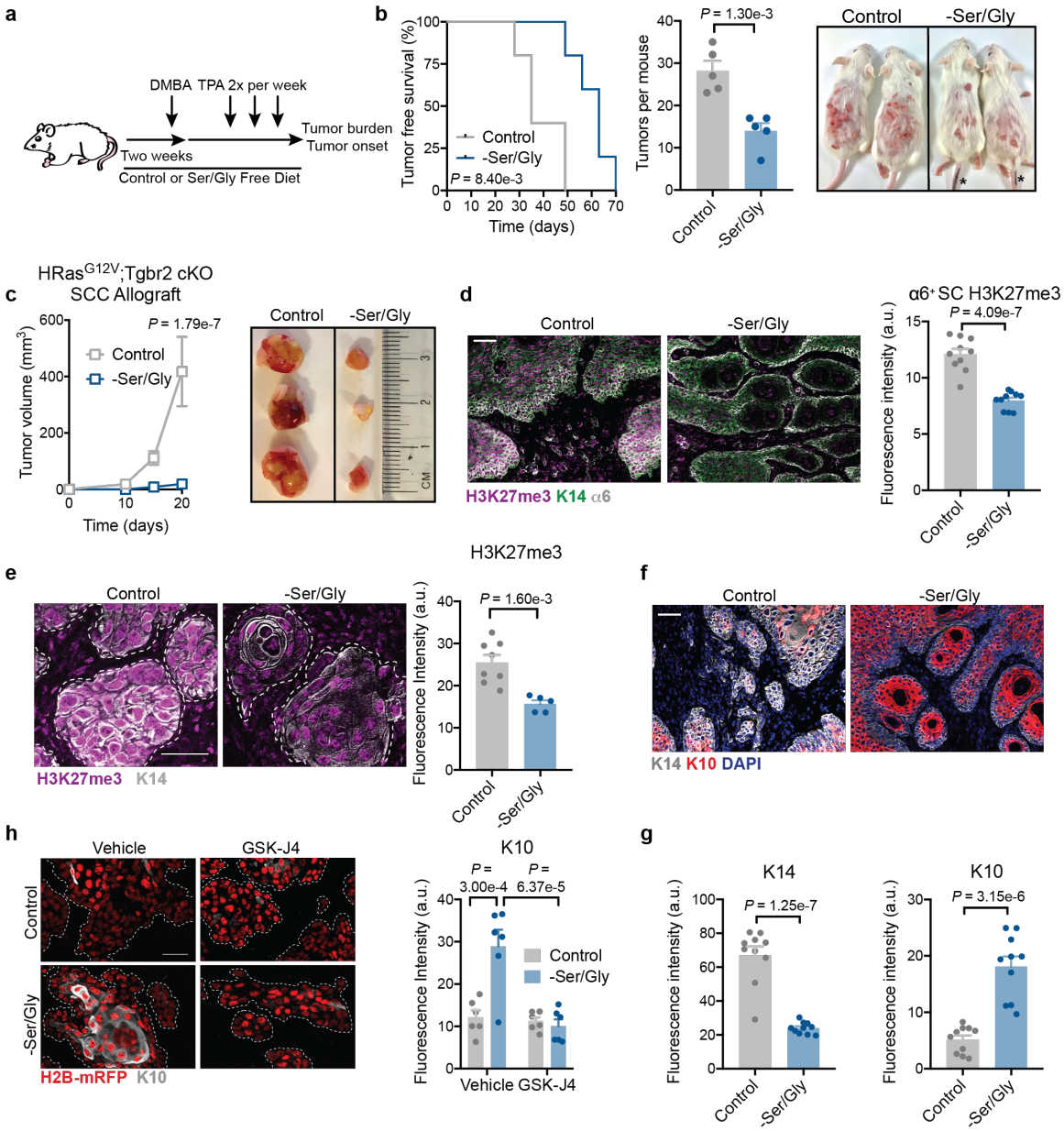

Fig 2.12 Dietary ser/gly restriction impairs tumor initiation and growth. a, Schematic of DMBA/TPA model of SCC initiation. **b,** Tumor free survival curve (left), tumor burden (center) and representative mice (right) in DMBA/TPA treated mice. **c,** Tumor growth of established SCCs injected intradermally. **d-e**, H3K27me3 levels in DMBA/TPA (**d**) and established SCC allografts (**e**). **f-g**, K14 and K10 staining (**f**) and quantification (**g**) in DMBA/TPA induced tumors. **h,** K10 staining in SCC allografts grown in mice treated with GSK-J4.

represent a liability for SCCs by driving differentiation. Indeed, tumors that formed under the selective pressure of Ser/Gly restriction exhibited reduced H3K27me3 and enhanced

differentiation, typified by reduced K14 and increased K10 staining, relative to controls (Fig. 2.12d-g). Pharmacologically inhibiting αKG-dependent H3K27me3 demethylases[160] prevented starvation-induced differentiation (Fig 2.12g).

Ser/Gly starvation also induced differentiation, H3K27me3 loss, and growth suppression in xenografts of human A431 and SCC9 lines (2.13a-f). Finally, analysis of 139 different cutaneous and head and neck human SCCs revealed that H3K27me3 levels correlated with SCC grade (Fig. 2.13g). Thus, my findings identify a strong link between Ser/Gly availability, H3K27me3 demethylation and tSC fate.

Fig 2.13 Human SCCs are sensitive to ser/gly restriction. a-c, K14/K10 staining (**a**), H3K27me3 staining (**b**) and growth (**c**) in A431 SCC xenografts. **d-f**, K14/K10 staining (**d**), H3K27me3 staining (**e**), and growth (**f**) in SCC9 SCC xenografts. **g,** Correlation of H3K27me3 IHC with histopathological tumor grade in cutaneous SCCs (cSCC) and head and neck SCCs (HNSCC).

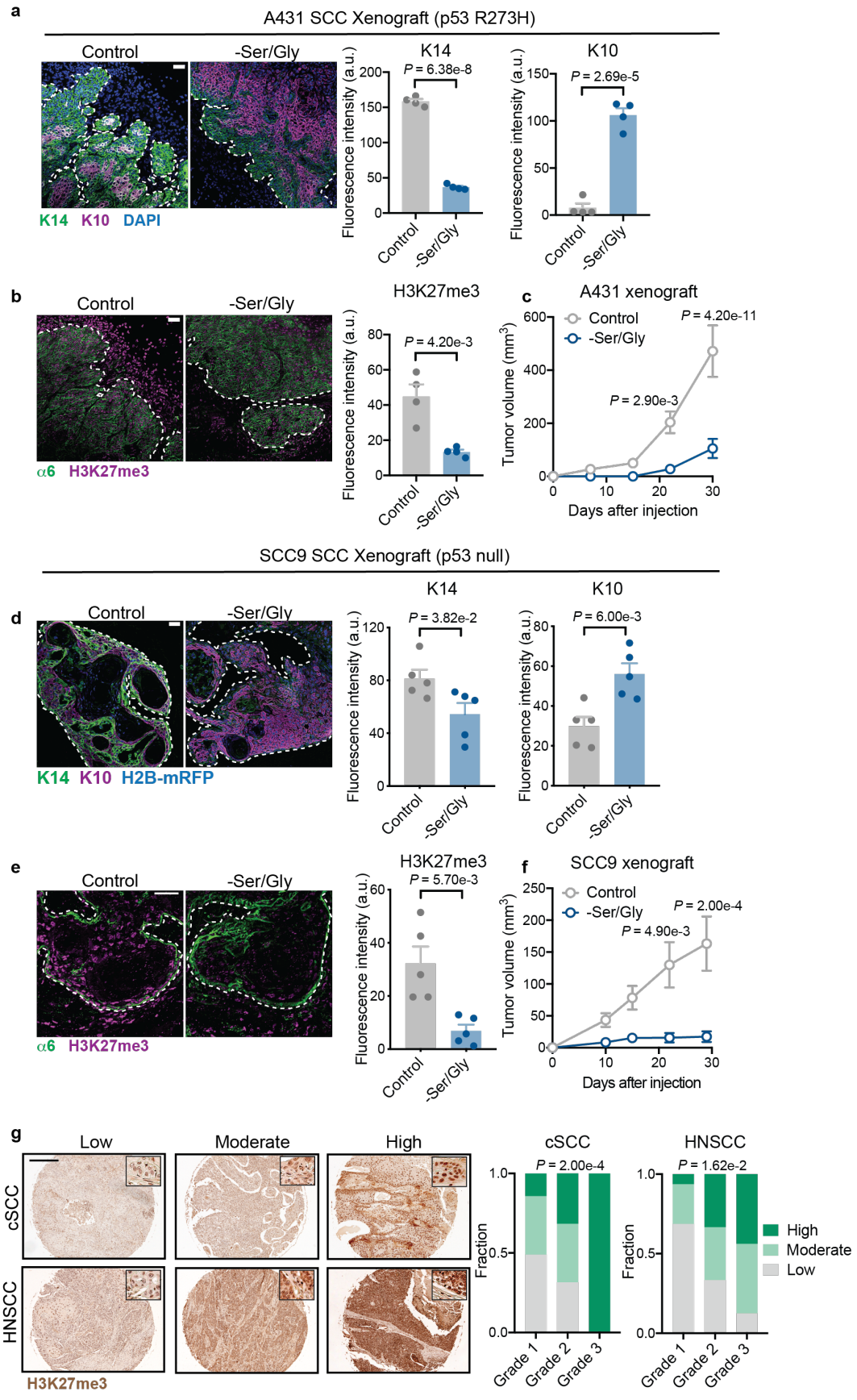
a
A431 SCC Xenograft (p53 R273H)
Control
-Ser/Gly
K14 K10 DAPI
K14
P = 6.38e-8
Fluorescence intensity (a.u.)
K10
P = 2.69e-5
b
H3K27me3
P = 4.20e-3
α6 H3K27me3
c
A431 xenograft
Control
-Ser/Gly
P = 4.20e-11
P = 2.90e-3
Tumor volume (mm3)
Days after injection
SCC9 SCC Xenograft (p53 null)
d
K14 K10 H2B-mRFP
P = 3.82e-2
P = 6.00e-3
e
H3K27me3
P = 5.70e-3
α6 H3K27me3
f
SCC9 xenograft
P = 2.00e-4
P = 4.90e-3
g
Low
Moderate
High
cSCC
HNSCC
H3K27me3
P = 2.00e-4
P = 1.62e-2
Fraction
Grade 1
Grade 2
Grade 3
High
Moderate
Low

2.2.6. Glucose-derived serine synthesis suppresses tumorigenesis and stemness

To determine whether the anti-tumor effects of Ser/Gly starvation are due to Ser/Gly starvation or SSP activation, I silenced *Phgdh* in SCCs (Fig. 2.14a,b). *In vivo*, *Phgdh* silencing prevented H3K27me3 loss upon Ser/Gly starvation (Fig. 2.14c). Consistent with driving differentiation, Ser/Gly starvation induced tSC depletion, as reflected by loss of cells expressing the tSC markers CD44 and SOX2. Silencing *Phgdh* expanded the tSC pool and prevented tSC loss upon dietary Ser/Gly starvation (Fig. 2.14d,e). Critically, SCC differentiation required an intact serine synthesis pathway, since *Phgdh* silencing blocked diet-induced differentiation, as assessed by K14/K10 staining (Fig. 2.14f,g).

These findings suggested that, in contrast to previous reports on melanoma and breast cancer[154,161], cell-autonomous SSP activation acts as a tumor suppressor in SCCs by driving SC depletion. Consistent with tSC expansion, sh*Phgdh* SCCs grew more rapidly than sh*Scramble* SCCs under normal growth conditions *in vivo* (Fig. 2.15a). Importantly, I could abrogate this advantage by putting *shPhgdh* SCCs on a Ser/Gly-free diet, which suppressed sh*Phgdh* SCC proliferation (Fig 2.15b,c). *Phgdh* ablation using CRISPR-Cas9 likewise enhanced tumor growth (Fig 2.15d-f). Together, these results underscore the advantage that SCC-SCs gain by silencing endogenous serine biosynthesis so long as exogenous serine is present to fulfill anabolic demands.

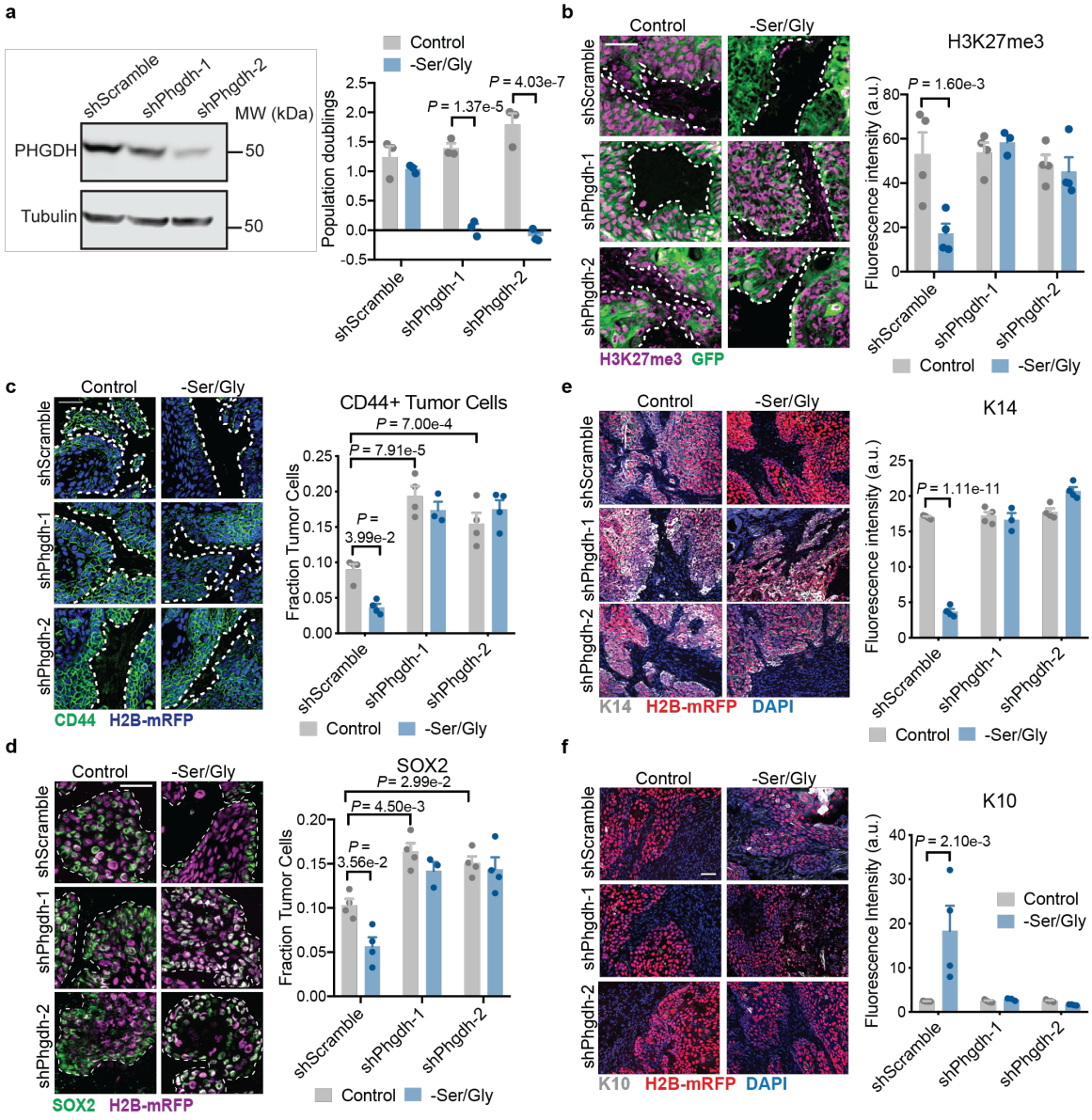

Fig 2.14 Glucose-derived serine synthesis suppresses SCC stem cell maintenance. a, Western blot (left) and growth during 48 hours of ser/gly starvation (right) of sh*Phgdh* mouse SCC lines. **b,** Immunofluorescence of H3K27me3 levels in sh*Phgdh* orthotopic allografts. **c-d**, Immunofluorescence of the stem cell markers CD44 (**c**) and SOX2 (**d**) in sh*Phgdh* orthotopic allografts. **e-f** Immunofluorescence of K14 (**e**) and K10 (**f**) in sh*Phgdh* orthotopic allografts.

Fig 2.15. Glucose derived serine synthesis suppresses tumorigenesis when extracellular serine is available. a, Growth of sh*Phgdh* orthotopic allografts on a control diet. **b-c**, Immunofluorescence (**b**) and analysis (**c**) of Ki67 staining, a marker of proliferation, in sh*Phgdh* allografts under control and ser/gly free diet conditions. **d,** Growth of sh*Phgdh* allografts under control and ser/gly free diet conditions. **e-f**, validation of PHGDH KO lines. sg*Phgdh* lines A1 and sg*Phgdh* C6 were used for subsequent experiments and are referred to as sg*Phgdh*-1 and sg*Phgdh*-6, respectively. **g,** Growth of sg*Phgdh* orthotopic allografts.

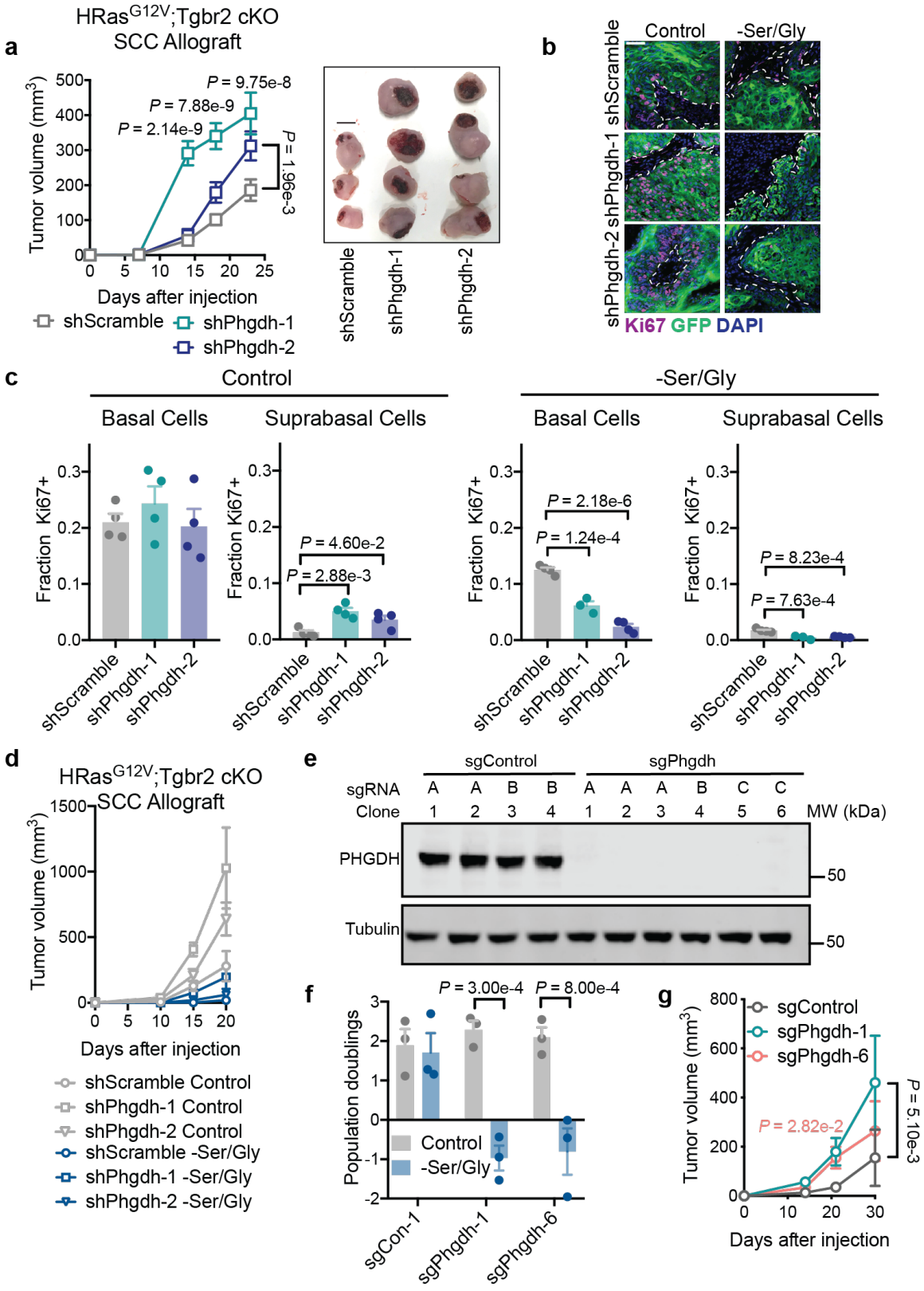
a
HRas^{G12V};Tgbr2 cKO
SCC Allograft
Tumor volume (mm^3)
P = 9.75e-8
P = 7.88e-9
P = 2.14e-9
P = 1.96e-3
Days after injection
shScramble
shPhgdh-1
shPhgdh-2
b
Control
-Ser/Gly
shScramble
shPhgdh-1
shPhgdh-2
Ki67 GFP DAPI
c
Control
-Ser/Gly
Basal Cells
Suprabasal Cells
Fraction Ki67+
P = 4.60e-2
P = 2.88e-3
P = 2.18e-6
P = 1.24e-4
P = 8.23e-4
P = 7.63e-4
d
HRas^{G12V};Tgbr2 cKO
SCC Allograft
Tumor volume (mm^3)
Days after injection
shScramble Control
shPhgdh-1 Control
shPhgdh-2 Control
shScramble -Ser/Gly
shPhgdh-1 -Ser/Gly
shPhgdh-2 -Ser/Gly
e
sgControl
sgPhgdh
sgRNA
Clone
MW (kDa)
PHGDH
Tubulin
50
f
P = 3.00e-4
P = 8.00e-4
Population doublings
Control
-Ser/Gly
sgCon-1
sgPhgdh-1
sgPhgdh-6
g
sgControl
sgPhgdh-1
sgPhgdh-6
P = 2.82e-2
P = 5.10e-3
Tumor volume (mm^3)
Days after injection

2.2.7. αKG drives tumor suppression and differentiation in SCCs

Our data suggest that by inducing the SSP, the consequential production of αKG can bias tSCs to differentiation and thereby suppress tumorigenesis. To directly test this model, I manipulated intracellular αKG and succinate by engineering SCC cells to silence either oxoglutarate dehydrogenase (*Ogdh*) which consumes αKG, or succinate dehydrogenase A (*Sdha*), which consumes succinate (Fig. 2.16a)[53]. As expected, intracellular αKG was increased in *shOgdh* lines while succinate was increased upon *Sdha* silencing (Fig. 2.16b).

While each hairpin reduced tumor growth on a normal diet, they had opposing effects upon Ser/Gly restriction (Fig. 2.16c). OGDH loss hampered SCC growth and was sufficient to drive H3K27me3 loss and tumor differentiation, as assessed by K14/K10 staining, even on a normal diet (Fig. 2.16d-f). This was not due to TCA cycle disruption, as SDHA loss failed to induce differentiation in control mice (Fig. 2.20e,f). Rather, SDHA silencing prevented both H3K27me3 loss and differentiation upon Ser/Gly restriction (Fig. 2.16d-f). As a result, *shSdha* tumors sustained growth in the absence of dietary Ser/Gly (Fig. 2.16c). Collectively, these findings are consistent with Ser/Gly starvation inducing activation of αKG-dependent dioxygenases that promote tumor suppressive differentiation programs.

Fig 2.16. αKG is necessary and sufficient for SCC differentiation. a, Schematic of the TCA cycle highlighting reactions catalyzed by OGDH and SDHA. **b,** GC-MS of intracellular αKG (left) and succinate (right) levels in sh*Renilla*, sh*Ogdh*, and sh*Sdha* SCC lines, verifying expected changes in metabolite abundance upon knockdown. **c,** Growth of indicated SCC lines injected orthotopically. **d,** H3K27me3 immunofluorescence of indicated SCC lines. **e-f**, Quantification (**e**) and immunofluorescence (**f**) of differentiation in indicated SCC lines, as assessed by K14/K10 staining.

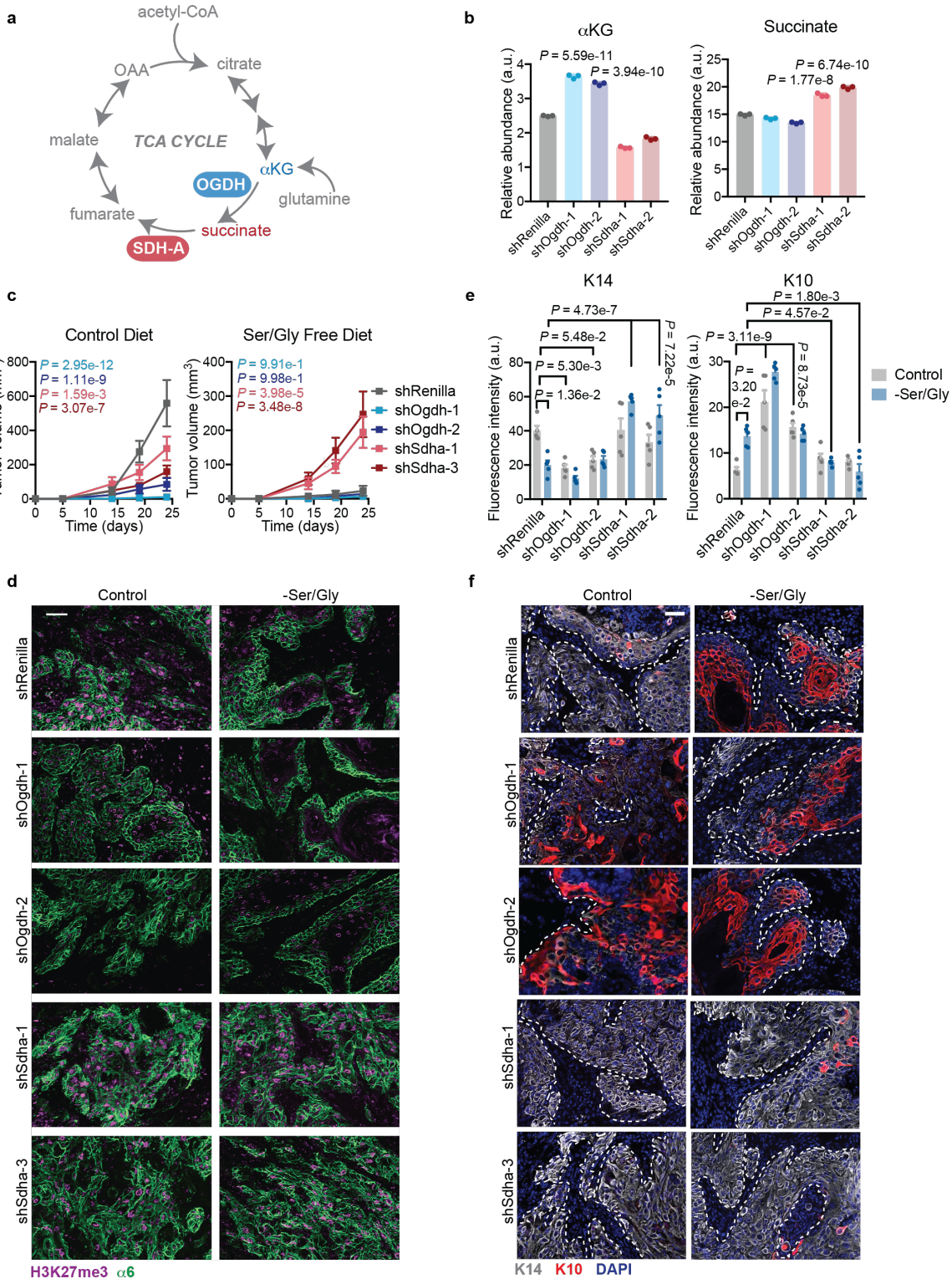
a
acetyl-CoA
citrate
OAA
malate
TCA CYCLE
αKG
OGDH
glutamine
fumarate
succinate
SDH-A
b
αKG
Succinate
Relative abundance (a.u.)
P = 5.59e-11
P = 3.94e-10
P = 6.74e-10
P = 1.77e-8
shRenilla
shOgdh-1
shOgdh-2
shSdha-1
shSdha-2
c
Control Diet
Ser/Gly Free Diet
Tumor volume (mm3)
Time (days)
P = 2.95e-12
P = 1.11e-9
P = 1.59e-3
P = 3.07e-7
P = 9.91e-1
P = 9.98e-1
P = 3.98e-5
P = 3.48e-8
shRenilla
shOgdh-1
shOgdh-2
shSdha-1
shSdha-3
e
K14
K10
Fluorescence intensity (a.u.)
P = 4.73e-7
P = 5.48e-2
P = 5.30e-3
P = 1.36e-2
P = 7.22e-5
P = 1.80e-3
P = 4.57e-2
P = 3.11e-9
P = 3.20 e-2
P = 8.73e-5
Control
-Ser/Gly
d
Control
-Ser/Gly
shRenilla
shOgdh-1
shOgdh-2
shSdha-1
shSdha-3
H3K27me3 α6
f
Control
-Ser/Gly
shRenilla
shOgdh-1
shOgdh-2
shSdha-1
shSdha-3
K14 K10 DAPI

2.3. DISCUSSION

In this study I discovered that environmental serine availability profoundly affects tumor initiation and SC fate. Pre-malignant EpdSCs that are destined to initiate tumors suppress *de novo* serine synthesis by increasing mitochondrial pyruvate consumption, resulting in endogenous serine auxotrophy. In WT EpdSCs, SSP activation facilitates αKG accumulation, which favors H3K27me3 demethylation and promotes terminal differentiation. The SSP also regulates SCC differentiation. In the presence of abundant serine, SSP inhibition triggered expansion of tSCs and promoted tumor growth. Conversely, enforcing serine synthesis using a Ser/Gly-free diet impaired tumor initiation in mice. Diet-mediated tumor suppression could be reversed by inhibiting αKG-dependent dioxygenases, underscoring αKG-dependent differentiation as a major route of tumor suppression. These findings are likely to have relevance to humans, since xenografts were sensitive to Ser/Gly starvation and H3K27me3 levels correlated positively with tumor grade in human SCCs. These results shed light on how SCs integrate nutrient availability with chromatin dynamics *in vivo* (Fig 2.17). This work was recently published in *Nature Cell Biology*[14].

Recent evidence supports my finding that NAD+ regeneration is limiting for serine biosynthesis[146]. Previous studies revealed that environmental or genetic manipulations that impose mitochondrial redox imbalances subsequently impair amino acid biosynthesis[146,147,150]. Here, I find that endogenous changes in central carbon metabolism, such as those found in $SOX2^{+}$ EpdSCs, similarly impair cytosolic NAD+ regeneration and amino acid biosynthesis. Collectively, these findings suggest that compartment-specific redox metabolism is likely to be an important regulator of cell fate decisions and nutrient stress responses. Although I cannot rule out the possibility that other mechanisms may restrict serine synthesis in pre-malignant EpdSCs, our data support a critical role for cytosolic NAD+ regeneration in regulating serine auxotrophy and EpdSC behavior.

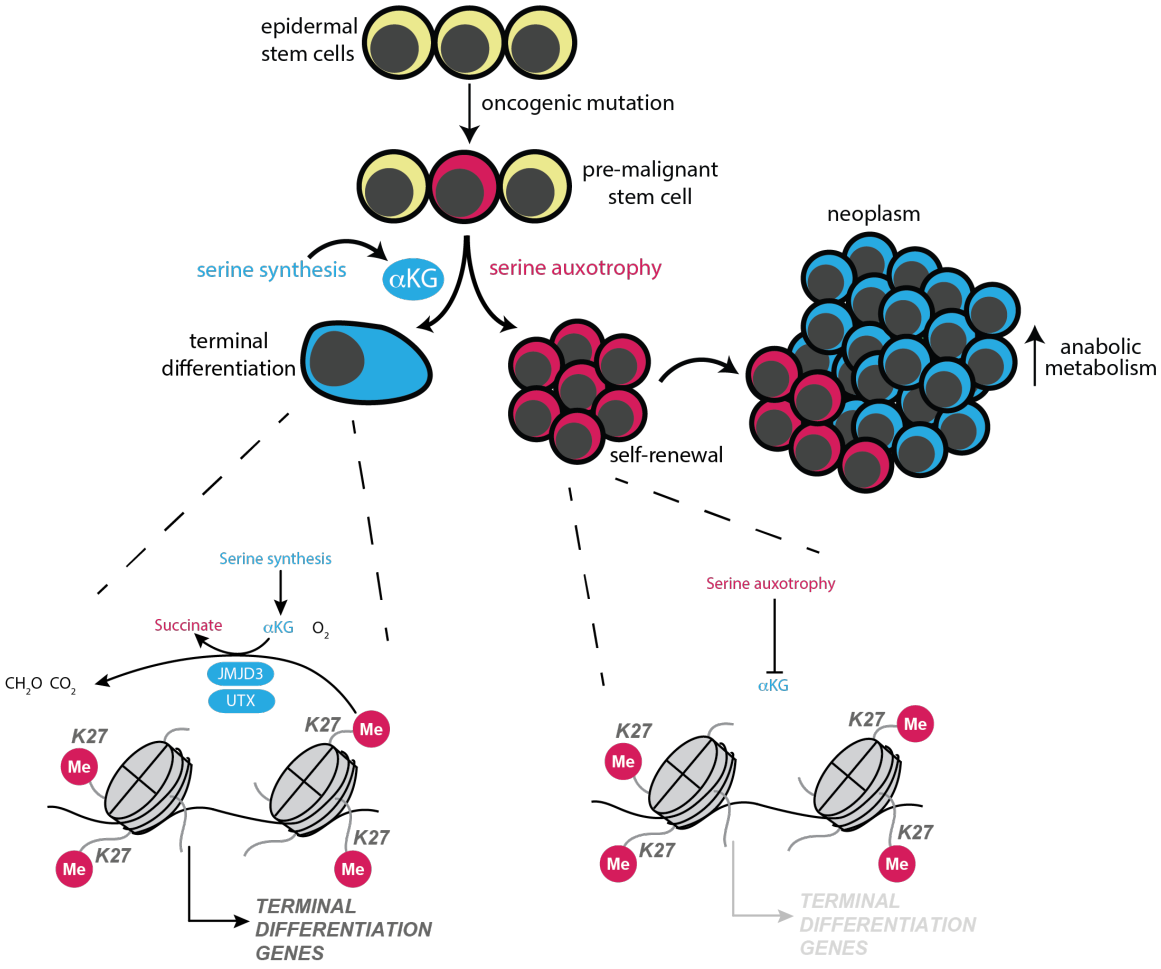

Fig 2.17 Extracellular serine controls epidermal stem cell fate and tumor initiation. Summary model of metabolic control of tumor initiation. Serine auxotrophy enforces oncogenic stem cell self-renewal but suppressing serine synthesis-derived αKG, which otherwise drives demethylation of H3K27me3, enabling expression of terminal differentiation genes.

Emerging evidence suggests that extracellular Ser/Gly restriction impairs tumor growth by imposing redox stress[116,117] and limiting one-carbon units that support proliferation[162]. My data extend the tumor suppressive effects of Ser/Gly deprivation to tumor initiation, while providing an additional mechanism by which Ser/Gly restriction can antagonize tumorigenesis. The degree

to which Ser/Gly restriction affects endogenous serine synthesis, αKG production, and differentiation programs in other cell types is an important area for future investigation.

Intriguingly, certain cancers harbor recurrent mutations in metabolic enzymes that poison αKG-dependent dioxygenases to suppress differentiation[30,31,38,163]. My data illustrate that even in the absence of such mutations, tSCs rewire intrinsic metabolic pathways to antagonize αKG-dependent chromatin remodeling. While I cannot exclude regulation of other αKG-dependent dioxygenases, I find that environmental Ser/Gly availability contributes to H3K27me3 demethylation, an established mediator of epidermal differentiation.

In conjunction with recent data that mutational status[53], nutrient availability[97,109,164] and other metabolic pathways[165] can suppress αKG-dependent dioxygenases, our work supports the notion that αKG may act generally as a metabolic tumor suppressor. The pathways that contribute to αKG pools may vary in a cell-type and context-specific manner[154,164,165]. It is intriguing to consider that while the TCA cycle produces αKG in mitochondria, the SSP generates αKG in the nucleo-cytosolic compartment, where it can act directly as a co-substrate for αKG-dependent dioxygenases. More broadly, my findings expose a way in which SCs balance metabolic demands for growth with those of regulating cell identity.

Consistent with recent work[17,116], I find that the SSP is critical for growth when extracellular serine is limiting. However, when extracellular serine is abundant, I find that the SSP is tumor suppressive. By contrast, certain established cancers including breast cancer and melanoma rely on SSP flux to maintain proliferation even in the presence of abundant extracellular serine[154,161]. Intriguingly, some of these tumors have evolved mechanisms such as *EZH2* overexpression[166] to suppress differentiation. Thus, plentiful exogenous serine may generally support tumor initiation and growth both by repressing differentiation and supporting proliferation.

A key question from this work is how SCs are able to initiate a tumor in the face of serine auxotrophy. Both normal and malignant SCs reside in proximity to the vasculature, and the perivascular niche is critical for maintaining tSC self-renewal[167,168]. It is therefore tempting to speculate that this niche also represents a rich nutrient source that enables tumorigenic SCs to rely on extracellular serine and suppress differentiation. Dietary Ser/Gly restriction disrupts SC maintenance, thereby establishing serine availability as a key regulator of cell fate during tumor initiation and growth. These findings raise the possibility that targeting serine uptake may be a promising therapeutic avenue to eliminate oncogenic stem cells by blunting their self-renewal and growth.

CHAPTER 3

PERSPECTIVES AND FUTURE DIRECTIONS

3.1 INTRODUCTION

Stem cells balance decisions of self-renewal and differentiation to maintain tissue homeostasis, and imbalances in this decision drive diverse pathologies including cancer and aging. Although numerous signaling and transcriptional pathways have been linked to stem cell fate regulation, the role of nutrients and metabolites in controlling stem cell behavior has been relatively less well explored. Moreover, whether or not endogenous metabolic pathways control key stem cell functions such as tumor initiation and lineage plasticity are poorly understood. Using the mammalian epidermis as a model system, I have explored these questions throughout the course of my thesis.

In particular, I have focused on how availability and uptake of the nutrient serine is linked to intracellular metabolic pathways that control abundance of the metabolite αKG, a critical co-substrate for chromatin modifying enzymes. I found that starving EpdSCs of serine triggers activation of the serine synthesis pathway, which drives αKG accumulation that is necessary and sufficient for epidermal differentiation and H3K27me3 demethylation. Accordingly, I found that serine availability controls the ability of a stem cell to initiate a neoplasm and properly respond to tissue injury. Finally, pre-malignant EpdSCs suppress endogenous serine synthesis to support their own self renewal. These findings have implications for therapeutic targeting of stem cells that initiate and sustain tumors and for enhancing wound repair. In this chapter I discuss three outstanding questions raised by my studies: the role of transporters in stem cell biology; the role of compartmentalized redox metabolism in controlling cell fate; and the mechanisms by which αKG might regulate stem cell fate.

3.2 METABOLITE TRANSPORTERS AS REGULATORS OF STEM CELL FATE

Both *in vitro* and *in vivo*, I have found that limiting extracellular serine drives changes in stem cell behavior. In EpdSCs and SCC-SCs, it drives differentiation; in pre-malignant EpdSCs it drives growth arrest; and in HFSCs it promotes lineage plasticity. Moreover, measurements of serine uptake demonstrated that pre-malignant EpdSCs increased serine uptake relative to WT EpdSCs. These studies point to a critical role of serine abundance in mediating stem cell behaviors. In particular, in the IFE, it is tempting to speculate that the balance of extracellular serine abundance and intracellular serine uptake is an endogenous driver of EpdSC differentiation, such that differentiation is coupled to enhanced serine synthesis-dependent αKG production.

Within a tissue, abundance of a nutrient that a cell experiences is likely determined by two key parameters: non-autonomous control by tissue vasculature (supply) and cell autonomous control by transporter expression (consumption). First, proximity of a cell to and structure of the vasculature is likely to be a key determinant of nutrient availability, since the vasculature delivers and drains nutrients and oxygen to and from a tissue[169,170]. In the skin, stem cells reside on the basement membrane and are therefore in close proximity to blood and lymphatic vasculature. These vascular niches have been implicated in stem cell proliferation and self-renewal in the skin, although their role in regulating nutrient homeostasis has not been well explored[91,167,168]. Despite this, manipulation of the vasculature is likely to have pleiomorphic effects beyond nutrient regulation, given the critical role of perivascular niche in signaling to stem cells[90,167,168]. Nevertheless, the epidermis itself is avascular, and therefore it is likely that EpdSCs have greater access to nutrients than their differentiated counterparts due to their proximity to the vasculature.

Secondly, nutrients are taken up into cells by transporters on the plasma membrane. Accordingly, it is tempting to speculate that transporter expression could determine the relative

abundance of a nutrient that a cell experiences, both based on the affinity of a particular transporter for its substrate and the amount of transporter a cell expresses. This effect has been well documented for glucose, where expression of the low affinity glucose transporter GLUT2 in metabolic organs enables sensing of circulating glucose levels to control systemic glucose homeostasis[171]. Moreover, acute regulation of GLUT1 plasma membrane localization enables rapid increases in glucose uptake upon growth factor stimulation[88]. Whether or not similar paradigms of nutrient sensing exist for other metabolites, such as serine, remains largely unexplored, and the role of transporters in controlling stem cell biology is not well understood.

Serine is thought to be transported into cells by Solute Carrier Family 1A4 (SLC1A4) and 1A5 (SLC1A5), both of which use sodium ion co-transport to drive uptake[172,173]. Serum serine levels are approximately 200±100 μM, and the Michaelis constants (an enzymatic measure of affinity) of SLC1A4 and SLC1A5 for serine are 100±20 μM and 250±40 μM, respectively[172–174]. Accordingly, SLC1A4 is predicted to be a high affinity serine transporter relative to SLC1A5 (Fig. 3.1a). Given increased serine uptake in pre-malignant $SOX2^+$ EpdSCs relative to WT EpdSCs, I asked whether or not this might be linked to differential expression of serine transporters. Consistent with its role as a high affinity serine transporter, I found that $SOX2^+$ EpdSCs expressed higher levels of *Slc1a4* mRNA and protein *in vitro* (Fig. 3.1b). Intriguingly, *in vivo*, SLC1A4 expression is restricted to EpdSCs within both WT and $SOX2^+$ epidermis, although its expression remains higher in $SOX2^+$ EpdSCs (Fig. 3.1c). That SLC1A4 is only expressed in stem cells within the epithelium raises the possibility that differentiation is endogenously coupled to a decrease in serine uptake and an increase in serine synthesis, driving αKG-dependent differentiation. Importantly, serine itself is an essential metabolite for epidermal barrier formation due to its role in sphingolipid biosynthesis[175,176], suggesting that differentiation would impose a significant

demand for serine synthesis in the absence of the ability of differentiated cells to consume serine from extracellular sources. Consistently, patients with PHGDH deficiency exhibit impaired epidermal differentiation that is associated with defects in sphingolipid biosynthesis[176,177].

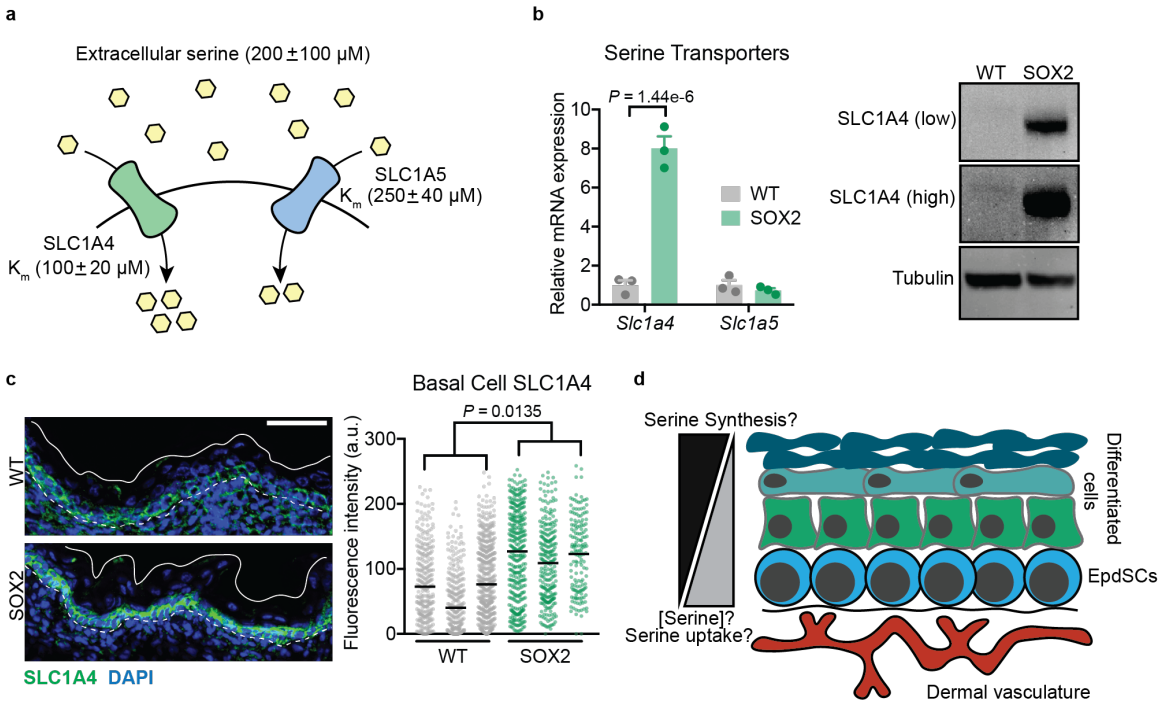

Fig. 3.1 SLC1A4 as a putative regulator of EpdSC fate. a, Enzymatic parameters of SLC1A4 and SLC1A5, two potential serine transporters. **b,** mRNA (left) and Western blot (right) of serine transporters in cultured EpdSCs. **c,** *In vivo* SLC1A4 expression. Dashed line indicates basement membrane, solid line indicates air-epithelial interface. **d,** Potential model for how serine availability and transport endogenously regulate epidermal differentiation.

Altogether, the combination of EpdSC proximity to the vasculature and restricted expression of SLC1A4 suggests a model wherein apparent serine availability endogenously controls epidermal differentiation (Fig. 3.1d). This would be consistent with our data that dietary Ser/Gly restriction increases EpdSC differentiation. Future studies should be aimed at manipulation of SLC1A4 to determine its role in epidermal differentiation, both via loss of function studies and overexpression of SLC1A4 mutants with varying affinities for serine[173] in differentiating cells. Reconstitution of SLC1A4 in cultured WT EpdSCs as well as cell free studies

will enable us to interrogate its biochemical function as a serine transporter in the epidermis. If SLC1A4 expression determines differentiation, I might expect that its overexpression in suprabasal cells would block their differentiation via suppression of serine synthesis dependent αKG production, while maintaining sphingolipid synthesis.

More broadly, given the restricted nature of SLC1A4 expression it is intriguing to consider whether or not a "transporter code" exists within tissues, such that the cohort of transporters particularly cell types express determines their function and fate. Moreover, transporters are appealing therapeutic targets given their plasma membrane localization and the possibility of developing competitive inhibitors for their substrates. Altogether, my functional studies on extracellular Ser/Gly restriction in Chapter 2 coupled with preliminary expression data presented here warrant further investigation of amino acid transporters as critical regulators of physiological stem cell functions.

3.3. COMPARTMENTALIZED REDOX METABOLISM AS A REGULATOR OF CELL FATE.

A major contribution of my work is the identification of cytosolic redox status as a determinant of serine synthesis in EpdSCs. Briefly, the first step of serine synthesis by PHGDH requires the reduction of NAD+ to NADH. Accordingly, sustaining serine synthesis requires a mechanism to regenerate NAD+ from NADH in the cytosol, which in most cells is accomplished via the conversion of pyruvate to lactate by lactate dehydrogenase[178]. I found that pre-malignant EpdSCs restricted serine synthesis by decreasing the conversion of pyruvate to lactate, instead oxidizing pyruvate in the TCA cycle. Notably, increasing NAD+ regeneration was sufficient to drive stem cell differentiation, presumably in part by enhancing serine synthesis. Interestingly, in

the intestinal crypt, blocking pyruvate entry into the mitochondria and subsequently shunting it to lactate enhances stem cell proliferation and self-renewal[179–181]. These studies provide evidence that compartmentalized redox status is a lineage specific determinant of cell fate and nutrient dependencies.

Previous studies have linked redox status to amino acid biosynthesis. Of note, these studies found that genetic and pharmacological suppression of mitochondrial NAD+ regeneration was sufficient to impair aspartate and serine biosynthesis[146,147,150,182]. Our work, in contrast, is the first demonstration of endogenous metabolic rewiring via changes in pyruvate fate controlling redox homeostasis. Moreover, they place these previous findings in the physiological context of tumor initiation and stem cell fate and provide evidence for distinct functions of cytosolic and mitochondrial redox homeostasis. Studying the role of redox metabolism in other physiological stem cell functions such as during wound healing may be of interest for future studies.

I suggest that in part, enhancing cytosolic NAD+ regeneration drives differentiation by enhancing αKG synthesis via serine synthesis. Future studies can take advantage of LbNOX expression, which I established and validated in the epidermis, to genetically enhance NAD+ regeneration in order to further investigate this process. Moreover, LbNOX can also be targeted to the mitochondria (mitoLbNOX)[148], and comparative analysis of the effects of mitoLbNOX and LbNOX may enable us to understand the physiological functions of compartmentalized redox metabolism in EpdSCs. It will be of particular interest to understand whether or not there are αKG-independent effects of cytosolic NAD+ regeneration on stem cell fate, such as through regulation of nucleotide synthesis or transcriptional co-repressors[183–186].

3.4 αKG AS A REGULATOR OF STEM CELL FATE IN THE EPIDERMIS

I found that extracellular serine abundance controls stem cell fate by regulating αKG levels. Limiting extracellular Ser/Gly triggers activation of the serine synthesis pathway, which subsequently leads to αKG accumulation that can drive EpdSC differentiation and H3K27me3. These studies build on previous work from our lab and others showing that the H3K27me3 methyltransferase EZH2 is essential for EpdSC self-renewal and that the demethylase JMJD3 is essential for differentiation[155,156,187]. Nevertheless, as discussed in Chapter 1, it remains challenging to understand how αKG mediates specific effects, given that multiple intracellular dioxygenases consume it as part of their reaction cycle. Indeed, although I find that pharmacological inhibition of JMJD3 is sufficient to reverse Ser/Gly starvation induced differentiation, and that H3K27me3 levels correlate with αKG-induced differentiation, it remains possible that additional dioxygenases are important in differentiation. For example, similar to H3K27me3, DNA methylation has been shown to be critical for EpdSC self-renewal[188], suggesting that TET enzymes that demethylate DNA may also play a role in αKG-dependent differentiation. Nevertheless, this work is the first to establish αKG as a regulator of adult stem cell behavior, building on work in embryonic stem cells that αKG is a key determinant of stem cell fate[29].

Multiple cancers harbor recurrent mutations in metabolic enzymes, such as isocitrate dehydrogenase 1 and 2 (IDH1/2) and succinate dehydrogenase (SDH) that result in accumulation of so-called oncometabolites that poison αKG-dependent dioxygenases. Notably, these oncometabolites largely function by locking stem cells in a hyperproliferative self-renewing state[21]. Consistently, αKG has been shown to suppress tumorigenesis and drive differentiation in multiple cancers including leukemia, pancreatic cancer, and intestinal cancer[52,53,111]. Thus, our work adds to a growing body of literature suggesting that αKG acts as a metabolic tumor

suppressor. Additionally, it is consistent with previous work showing that environmental constraints such as glutamine limitation and hypoxia can limit αKG-dependent dioxygenase function[52,97,109], suggesting that cancer cells can engage multiple mechanisms to evade the tumor suppressive effects of αKG. Moreover, it provides evidence that stem cells can rewire endogenous metabolic pathways to limit αKG production, such that even under serine limited conditions pre-malignant EpdSCs can prevent differentiation by suppressing serine synthesis.

An important question is understanding whether or not it will be feasible to enhance αKG production to suppress tumorigenesis. While this represents an appealing route forward, it should be noted that αKG accumulation may not always be beneficial. For example, in breast cancer, αKG promotes metastatic colonization of the lung by enhancing activity of αKG-dependent collagen hydroxylases[164]. In pediatric ependymomas, αKG was recently shown to be critical in establishing epigenomic programs that support proliferation[104]. These studies highlight the importance of understanding the specific mechanisms by which αKG mediates its diverse effects, so as to better refine our ability to target this critical metabolic axis.

3.5 CONCLUSIONS

In this thesis, I aimed to explore metabolic control of stem cell function in the skin. In doing so, I uncovered the mechanisms by which nutrient availability is integrated with stem cell fate decisions during tumor initiation and progression and wound repair. I anticipate that these findings will have implications beyond the skin. It may be of particular interest to study the links between αKG and amino acid uptake in stem cells that initiate neoplasms driven by IDH mutations, such as those of the blood and brain. Additionally, I anticipate that understanding the links between endogenous metabolic pathways and transcriptional programs in stem cells will be broadly

relevant in pathologies outside of cancer, including inflammatory diseases, wound healing, diabetes and degenerative diseases. Finally, building on our knowledge of the mechanisms by which serine, αKG and cell fate are linked will enable directed therapies to enhance epidermal wound repair while suppressing tumorigenesis.

MATERIALS AND METHODS

Cell culture. Primary EpdSCs from WT and SOX2^{+} mice, HRas^{G12V} transduced EpdSCs, and SCC lines were grown under standard tissue culture conditions, 37 ºC and 7.5% CO_2. Cells were cultured in E-low calcium (50 μM Ca^{2+}) medium (E-low) made in house from DMEM/F12 medium supplemented with 15% chelated FBS, 5 μg/mL insulin, 5 μg/mL transferrin, 2 nM triiodothyroxine, 40 μg/mL hydrocortisone and 10 nM cholera toxin. For all experiments, cells were switched from E-low growth medium to E-low lacking pyruvate, aspartate, glutamate, and glutamine reconstituted with 4 mM glutamine, 25 mM glucose, 15% chelated dialyzed FBS (GeminiBio), and ±0.32 mM Ser/Gly (experimental E-low medium). A431 SCCs were grown in DMEM supplemented with 10% FBS and 1 mM sodium pyruvate. SCC9 SCCs were grown in E-low medium supplemented to 1.5 mM Ca^{2+}. A mix of male and female cells were used for all studies. Independently derived littermate lines were used for comparisons. Unless noted in legends, WT-1 and SOX2-1 lines were used.

Mice. All animal experiments were performed in the AAALAC-accredited Comparative Bioscience Center at the Rockefeller University. Experiments were in accordance with NIH guidelines for Animal Care and Use, approved and overseen by The Rockefeller University's Institutional Animal Care and Use Committee. *Rosa26-CAG-loxP-stop-loxP-Sox2-IRES-eGFP* mice were donated by J. Que and maintained in a B6/svev129 mixed background. *Krt14-cre(tg), Krt14-creER(tg),* and *Krt10-H2B-mRFP(tg)* mice were maintained in a CD-1-ICR background. *Sox9-CreER;R26-LSL-YFP* mice were maintained in a mixed B6/CD1 background. For analysis of WT and SOX2^{+} mice, a mix of males and females were used. *Krt14-CreER*;*R26-LSL-Sox2-IRES-GFP* and *Sox9-CreER;R26-LSL-YFP* mice were treated with 5 100 μL doses of 2% w/v tamoxifen (Sigma) beginning at P50. For tumor allografts, 6-8 week old female *Nude* (Nu/Nu) mice were used. For DMBA/TPA experiments, P60 female FvB mice were used.

Primary culture derivation. P0 mice were euthanized by decapitation, backskin was dissected off and incubated in a 1:1 mix of dispase and PBS overnight at 4 ºC. Epidermis was removed from the dermis and incubated in a 1:1 mix of 0.25% trypsin/EDTA and versene for 10 min at room temperature. The epidermal

fraction was mechanically dissociated to a single cell suspension, filtered through a 40 μm filter and cultured in E-low medium.

Growth curves. 5000 WT, $SOX2^+$ or HT-SCC cells were plated in triplicate into a black 96 well plate (Nunc). The next day (day 0), one plate was fixed with 4% PFA for 10 min. Remaining cells were treated with indicated medium/reagent, and at indicated times were subsequently fixed, stained with DAPI, and counted using a BioTek Cytation5. For chemical treatments, cells were pre-treated for 4 h prior to switching to control or serine/glycine (Ser/Gly)-free experimental E-low medium. For partial Ser/Gly starvation experiments, cells were cultured in medium with 17.065 mg/L serine and 12.19 mg/L glycine. Population doublings were calculated as the $\log_2$ fold change in cell number relative to day 0.

Scratch wound. HFSCs were seeded in a 6 well plate. When cultures were confluent, cells were washed once with PBS and switched into control or ser/gly free medium. A P200 pipet tip was dragged once down the length of each well to generate a wound, and cells were imaged using phase contrast microscopy and indicated time points.

In vitro **drug treatments.** Drugs were added at the following concentrations: α-ketobutyrate 1 mM, dichloroacetate 5 mM, UK-5099 500 nM, pyruvate 2 mM, lactate 2 mM, formate 1 mM, dimethyl-α-ketoglutarate 4 mM, 4 mM, eGSH 1 mM, Trolox 500 nM, GSK-J4 10 μM, GSK-343 10 μM, Nutlin-3a 10 μM.

Nutrient uptake. 150,000 WT or 300,000 $SOX2^+$ cells were seeded into 6 well plates (Corning). The following day, medium was aspirated and replaced with 1 mL of experimental E-low medium containing Ser/Gly. At the same time, 1 mL of medium was added to a control 6 well plate lacking cells. 24 h later, media was collected and spun at max speed at 4 ºC for 20 min. 50 μL of the supernatant was added to 1 mL of ice-cold 80% methanol supplemented with 2 μM deuterated 2-hydroxyglutarate (D-2-hydroxyglutaric-2,3,3,4,4-d5 acid (d5-2HG)) as an internal standard and analyzed by mass spectrometry. Glutamine

consumption, glutamate secretion and lactate secretion were measured using a YSI 2950 series biochemistry analyzer (YSI Life Sciences). Metabolite consumption and secretion was determined relative to fresh medium and the values were normalized to the average protein content in each condition where indicated.

Serine standard curve. Serine (0-20 nmol) was dissolved in 50 µL of water and mixed with ice-cold 80% methanol supplemented with d5-2HG. After overnight incubation at -20°C, the serine standards were dried in an evaporator (Genevac EZ-2 Elite), derivatized as described in **GC-MS metabolite profiling** and analyzed using an Agilent 7890A GC coupled to Agilent 5975C mass selective detector. A standard curve was obtained by plotting d5-2HG-normalized serine peak area against the amount serine. The linear regression equation was calculated by the least squares method using Microsoft Excel.

Estimation of serine synthesis. To quantify the amount of serine consumption, the MS peaks representing serine were extracted and integrated using MassHunter software, normalized to the internal standard (d5-2HG) peak area and quantified against the serine standard curve. The calculated values were normalized to the average protein content of all wells in each condition (µmol serine/mg protein). Serine biosynthetic demand in the absence of exogenous Ser/Gly was estimated using a serine standard curve to calculate serine uptake (from Fig. 1c) in the presence of Ser/Gly and serine secretion in the absence of Ser/Gly, while intracellular glutamine availability was estimated using a YSI analyzer as glutamine consumption minus glutamate secretion. Since serine synthesis produces a mole of αKG per mole of serine, the fraction of intracellular glutamine used to meet serine biosynthetic demand approximates the fraction of glutamine used to produce αKG via this pathway. See Supplementary Tables 2 and 3 for more information.

GC-MS metabolite profiling. For all metabolite experiments, 150,000 WT or 300,000 $SOX2^+$ cells were seeded in 6-well plates under standard culture conditions and changed into the corresponding experimental

E-low media the next day. For isotope tracing experiments, cells were cultured for 4 h in indicated experimental E-low medium reconstituted with uniformly labeled ^{13}C-serine, glycine, glucose or glutamine (Cambridge Isotope Labs) following 16 hours of culture in experimental E-low medium with or without Ser/Gly. For serum, blood was collected from the retro-orbital sinus and allowed to clot on ice for 30 min. Samples were then spun at 1,000 *g* for 10 min and supernatant (serum) was collected. Metabolites were extracted with 1 mL of ice-cold 80% methanol supplemented with d5-2HG.

After overnight incubation at -80°C, cell lysates were centrifuged at 21,000 *g* for 20 min and protein-free supernatants were dried in an evaporator (Genevac EZ-2 Elite). Metabolites were resuspended in 50 μL of 40 mg/mL methoxyamine hydrochloride (Sigma) in pyridine (ThermoFisher) by incubation at 30°C for 2 h and further derivatized by addition of 80 μL of MSTFA (ThermoFisher) and 70 μL ethyl acetate (Sigma). After 30 min incubation at 37°C, samples were analyzed using an Agilent 7890A GC coupled to Agilent 5975C mass selective detector. The GC was run in splitless mode using constant helium gas flow at 1 mL/min. A microliter of derivatized sample was injected onto an HP-5MS column and the GC oven temperature ramped from 60°C to 290°C over 25 min.

GC-MS analysis. Peaks representing metabolites of interest were extracted and integrated using MassHunter software (Agilent Technologies) and verified relative to known spectra for each metabolite. The following ions were used for quantification of metabolite levels: d5-2HG *m/z* 354; alanine, *m/z* 218; αKG, *m/z* 304; asparagine, *m/z* 231; aspartate, *m/z* 334; citrate, *m/z* 465; cysteine, *m/z* 322; fumarate, *m/z* 245; glutamate, *m/z* 363; glutamine, *m/z* 362; glycine, *m/z* 276; isoleucine, *m/z* 260; leucine, *m/z* 260; malate, *m/z* 335; methionine, *m/z* 250; phenylalanine, *m/z* 294; proline, *m/z* 216; serine *m/z* 306; succinate, *m/z* 247; threonine, *m/z* 320; tryptophan, *m/z* 405; tyrosine, *m/z* 382; and valine, *m/z* 246; pyruvate, *m/z* 115; lactate *m/z* 219. All values were normalized to both the internal standard peak area and the protein content of triplicate samples. Enrichment of ^{13}C was determined by quantifying the abundance of the following ions: citrate, *m/z* 465-482; glycine, *m/z* 276-286; and serine, *m/z* 306-317. Correction for naturally occurring isotopes was performed using IsoCor software[189].

NAD+/NADH ratio quantification. The NAD+/NADH ratio was quantified using an enzymatic colorimetric Abcam kit according to manufacturer's instructions. Briefly, cells were lysed with 450 μL NADH/NAD extraction buffer and then spun for 5 min at 4ºC at maximum speed. Supernatant was filtered through a 10 kDa spin column (BioVision) and 200 μL was used for total NAD+ and NADH quantification. The remaining extract was heated at 60ºC for 30 min to decompose NAD+. 50 μL of sample was mixed with 100 μL of reaction mixture and incubated for 5 min at room temperature. 10 μL of developing solution was added and the reaction was incubated for 1 h at room temperature. Absorbance was measured at 450 nm using a BioTek Cytation 5 plate reader and NAD+ and NADH amounts were calculated using a standard curve of purified NADH. The NAD+/NADH ratio was calculated as $(NAD(H)_{total} - NADH)/NADH$.

Immunofluorescence and image analysis. For immunofluorescence, samples were dissected off of mice, were pre-fixed in 4% PFA for 1 h at 4°C and then incubated with 30% w/v sucrose overnight, embedded in Optimal Cutting Temperature (OCT) compound (Tissue Tek), and sectioned at a thickness of 12 μm. For *in vitro* immunofluorescence, cells were seeded into fibronectin coated glass chamber-slides (Millipore), and fixed for 10 min in 4% PFA at room temperature. To determine HFSC proliferation in waxing experiments, skin was scraped to remove fat, incubated in 2.5 U/mL dispase + 20 mM EDTA for 2 hr at 37ºC, and then HFs were separated from the epidermis manually. Samples were blocked at room temperature in Gelatin Block (2% fish gelatin, 5% normal donkey serum, 1% bovine serum albumin, 0.3% Triton, in PBS). Samples were incubated with primary antibody overnight at 4°C, washed in PBS, and exposed to secondary antibody for 1 h at room temperature. Samples were mounted in ProLong Gold with DAPI (Life Tech) prior to imaging. The following primary antibodies and dilutions were used: GFP (chicken, 1:2000, Abcam), GFP (goat, 1:1000 VWR), K5 (guinea pig, 1:500, E. Fuchs), K10 (rabbit, 1:1000, Covance), RFP (rat, 1:1000, Chromotek), RFP (goat, 1:500, MYBioSource), K14 (rabbit, 1:1000, E. Fuchs), K14 (chicken, 1:1000, Covance), Involucrin (rabbit, 1:1000, Covance), SOX2 (rabbit, 1:300, Abcam), cleaved caspase 3 (rabbit, 1:200, Cell Signaling), integrin-α6 (rat, 1:2000, eBioscience), H3K27me3 (rabbit, 1:500, Millipore), FLAG M2 (mouse, 1:1000, Sigma), CD44 (rat, 1:200, BD

Bioscience), Ki-67 (rabbit, 1:200, Cell Signaling), K24 (Fuchs lab, 1:5000), KLF5 (goat, 1:100, R&D), SLC1A4 (rabbi, 1:200, Cell Signaling). Secondary antibodies were conjugated to Alexa Fluor™ 488, RRX, or 647 (1:1000, Life Technologies A-11006). Phalloidin conjugated to Alexa Fluor™ 564 or 647 (165 nM working concentration, ThermoFisher) were used and stained simultaneously with secondary antibodies. Images were captured on a Zeiss Axioplan2 using a Plan-Apochromat 20x/0.8 air objective or 40x/0.8 oil immersion objective. Images were processed using ImageJ and Adobe Photoshop CS5. See Reporting Summary for antibody catalog numbers.

To quantify fluorescence in SCCs of progenitor and differentiated cell markers, tumor cells were masked on GFP (for K14, K10 and involucrin) or DAPI/H2B-mRFP (for H3K27me3) and pixel intensity was analyzed within the mask on the marker of interest. In the absence of a mask for cells of interest, fluorescence was quantified manually through ROI selection. To quantify mitotic spindle axis, a straight line was drawn between the middle of two daughter nuclei marked by K14, and the angle between this line and the basement membrane, as stained by keratin-14, was quantified. Mitotic angles < 30^{o} were classified as planar, and angles >30^{o} were classified as nonplanar.

Immunohistochemistry. All human samples were derived from commercially purchased, de-identified paraffin embedded tissue arrays (Biomax SK802b, HN803e). Arrays were baked at 60^{o}C for 30 min and then deparaffinized by washing 2x10 times in Citrus Clearing Solvent (ThermoFisher) followed by 2x10 washes in 100% ethanol (EtOH), 1x10 wash in 95% EtOH, and 1x10 wash in 70% EtOH. Antigen retrieval was then performed in pH 6.0 Citrate (Vector Laboratories) by heating slides to 125^{o}C for 30 s and 90^{o}C for 10 s in a pressure cooker. Slides were stained according to VECTASTAIN® Elite® ABC Universal PLUS Kit manufacturer instructions (Vector Laboratories). Briefly, slides were permeabilized for 5 min in 0.1% TBS-T, blocked in BLOXALL peroxidase block for 10 min and horse serum for 20 min. Arrays were incubated in primary antibody (H3K27me3 rabbit, 1:500, Millipore) overnight at 4^{o}C. The next day, slides were incubated with secondary antibody (Horse anti-mouse/rabbit IgG, biotinylated) for 30 min at room temperature. Slides were incubated in VECTASTAIN Elite ABC Reagent for 30 min at room temperature,

and then in a 1:1 mixture of ImPACT® DAB EqV Reagent 1 (Chromogen) and Reagent 2 (Diluent) for 2 min. After development, slides were incubated in hematoxylin (Sigma) for 1 min, washed 3x in water, washed 1x in acid alcohol (1% HCl in 95% EtOH), washed 3x in water, washed 1x in Bluing Reagent (Fisher), washed 1x in water, and then dehydrated by washing 10x 70% EtOH, 10x 95% EtOH, 2x10 100% EtOH, 2x10 Citrus Clearing Solvent. Slides were mounted with Cytoseal 60 (ThermoFisher). Images were captured using a BioTek Cytation 5 using a 4x or 20x air objective. See Reporting Summary for antibody catalog numbers.

To score arrays for H3K27me3 intensity, investigators were blinded to tumor stage, lineage and anatomic location. Within a tissue core, lymphocytes were used as an internal control for high H3K27me3 staining. Staining intensity within tumor cells was scored "high" if intensity was at least ~70% as intense as lymphocytes, "moderate" if intensity was ~30-70% as intense as lymphocytes, or "weak" if staining was <30% as intense as lymphocytes. After scoring, investigators were unblinded to bin scoring results based on histopathological grade. Images were processed in ImageJ and Photoshop.

Hematoxylin & eosin. Slides were washed in water, incubated in hematoxylin for 2 min, washed in water 3x, washed once in acid alcohol, washed twice in water, washed once in Bluing reagent, and washed once in water. Slides were subsequently dehydrated with 10 washes each in subsequent 80%, 95% and 100% EtOH, followed by eosin staining for 1 minute, 2 x 20x washes in 100% EtOH and 2 x 20x washes in Citrus Clearing Solvent. Slides were mounted with Cytoseal 60 and imaged on a Zeiss Axioplan2 using a Plan-Apochromat 20x/0.8 air objective. Images were processed in ImageJ and Photoshop.

Western Blot. Triplicate wells were lysed in chilled RIPA buffer containing cOmplete protease inhibitors and PhoSTOP phosphatase inhibitors (Roche). Protein was quantified using a Pearce BCA protein quantification kit. 15 μg of protein was loaded for SDS-PAGE and standard western blotting procedures. For histone extraction, 1 x 10^6 cells were suspended in Laemmli buffer and sonicated 15X, 30 s on/off. β-mercaptoethanol and bromophenol blue were added, samples were boiled, and 6 μL was loaded for standard

western blotting procedures. Membranes were blocked in LiCOR blocking buffer. Membranes were incubated in primary antibody overnight in blocking buffer with 0.2% Tween-20 at 4ºC, and incubated in secondary antibody diluted in blocking buffer with 0.2% Tween-20 and 0.01% SDS for 1 h at room temperature. The following primary antibodies and dilutions were used: PHGDH (rabbit, 1:2000, Sigma), PSAT1 (mouse, 1:500, Sigma) PSPH (rabbit, 1:500, Sigma), SHMT1 (rabbit, 1:1000, Cell Signaling), SHMT2 (rabbit, 1:1000, Cell Signaling), OGDH (rabbit, 1:1000, ProteinTech), SDH-A (mouse, 1:1000, abcam), H3K27me3 (rabbit, 1:1000, Millipore), α-tubulin (mouse, 1:10000, Sigma), total H3 (mouse, 1:10000, abcam), β-actin (rabbit, 1:1000, Cell Signaling), SLC1A4 (rabbit, 1:1000, Cell Signaling). The following LiCOR secondary antibodies were used, all at 1:10000: IRDye 800CW donkey anti-mouse IgG, IRDye 800CW donkey anti-rabbit IgG, IRDye 680 LT donkey anti-mouse IgG, IRDye 680LT donkey anti-rabbit IgG. Membranes were imaged via fluorescence on an Odyssey CLx Imager and processed using Adobe Photoshop CS5. See Reporting Summary for antibody catalog numbers.

qRT-PCR. Triplicate wells were lysed in 200 μL TRIzol. RNA was extracted using a Zymo Direct-zol RNA miniprep kit, and 100 ng of RNA was used for cDNA synthesis with a SuperScript VILO cDNA synthesis kit (ThermoFisher). cDNA was diluted 1:5 for qPCR. cDNAs were mixed with indicated gene-specific primers listed in Supplementary Table 7 and SYBR green PCR Master Mix (Sigma), and qRT-PCR was performed on an Applied Biosystems 7900HT Fast Real-Time PCR system. Values were normalized to expression of β-actin.

EdU incorporation. Mice were treated with 0.02 CC of 5 mg/mL EdU for 1 hour prior to sacrifice. EdU staining was performed following incubation of slides with secondary antibody. AF-647 azide, copper sulfate and EdU additive buffer and reaction buffers (Life Technology) were added to slides. Slides were incubated for 20 min at room temperature, washed and mounted for imaging.

Tumor allograft, xenograft and growth curves. 200,000 mouse ($Hras^{G12V}$;Tgbr2 cKO) or human (SCC9, or A431) SCC cells diluted 1:1 in growth factor-reduced, phenol red-free Matrigel (Corning) were injected

intradermally into the backs of *Nude* mice. For sh*Sdha* and sh*Ogdh* experiments, mice were treated with 100 mg/L doxycycline and 2% w/v sucrose in drinking water starting 5 days after grafting. For GSK-J4 treatment, mice were treated daily for five days intraperitoneally with 10 mg/kg GSK-J4, beginning 5 days after grafting. For rapamycin treatment, mice were treated daily for five days intraperitoneally with 4 mg/kg rapamycin, beginning 5 days after grafting. Tumors were measured at indicated time points. Tumor size was measured using a digital caliper, and volume was calculated using the formula $(\pi(\text{length} \times \text{width})^2)/6$.

Serine/glycine free diet. Purified control amino acid diet (5CC7) and diet lacking serine and glycine (5BJX) (WF Fisher and Sons) were formulated as previously described[116,117]. Mice were maintained on diets for at least two weeks prior to initiating experiments. Pregnant females were placed on diet on the day of plug.

DMBA/TPA two step chemical carcinogenesis protocol. P60 female WT FvB mice were placed on control or serine/glycine free diet. Two weeks later, mice were treated topically with a single 100 μL dose of 400 nmol DMBA (Sigma) diluted in acetone. Beginning the following week, mice were treated 2x/week topically with 100 μL of 20 nmol TPA (Sigma) diluted in ethanol and monitored for tumors.

Wounding. Second telogen mice were used for wounding experiments. Mice were anesthetized with isofluorane and shaved for partial thickness and full thickness wounds. For partial thickness wounding, skin was gently stretched and a Dremel tool with a polishing tool was used to make abrasions of the epidermis by polishing the skin 4-5 times (100 series rotary tool and 520 polishing tool from Dremel Inc.). For full thickness wounding, a 6 mm punch biopsy (Miltex) was taken. For depilation, molten wax was applied onto the hair coats and peeled off after hardening.

CRISPR/Cas9 editing of SCC cells. Guide RNA (gRNA) targeting the second and fourth exons of *Phgdh* were designed using GuideScan software[70]. Synthetic gRNAs, negative control gRNA, Atto550-trRNA, and recombinant Cas9 were purchased from IDTdna. gRNA:trRNA:Cas9 complexes were assembled and transfected into SCC cells following manufacturers protocol (IDTdna.com: Cationic lipid delivery of

CRISPR ribonucleoprotein complexes into mammalian cells) using RNAiMAX (ThermoFisher) reagent as the transfection reagent. 48 h post transfection single GFP+/Atto550+/DAPI- cells were sorted into 96 well plates and allowed to grow into clonal cell lines. To screen cells for Phgdh knockout, genomic DNA was isolated from each clone. Short PCR amplicons including the gRNA target region were generated, barcoded, sequenced in a multiplex fashion on an Illumina MiSeq Nano using a modified version of the *16S metagenomics sequencing library preparation* protocol from illumima. Knockout was confirmed by western blot. sgRNA sequences are provided in Supplementary Table 6.

shRNA mediated knockdown and viral infection. Following *Phgdh* hairpin screening via transient transfection, efficient hairpins were subcloned into pLKO-H2B-mRFP1 vectors. sh*Ogdh* and sh*Sdha* hairpins were packaged into LT3-GEPIR doxycycline inducible vectors[53] (donated by S. Lowe) and validated following culture of cells in 1 μg/mL doxycycline hyclate (Sigma) for 24 h. For *LbNOX* expression, *LbNOX-Flag* (Addgene #75285) was amplified and subcloned with an N-terminal P2A site into pLKO-H2B-mRFP1. Vectors were packaged into lentivirus using calcium chloride transfection of 293TN cells (Invitrogen) with packaging plasmids pMD2.G and pPAX2 (Addgene #12259 and #12260, respectively). Viral supernatant was collected 46 h after transfection and filtered through a 0.45 μm filter. Cells were then transduced and two days later were purified using fluorescence associated cell sorting (FACS) based on mRFP1 expression. For sh*Renilla*, sh*Ogdh,* and sh*Sdha* lines, infected cells were selected using 1 μg/mL puromycin for 24 h. shRNA sequences are provided in Supplementary Table 5.

Statistics and Reproducibility

Statistical analyses were performed using Prism 7 and 8 (Graphpad) software. All *in vitro* experiments shown were repeated at least twice in triplicate with similar results, and representative data are shown unless otherwise indicated. All *in vivo* experiments were repeated in at least three biological replicates with similar results. Unpaired two-tailed Student's *t*-tests were used to ascertain statistical significance between two groups. One-way ANOVA was used to assess statistical significance between three or more groups with

one experimental parameter, while two-way ANOVA was used to assess statistical significance between groups with two experimental parameters. See Fig. legends for more information on statistical tests. Mice were randomly allocated to control or experimental conditions. Experimenters were not blinded to conditions during data collection or analysis, except for scoring of H3K27me3 staining by IHC, where investigators were blinded to tumor histological grade.

APPENDIX

Table 2.1. Serine standard curve data

Serine (nmol)	D5-2HG normalized peak area
0	0.027213558
0	0.011766296
0.1	0.025398432
0.1	0.028388756
0.5	0.114490747
0.5	0.102225692
1	0.217915223
1	0.251592868
2.5	0.464356491
2.5	0.508034819
5	1.251600614
5	0.850940717
10	2.508784279
10	2.423833354
20	3.985209204
20	4.160433295
Standard curve:	**$y = 0.212x$ ($R^2 = 0.98673$)**

Table 2.2. Extracellular glutamine, glutamate and serine data

Parameter	Mean (n = 6)	Standard Deviation
Gln consumption (mmol/mg protein)	6.439	0.4965
Glu secretion (mmol/mg protein)	1.14	0.02147
Intracellular Gln (Gln consumed - Glu secreted) (mmol/mg protein)	5.299	0.4858
Ser consumption (mmol/mg protein)	0.5164	0.1203
Ser secretion (mmol/mg protein)	0.05072	0.01014
Serine synthesis (Ser consumption + Ser secretion) (mmol/mg protein)	0.5671	0.1193
Fraction of Intracellular Gln (Ser synth/Intracellular Gln)	0.1092	0.03382

Table 2.3 shRNA sequences

sh*Scramble*	CAACAAGATGAAGAGCACCA
sh*Phgdh-1*	CCGAATGCAATCCTTTGGAAT
sh*Phgdh-2*	CGTGAACTTGGTGAACGCTAA
sh*Renilla*	TAGATAAGCATTATAATTCCT
sh*Ogdh-1*	TAAATGAAACATTTTGTCCTG
sh*Ogdh-2*	TAGCAATTCTGCATACTTCTG
sh*Sdha-1*	TTAATTGAAGGAACTTTATCTC
sh*Sdha-2*	TTCATAACCGATTCTTCTCCAG
sh*Sdha-3*	TCTGATGTTCTTATACTTCCAT

Table 2.4 sgRNA sequences

sg*Phgdh-A*	AATGAGGCCTTCACAGTCCT
sg*Phgdh-B*	CCAGAACTTACTTCATGACT
sg*Phgdh-C*	TGGCAAATGGGACCGGAAGA

Table 2.5 RT-qPCR primers

Ldha_F	AGGCTCCCCAGAACAAGATT
Ldha_R	TCTCGCCCTTGAGTTTGTCT
Pdk1_F	GTGCCCCTGGCTGGGTTTGG
Pdk1_R	CCAGGCGTCCCATGTGCGTT
Pcx_F	GGCCAAGGAAAATGGTGTAG
Pcx_R	CTTCC ACCTT GTCTCCCATC
Pdha1_F	ACACAGCATGAGTGACCCTG
Pdha1_R	CACCCATCCACCCACCTAAC
Pdhb_F	TGGTGCTGATGTCCCTATGC
Pdhb_R	CCTTCCAGTGAAAGAGGGCA
Krt-14_F	CGCCGCCCCTGGTGTGG
Krt-14_R	ATCTGGCGGTTGGTGGAGGTCA
Krt-5_F	AACATTTTGGGGTCTGGGTCAC
Krt-F_R	GGCCCACAGAGACTGCTTCTTT
Lor_F	TCACTCATCTTCCCTGGTGCTT
Lor_R	GTCTTTCCACAACCCACAGGA
Flg_F	GGAGGCATGGTGGAACTGA
Flg_R	TGTTTATCTTTTCCCTCACTTCTACATC
Tp53_F	CTAGCATTC AGGCCCTCATC
Tp53_R	TCCGACTGTGACTCCTCCAT

Cdkn1a_F	CGGTGTCAGAGTC TAGGGGA
Cdkn1a_R	ATCACCAGGATTGGACATGG
Mdm2_F	TGTCT GTGTCTACCGAGGGTG
Mdm2_R	TCCAACGGACTTTAACAACTTCA
Actin_F	GCTCTTTCCAGCCTTCCTT
Actin_R	CTTCTGCATCCTGTCAGCAA

REFERENCES

1. Rogers, K. W. & Schier, A. F. Morphogen Gradients: From Generation to Interpretation. *Annu. Rev. Cell Dev. Biol.* **27**, 377–407 (2011).
2. Bedzhov, I., Graham, S. J. L., Leung, C. Y. & Zernicka-Goetz, M. Developmental plasticity, cell fate specification and morphogenesis in the early mouse embryo. *Philosophical Transactions of the Royal Society B: Biological Sciences* vol. 369 (2014).
3. Ge, Y. & Fuchs, E. Stretching the limits: from homeostasis to stem cell plasticity in wound healing and cancer. *Nat. Rev. Genet.* **19**, 311–325 (2018).
4. De Robertis, E. M. Spemann's organizer and self-regulation in amphibian embryos. *Nature Reviews Molecular Cell Biology* vol. 7 296–302 (2006).
5. Yu, S. *et al.* Paneth Cell Multipotency Induced by Notch Activation following Injury. *Cell Stem Cell* **23**, 46-59.e5 (2018).
6. Takahashi, K. & Yamanaka, S. Induction of pluripotent stem cells from mouse embryonic and adult fibroblast cultures by defined factors. *Cell* **126**, 663–76 (2006).
7. Adam, R. C. & Fuchs, E. The Yin and Yang of Chromatin Dynamics In Stem Cell Fate Selection. *Trends in Genetics* vol. 32 89–100 (2016).
8. Schvartzman, J. M., Thompson, C. B. & Finley, L. W. S. Metabolic regulation of chromatin modifications and gene expression. *J. Cell Biol.* **217**, 2247–2259 (2018).
9. Su, X., Wellen, K. E. & Rabinowitz, J. D. Metabolic control of methylation and acetylation. *Curr. Opin. Chem. Biol.* **30**, 52–60 (2016).
10. Reid, M. A., Dai, Z. & Locasale, J. W. The impact of cellular metabolism on chromatin dynamics and epigenetics. *Nature Cell Biology* vol. 19 1298–1306 (2017).
11. Sullivan, M. R. & Vander Heiden, M. G. Determinants of nutrient limitation in cancer. *Critical Reviews in Biochemistry and Molecular Biology* vol. 54 193–207 (2019).
12. Thompson, C. B. & Bielska, A. A. Growth factors stimulate anabolic metabolism by directing nutrient uptake. *J. Biol. Chem.* **294**, 17883–17888 (2019).
13. Vardhana, S. A. *et al.* Glutamine independence is a selectable feature of pluripotent stem cells. *Nat. Metab.* **1**, 676–687 (2019).
14. Baksh, S. C. *et al.* Extracellular serine controls epidermal stem cell fate and tumour initiation. *Nat. Cell Biol.* 1–12 (2020) doi:10.1038/s41556-020-0525-9.
15. Cheng, C. W. *et al.* Ketone Body Signaling Mediates Intestinal Stem Cell Homeostasis and Adaptation to Diet. *Cell* **178**, 1115-1131.e15 (2019).
16. Sullivan, M. R. *et al.* Quantification of microenvironmental metabolites in murine cancers reveals determinants of tumor nutrient availability. *Elife* **8**, (2019).
17. Sullivan, M. R. *et al.* Increased Serine Synthesis Provides an Advantage for Tumors Arising in Tissues Where Serine Levels Are Limiting. *Cell Metab.* (2019) doi:10.1016/J.CMET.2019.02.015.
18. Ngo, B. *et al.* Limited Environmental Serine and Glycine Confer Brain Metastasis Sensitivity to PHGDH Inhibition. *Cancer Discov.* (2020) doi:10.1158/2159-8290.CD-19-1228.
19. Pan, M. *et al.* Regional glutamine deficiency in tumours promotes dedifferentiation through inhibition of histone demethylation. *Nat. Cell Biol.* **18**, 1090–1101 (2016).
20. Elia, I. *et al.* Breast cancer cells rely on environmental pyruvate to shape the metastatic niche. *Nature* **568**, 117–121 (2019).
21. Intlekofer, A. M. & Finley, L. W. S. Metabolic signatures of cancer cells and stem cells.

Nat. Metab. **1**, 177–188 (2019).
22. Koivunen, P. *et al.* Transformation by the (R)-enantiomer of 2-hydroxyglutarate linked to EGLN activation. *Nature* **483**, 484–488 (2012).
23. Losman, J.-A. *et al.* (R)-2-hydroxyglutarate is sufficient to promote leukemogenesis and its effects are reversible. *Science* **339**, 1621–5 (2013).
24. Laukka, T., Myllykoski, M., Looper, R. E. & Koivunen, P. Cancer-associated 2-oxoglutarate analogues modify histone methylation by inhibiting histone lysine demethylases. *J. Mol. Biol.* **430**, 3081–3092 (2018).
25. Koivunen, P. *et al.* Inhibition of hypoxia-inducible factor (HIF) hydroxylases by citric acid cycle intermediates: Possible links between cell metabolism and stabilization of HIF. *J. Biol. Chem.* **282**, 4524–4532 (2007).
26. Chakraborty, A. A. *et al.* Histone demethylase KDM6A directly senses oxygen to control chromatin and cell fate. *Science (80-.).* **363**, 1217–1222 (2019).
27. Pritchard, J. B. Intracellulara-KetoglutarateControlsthe Efficacyof Renal OrganicAnionTransport. **274**, 1278–1284 (1995).
28. Ward, P. S. *et al.* The potential for isocitrate dehydrogenase mutations to produce 2-hydroxyglutarate depends on allele specificity and subcellular compartmentalization. *J. Biol. Chem.* **288**, 3804–3815 (2013).
29. Carey, B. W., Finley, L. W. S., Cross, J. R., Allis, C. D. & Thompson, C. B. Intracellular α-ketoglutarate maintains the pluripotency of embryonic stem cells. *Nature* **518**, 413–416 (2014).
30. Lu, C. *et al.* IDH mutation impairs histone demethylation and results in a block to cell differentiation. *Nature* **483**, 474–478 (2012).
31. Xiao, M. *et al.* Inhibition of α-KG-dependent histone and DNA demethylases by fumarate and succinate that are accumulated in mutations of FH and SDH tumor suppressors. *Genes Dev.* **26**, 1326–38 (2012).
32. Chowdhury, R. *et al.* The oncometabolite 2-hydroxyglutarate inhibits histone lysine demethylases. *EMBO Rep.* **12**, 463–469 (2011).
33. Selak, M. A. *et al.* Succinate links TCA cycle dysfunction to oncogenesis by inhibiting HIF-α prolyl hydroxylase. *Cancer Cell* **7**, 77–85 (2005).
34. Letouzé, E. *et al.* SDH Mutations Establish a Hypermethylator Phenotype in Paraganglioma. *Cancer Cell* **23**, 739–752 (2013).
35. Adam, J. *et al.* Renal Cyst Formation in Fh1-Deficient Mice Is Independent of the Hif/Phd Pathway: Roles for Fumarate in KEAP1 Succination and Nrf2 Signaling. *Cancer Cell* **20**, 524–537 (2011).
36. Ward, P. S. *et al.* The Common Feature of Leukemia-Associated IDH1 and IDH2 Mutations Is a Neomorphic Enzyme Activity Converting α-Ketoglutarate to 2-Hydroxyglutarate. *Cancer Cell* **17**, 225–234 (2010).
37. Dang, L. *et al.* Cancer-associated IDH1 mutations produce 2-hydroxyglutarate. *Nature* **462**, 739–744 (2009).
38. Figueroa, M. E. *et al.* Leukemic IDH1 and IDH2 Mutations Result in a Hypermethylation Phenotype, Disrupt TET2 Function, and Impair Hematopoietic Differentiation. *Cancer Cell* **18**, 553–567 (2010).
39. Saha, S. K. *et al.* Mutant IDH inhibits HNF-4α to block hepatocyte differentiation and promote biliary cancer. *Nature* **513**, 110–114 (2014).
40. Lu, C. *et al.* Induction of sarcomas by mutant IDH2. *Genes Dev.* **27**, 1986–1998 (2013).

41. Sasaki, M. *et al.* IDH1(R132H) mutation increases murine haematopoietic progenitors and alters epigenetics. *Nature* **488**, 656–659 (2012).
42. Bardella, C. *et al.* Expression of Idh1R132H in the Murine Subventricular Zone Stem Cell Niche Recapitulates Features of Early Gliomagenesis. *Cancer Cell* **30**, 578–594 (2016).
43. Díaz-Castro, B. *et al.* Resistance of glia-like central and peripheral neural stem cells to genetically induced mitochondrial dysfunction—differential effects on neurogenesis. *EMBO Rep.* **16**, 1511–1519 (2015).
44. Piruat, J. I., Pintado, C. O., Ortega-Sáenz, P., Roche, M. & López-Barneo, J. The Mitochondrial SDHD Gene Is Required for Early Embryogenesis, and Its Partial Deficiency Results in Persistent Carotid Body Glomus Cell Activation with Full Responsiveness to Hypoxia. *Mol. Cell. Biol.* **24**, 10933–10940 (2004).
45. Ouspenskaia, T., Matos, I., Mertz, A. F., Fiore, V. F. & Fuchs, E. WNT-SHH Antagonism Specifies and Expands Stem Cells prior to Niche Formation. *Cell* **164**, 156–169 (2016).
46. Matos, I. *et al.* Progenitors oppositely polarize wnt activators and inhibitors to orchestrate tissue development. *Elife* **9**, (2020).
47. Agathocleous, M. *et al.* Ascorbate regulates haematopoietic stem cell function and leukaemogenesis. *Nature* **549**, 476–481 (2017).
48. Cimmino, L. *et al.* Restoration of TET2 Function Blocks Aberrant Self-Renewal and Leukemia Progression. *Cell* **170**, 1079-1095.e20 (2017).
49. Ho, T. T. *et al.* Autophagy maintains the metabolism and function of young and old stem cells. *Nature* **543**, 205–210 (2017).
50. Chisolm, D. A. *et al.* CCCTC-Binding Factor Translates Interleukin 2- and α-Ketoglutarate-Sensitive Metabolic Changes in T Cells into Context-Dependent Gene Programs. *Immunity* **47**, 251-267.e7 (2017).
51. Klysz, D. *et al.* Glutamine-dependent α-ketoglutarate production regulates the balance between T helper 1 cell and regulatory T cell generation. *Sci. Signal.* **8**, (2015).
52. Tran, T. Q. *et al.* α-Ketoglutarate attenuates Wnt signaling and drives differentiation in colorectal cancer. *Nat. Cancer* **1**, 345–358 (2020).
53. Morris, J. P. *et al.* α-Ketoglutarate links p53 to cell fate during tumour suppression. *Nature* **573**, 595–599 (2019).
54. Mardis, E. R. *et al.* Recurring Mutations Found by Sequencing an Acute Myeloid Leukemia Genome. *N. Engl. J. Med.* **361**, 1058–1066 (2009).
55. Yan, H. *et al. IDH1* and *IDH2* Mutations in Gliomas. *N. Engl. J. Med.* **360**, 765–773 (2009).
56. Chen, C. *et al.* Cancer-associated IDH2 mutants drive an acute myeloid leukemia that is susceptible to Brd4 inhibition. *Genes Dev.* **27**, 1974–1985 (2013).
57. Bejarano-García, J. A. *et al.* Sensitivity of hematopoietic stem cells to mitochondrial dysfunction by SdhD gene deletion. *Cell Death Dis.* **7**, (2016).
58. Guitart, A. V. *et al.* Fumarate hydratase is a critical metabolic regulator of hematopoietic stem cell functions. *J. Exp. Med.* **214**, 719–735 (2017).
59. Cardaci, S. *et al.* Pyruvate carboxylation enables growth of SDH-deficient cells by supporting aspartate biosynthesis. *Nat. Cell Biol.* **17**, 1317–1326 (2015).
60. Kulkarni, R. A. *et al.* A chemoproteomic portrait of the oncometabolite fumarate. *Nat. Chem. Biol.* **15**, 391–400 (2019).
61. Lemonnier, F. *et al.* The IDH2 R172K mutation associated with angioimmunoblastic T-cell lymphoma produces 2HG in T cells and impacts lymphoid development. *Proc. Natl.*

Acad. Sci. U. S. A. **113**, 15084–15089 (2016).
62. Weng, H. *et al.* METTL14 Inhibits Hematopoietic Stem/Progenitor Differentiation and Promotes Leukemogenesis via mRNA m6A Modification. *Cell Stem Cell* **22**, 191-205.e9 (2018).
63. Cheng, Y. *et al.* m6A RNA Methylation Maintains Hematopoietic Stem Cell Identity and Symmetric Commitment. *Cell Rep.* **28**, 1703-1716.e6 (2019).
64. Batista, P. J. *et al.* M6A RNA modification controls cell fate transition in mammalian embryonic stem cells. *Cell Stem Cell* **15**, 707–719 (2014).
65. Hasemann, M. S. *et al.* C/EBPα Is Required for Long-Term Self-Renewal and Lineage Priming of Hematopoietic Stem Cells and for the Maintenance of Epigenetic Configurations in Multipotent Progenitors. *PLoS Genet.* **10**, e1004079 (2014).
66. Su, R. *et al.* R-2HG Exhibits Anti-tumor Activity by Targeting FTO/m6A/MYC/CEBPA Signaling. *Cell* **172**, 90-105.e23 (2018).
67. Hyung, C. S. *et al.* C/EBPα determines hematopoietic cell fate in multipotential progenitor cells by inhibiting erythroid differentiation and inducing myeloid differentiation. *Blood* **107**, 4308–4316 (2006).
68. Liu, P.-S. *et al.* α-ketoglutarate orchestrates macrophage activation through metabolic and epigenetic reprogramming. *Nat. Immunol.* (2017) doi:10.1038/ni.3796.
69. Finley, L. W. S. *et al.* Pluripotency transcription factors and Tet1/2 maintain Brd4-independent stem cell identity. *Nat. Cell Biol.* **20**, 565–574 (2018).
70. Costa, Y. *et al.* NANOG-dependent function of TET1 and TET2 in establishment of pluripotency. *Nature* **495**, 370–374 (2013).
71. Martello, G. & Smith, A. The Nature of Embryonic Stem Cells. *Annu. Rev. Cell Dev. Biol.* **30**, 647–675 (2014).
72. Di Micco, R. *et al.* Control of embryonic stem cell identity by brd4-dependent transcriptional elongation of super-enhancer-associated pluripotency genes. *Cell Rep.* **9**, 234–247 (2014).
73. Chen, X. *et al.* Integration of External Signaling Pathways with the Core Transcriptional Network in Embryonic Stem Cells. *Cell* **133**, 1106–1117 (2008).
74. Hamilton, W. B. *et al.* Dynamic lineage priming is driven via direct enhancer regulation by ERK. *Nature* **575**, 355–360 (2019).
75. Hwang, I.-Y. *et al.* Psat1-Dependent Fluctuations in α-Ketoglutarate Affect the Timing of ESC Differentiation. *Cell Metab.* **24**, 494–501 (2016).
76. TeSlaa, T. *et al.* α-Ketoglutarate Accelerates the Initial Differentiation of Primed Human Pluripotent Stem Cells. *Cell Metab.* **24**, 485–493 (2016).
77. Tischler, J. *et al.* Metabolic regulation of pluripotency and germ cell fate through α-ketoglutarate. *EMBO J.* **38**, (2019).
78. Weinberger, L., Ayyash, M., Novershtern, N. & Hanna, J. H. Dynamic stem cell states: Naive to primed pluripotency in rodents and humans. *Nature Reviews Molecular Cell Biology* vol. 17 155–169 (2016).
79. Schvartzman, J. M., Reuter, V. P., Koche, R. P. & Thompson, C. B. 2-hydroxyglutarate inhibits MyoD-mediated differentiation by preventing H3K9 demethylation. *Proc. Natl. Acad. Sci. U. S. A.* **116**, 12851–12856 (2019).
80. Iwafuchi-Doi, M. & Zaret, K. S. Cell fate control by pioneer transcription factors. *Dev.* **143**, 1833–1837 (2016).
81. Calo, E. & Wysocka, J. Modification of Enhancer Chromatin: What, How, and Why?

Molecular Cell vol. 49 825–837 (2013).
82. Sciacovelli, M. *et al.* Fumarate is an epigenetic modifier that elicits epithelial-to-mesenchymal transition. *Nature* **537**, 544–547 (2016).
83. Yu, M. & Ren, B. The Three-Dimensional Organization of Mammalian Genomes. *Annu. Rev. Cell Dev. Biol.* **33**, 265–289 (2017).
84. Flavahan, W. A. *et al.* Insulator dysfunction and oncogene activation in IDH mutant gliomas. *Nature* **529**, 110–114 (2016).
85. Flavahan, W. A. *et al.* Altered chromosomal topology drives oncogenic programs in SDH-deficient GISTs. *Nature* **575**, 229–233 (2019).
86. Modrek, A. S. *et al.* Low-Grade Astrocytoma Mutations in IDH1, P53, and ATRX Cooperate to Block Differentiation of Human Neural Stem Cells via Repression of SOX2. *Cell Rep.* **21**, 1267–1280 (2017).
87. Chen, H., Tian, Y., Shu, W., Bo, X. & Wang, S. Comprehensive Identification and Annotation of Cell Type-Specific and Ubiquitous CTCF-Binding Sites in the Human Genome. *PLoS One* **7**, e41374 (2012).
88. Waldhart, A. N. *et al.* Phosphorylation of TXNIP by AKT Mediates Acute Influx of Glucose in Response to Insulin. *Cell Rep.* **19**, 2005–2013 (2017).
89. Rodríguez-Colman, M. J. *et al.* Interplay between metabolic identities in the intestinal crypt supports stem cell function. *Nature* **543**, 424–427 (2017).
90. Crane, G. M., Jeffery, E. & Morrison, S. J. Adult haematopoietic stem cell niches. *Nat. Rev. Immunol.* **17**, 573–590 (2017).
91. Gur-Cohen, S. *et al.* Stem cell-driven lymphatic remodeling coordinates tissue regeneration. *Science (80-.).* **366**, 1218–1225 (2019).
92. Tavazoie, M. *et al.* A Specialized Vascular Niche for Adult Neural Stem Cells. *Cell Stem Cell* **3**, 279–288 (2008).
93. Sullivan, M. R. *et al.* Increased Serine Synthesis Provides an Advantage for Tumors Arising in Tissues Where Serine Levels Are Limiting. *Cell Metab.* (2019) doi:10.1016/J.CMET.2019.02.015.
94. Lee, P., Chandel, N. S. & Simon, M. C. Cellular adaptation to hypoxia through hypoxia inducible factors and beyond. *Nature Reviews Molecular Cell Biology* vol. 21 268–283 (2020).
95. Sergiy, M. N. *et al.* Acidic pH is a metabolic switch for 2-Hydroxyglutarate generation and signaling. *J. Biol. Chem.* **291**, 20188–20197 (2016).
96. Intlekofer, A. M. *et al.* L-2-Hydroxyglutarate production arises from noncanonical enzyme function at acidic pH. *Nat. Chem. Biol.* **13**, 494–500 (2017).
97. Intlekofer, A. M. *et al.* Hypoxia Induces Production of L-2-Hydroxyglutarate. *Cell Metab.* **22**, 304–311 (2015).
98. Scully, D. *et al.* Hypoxia promotes production of neural crest cells in the embryonic head. *Dev.* **143**, 1742–1752 (2016).
99. Barriga, E. H., Maxwell, P. H., Reyes, A. E. & Mayor, R. The hypoxia factor Hif-1α controls neural crest chemotaxis and epithelial to mesenchymal transition. *J. Cell Biol.* **201**, 759–776 (2013).
100. De Filippis, L. & Delia, D. Hypoxia in the regulation of neural stem cells. *Cellular and Molecular Life Sciences* vol. 68 2831–2844 (2011).
101. Mazumdar, J. *et al.* O2 regulates stem cells through Wnt/β-catenin signalling. *Nat. Cell Biol.* **12**, 1007–1013 (2010).

102. Simsek, T. *et al.* The distinct metabolic profile of hematopoietic stem cells reflects their location in a hypoxic niche. *Cell Stem Cell* **7**, 380–390 (2010).
103. Takubo, K. *et al.* Regulation of glycolysis by Pdk functions as a metabolic checkpoint for cell cycle quiescence in hematopoietic stem cells. *Cell Stem Cell* **12**, 49–61 (2013).
104. Michealraj, K. A. *et al.* Metabolic Regulation of the Epigenome Drives Lethal Infantile Ependymoma. *Cell* **0**, (2020).
105. Spencer, J. A. *et al.* Direct measurement of local oxygen concentration in the bone marrow of live animals. *Nature* **508**, 269–273 (2014).
106. Acar, M. *et al.* Deep imaging of bone marrow shows non-dividing stem cells are mainly perisinusoidal. *Nature* **526**, 126–130 (2015).
107. Altman, B. J., Stine, Z. E. & Dang, C. V. From Krebs to clinic: glutamine metabolism to cancer therapy. *Nat. Rev. Cancer* **16**, 619–634 (2016).
108. Tyrakis, P. A. *et al.* S-2-hydroxyglutarate regulates CD8+ T-lymphocyte fate. *Nature* **540**, 236–241 (2016).
109. Pan, M. *et al.* Regional glutamine deficiency in tumours promotes dedifferentiation through inhibition of histone demethylation. *Nat. Cell Biol.* **18**, 1090–1101 (2016).
110. Ishak Gabra, M. B. *et al.* Dietary glutamine supplementation suppresses epigenetically-activated oncogenic pathways to inhibit melanoma tumour growth. *Nat. Commun.* **11**, 3326 (2020).
111. Raffel, S. *et al.* BCAT1 restricts αKG levels in AML stem cells leading to IDHmut-like DNA hypermethylation. *Nature* **551**, 384–388 (2017).
112. Taya, Y. *et al.* Depleting dietary valine permits nonmyeloablative mouse hematopoietic stem cell transplantation. *Science (80-.).* **354**, 1152–1155 (2016).
113. Mayers, J. R. *et al.* Tissue of origin dictates branched-chain amino acid metabolism in mutant Kras-driven cancers. *Science (80-.).* **353**, 1161–1165 (2016).
114. Possemato, R. *et al.* Functional genomics reveal that the serine synthesis pathway is essential in breast cancer. *Nature* **476**, 346–350 (2011).
115. Samanta, D. *et al.* PHGDH Expression Is Required for Mitochondrial Redox Homeostasis, Breast Cancer Stem Cell Maintenance, and Lung Metastasis. *Cancer Res.* **76**, 4430–42 (2016).
116. Maddocks, O. D. K. *et al.* Modulating the therapeutic response of tumours to dietary serine and glycine starvation. *Nature* **544**, 372–376 (2017).
117. Maddocks, O. D. K. *et al.* Serine starvation induces stress and p53-dependent metabolic remodelling in cancer cells. *Nature* **493**, 542–546 (2012).
118. Gonzales, K. A. U. & Fuchs, E. Skin and Its Regenerative Powers: An Alliance between Stem Cells and Their Niche. *Dev. Cell* **43**, 387–401 (2017).
119. Flores, A. *et al.* Lactate dehydrogenase activity drives hair follicle stem cell activation. *Nat. Cell Biol.* **19**, 1017–1026 (2017).
120. Zhang, Z. *et al.* Differential glucose requirement in skin homeostasis and injury identifies a therapeutic target for psoriasis article. *Nat. Med.* **24**, 617–627 (2018).
121. Martincorena, I. *et al.* High burden and pervasive positive selection of somatic mutations in normal human skin. *Science (80-.).* **348**, (2015).
122. Martincorena, I. *et al.* Somatic mutant clones colonize the human esophagus with age. *Science* eaau3879 (2018) doi:10.1126/science.aau3879.
123. Blokzijl, F. *et al.* Tissue-specific mutation accumulation in human adult stem cells during life. *Nature* **538**, 260–264 (2016).

124. Jaiswal, S. *et al.* Age-Related Clonal Hematopoiesis Associated with Adverse Outcomes. *N. Engl. J. Med.* **371**, 2488–2498 (2014).
125. Genovese, G. *et al.* Clonal Hematopoiesis and Blood-Cancer Risk Inferred from Blood DNA Sequence. *N. Engl. J. Med.* **371**, 2477–2487 (2014).
126. Lapouge, G. *et al.* Identifying the cellular origin of squamous skin tumors. *Proc. Natl. Acad. Sci. U. S. A.* **108**, 7431–6 (2011).
127. Barker, N. *et al.* Crypt stem cells as the cells-of-origin of intestinal cancer. *Nature* **457**, 608–611 (2009).
128. White, A. C. & Lowry, W. E. Refining the role for adult stem cells as cancer cells of origin. *Trends Cell Biol.* **25**, 11–20 (2015).
129. White, A. C. *et al.* Defining the origins of Ras/p53-mediated squamous cell carcinoma. *Proc. Natl. Acad. Sci. U. S. A.* **108**, 7425–30 (2011).
130. Brown, S. *et al.* Correction of aberrant growth preserves tissue homeostasis. *Nature* **548**, 334–337 (2017).
131. Dow, L. E. *et al.* Apc Restoration Promotes Cellular Differentiation and Reestablishes Crypt Homeostasis in Colorectal Cancer. *Cell* **161**, 1539–1552 (2015).
132. Ying, Z., Sandoval, M. & Beronja, S. Oncogenic activation of PI3K induces progenitor cell differentiation to suppress epidermal growth. *Nat. Cell Biol.* 1 (2018) doi:10.1038/s41556-018-0218-9.
133. Warrell, R. P. *et al.* Differentiation Therapy of Acute Promyelocytic Leukemia with Tretinoin (All-trans-Retinoic Acid). *N. Engl. J. Med.* **324**, 1385–1393 (1991).
134. Boumahdi, S. *et al.* SOX2 controls tumour initiation and cancer stem-cell functions in squamous-cell carcinoma. *Nature* **511**, 246–250 (2014).
135. Sendoel, A. *et al.* Translation from unconventional 5′ start sites drives tumour initiation. *Nature* **541**, 494–499 (2017).
136. Maier, S. *et al.* SOX2 amplification is a common event in squamous cell carcinomas of different organ sites. *Hum. Pathol.* **42**, 1078–1088 (2011).
137. Blanco, S. *et al.* Stem cell function and stress response are controlled by protein synthesis. *Nature* **534**, 335–340 (2016).
138. Saxton, R. A. & Sabatini, D. M. mTOR Signaling in Growth, Metabolism, and Disease. *Cell* **168**, 960–976 (2017).
139. Agathocleous, M. *et al.* Ascorbate regulates haematopoietic stem cell function and leukaemogenesis. *Nature* **549**, 476–481 (2017).
140. Gao, X. *et al.* Dietary methionine influences therapy in mouse cancer models and alters human metabolism. *Nature* **572**, 397–401 (2019).
141. Liu, K. *et al.* Sox2 Cooperates with Inflammation-Mediated Stat3 Activation in the Malignant Transformation of Foregut Basal Progenitor Cells. *Cell Stem Cell* **12**, 304–315 (2013).
142. Hosios, A. M. *et al.* Amino Acids Rather than Glucose Account for the Majority of Cell Mass in Proliferating Mammalian Cells. *Dev. Cell* **36**, 540–549 (2016).
143. Yang, M. & Vousden, K. H. Serine and one-carbon metabolism in cancer. *Nat. Rev. Cancer* **16**, 650–662 (2016).
144. Michelakis, E. D., Webster, L. & Mackey, J. R. Dichloroacetate (DCA) as a potential metabolic-targeting therapy for cancer. *Br. J. Cancer* **99**, 989–94 (2008).
145. Halestrap, A. P. The mitochondrial pyruvate carrier. Kinetics and specificity for substrates and inhibitors. *Biochem. J.* **148**, 85–96 (1975).

146. Diehl, F. F., Lewis, C. A., Fiske, B. P. & Vander Heiden, M. G. Cellular redox state constrains serine synthesis and nucleotide production to impact cell proliferation. *Nature Metabolism* vol. 1 861–867 (2019).
147. Sullivan, L. B. *et al.* Supporting Aspartate Biosynthesis Is an Essential Function of Respiration in Proliferating Cells. *Cell* **162**, 552–63 (2015).
148. Titov, D. V *et al.* Complementation of mitochondrial electron transport chain by manipulation of the NAD+/NADH ratio. *Science* **352**, 231–5 (2016).
149. Williamson, D. H., Lund, P. & Krebs, H. A. The redox state of free nicotinamide-adenine dinucleotide in the cytoplasm and mitochondria of rat liver. *Biochem. J.* **103**, 514–27 (1967).
150. Birsoy, K. *et al.* An Essential Role of the Mitochondrial Electron Transport Chain in Cell Proliferation Is to Enable Aspartate Synthesis. *Cell* **162**, 540–551 (2015).
151. Beronja, S., Livshits, G., Williams, S. & Fuchs, E. Rapid functional dissection of genetic networks via tissue-specific transduction and RNAi in mouse embryos. *Nat. Med.* **16**, 821–827 (2010).
152. Lechler, T. & Fuchs, E. Asymmetric cell divisions promote stratification and differentiation of mammalian skin. *Nature* **437**, 275–280 (2005).
153. Asare, A., Levorse, J. & Fuchs, E. Coupling organelle inheritance with mitosis to balance growth and differentiation. *Science* **355**, eaah4701 (2017).
154. Possemato, R. *et al.* Functional genomics reveal that the serine synthesis pathway is essential in breast cancer. *Nature* **476**, 346–350 (2011).
155. Ezhkova, E. *et al.* Ezh2 Orchestrates Gene Expression for the Stepwise Differentiation of Tissue-Specific Stem Cells. *Cell* **136**, 1122–1135 (2009).
156. Sen, G. L., Webster, D. E., Barragan, D. I., Chang, H. Y. & Khavari, P. A. Control of differentiation in a self-renewing mammalian tissue by the histone demethylase JMJD3. *Genes Dev.* **22**, 1865–70 (2008).
157. Maddocks, O. D. K., Labuschagne, C. F., Adams, P. D. & Vousden, K. H. Serine Metabolism Supports the Methionine Cycle and DNA/RNA Methylation through De Novo ATP Synthesis in Cancer Cells. *Mol. Cell* **61**, 210–221 (2016).
158. Hamanaka, R. B. *et al.* Mitochondrial reactive oxygen species promote epidermal differentiation and hair follicle development. *Sci. Signal.* **6**, ra8 (2013).
159. Reeves, M. Q., Kandyba, E., Harris, S., Del Rosario, R. & Balmain, A. Multicolour lineage tracing reveals clonal dynamics of squamous carcinoma evolution from initiation to metastasis. *Nat. Cell Biol.* **20**, 699–709 (2018).
160. Kruidenier, L. *et al.* A selective jumonji H3K27 demethylase inhibitor modulates the proinflammatory macrophage response. *Nature* **488**, 404–408 (2012).
161. Locasale, J. W. *et al.* Phosphoglycerate dehydrogenase diverts glycolytic flux and contributes to oncogenesis. *Nat. Genet.* **43**, 869–874 (2011).
162. Labuschagne, C. F., van den Broek, N. J. F., Mackay, G. M., Vousden, K. H. & Maddocks, O. D. K. Serine, but Not Glycine, Supports One-Carbon Metabolism and Proliferation of Cancer Cells. *Cell Rep.* **7**, 1248–1258 (2014).
163. Letouzé, E. *et al.* SDH Mutations Establish a Hypermethylator Phenotype in Paraganglioma. *Cancer Cell* **23**, 739–752 (2013).
164. Elia, I. *et al.* Breast cancer cells rely on environmental pyruvate to shape the metastatic niche. *Nature* **568**, 117–121 (2019).
165. Raffel, S. *et al.* BCAT1 restricts αKG levels in AML stem cells leading to IDHmut-like

DNA hypermethylation. *Nature* **551**, 384–388 (2017).
166. Chang, C.-J. *et al.* EZH2 Promotes Expansion of Breast Tumor Initiating Cells through Activation of RAF1-β-Catenin Signaling. *Cancer Cell* **19**, 86–100 (2011).
167. Beck, B. *et al.* A vascular niche and a VEGF–Nrp1 loop regulate the initiation and stemness of skin tumours. *Nature* **478**, 399–403 (2011).
168. Oshimori, N., Oristian, D. & Fuchs, E. TGF-β Promotes Heterogeneity and Drug Resistance in Squamous Cell Carcinoma. *Cell* **160**, 963–976 (2015).
169. Schwörer, S., Vardhana, S. A. & Thompson, C. B. Cancer Metabolism Drives a Stromal Regenerative Response. *Cell Metabolism* vol. 29 576–591 (2019).
170. van Gastel, N. *et al.* Lipid availability determines fate of skeletal progenitor cells via SOX9. *Nature* **579**, 111–117 (2020).
171. Thorens, B. GLUT2, glucose sensing and glucose homeostasis. *Diabetologia* vol. 58 221–232 (2015).
172. Scopelliti, A. J., Font, J., Vandenberg, R. J., Boudker, O. & Ryan, R. M. Structural characterisation reveals insights into substrate recognition by the glutamine transporter ASCT2/SLC1A5. *Nat. Commun.* **9**, 38 (2018).
173. Scopelliti, A. J., Heinzelmann, G., Kuyucak, S., Ryan, R. M. & Vandenberg, R. J. Na+ interactions with the neutral amino acid transporter ASCT1. *J. Biol. Chem.* **289**, 17468–79 (2014).
174. Sullivan, M. R. *et al.* Increased Serine Synthesis Provides an Advantage for Tumors Arising in Tissues Where Serine Levels Are Limiting. *Cell Metab.* **30**, (2019).
175. Holleran, W. M. *et al.* Sphingolipids are required for mammalian epidermal barrier function: Inhibition of sphingolipid synthesis delays barrier recovery after acute perturbation. *J. Clin. Invest.* **88**, 1338–1345 (1991).
176. Takeichi, T. *et al.* Reduction of stratum corneum ceramides in Neu-Laxova syndrome caused by phosphoglycerate dehydrogenase deficiency. *J. Lipid Res.* **59**, 2413–2420 (2018).
177. Shaheen, R. *et al.* Neu-Laxova Syndrome, an Inborn Error of Serine Metabolism, Is Caused by Mutations in PHGDH. *Am. J. Hum. Genet.* **94**, 898–904 (2014).
178. Hosios, A. M. & Vander Heiden, M. G. The redox requirements of proliferating mammalian cells. *J. Biol. Chem.* **293**, 7490–7498 (2018).
179. Schell, J. C. *et al.* Control of intestinal stem cell function and proliferation by mitochondrial pyruvate metabolism. *Nat. Cell Biol.* **19**, 1027–1036 (2017).
180. Bensard, C. L. *et al.* Regulation of Tumor Initiation by the Mitochondrial Pyruvate Carrier. *Cell Metab.* **31**, 284-300.e7 (2020).
181. Sandoval, I. T. *et al.* A metabolic switch controls intestinal differentiation downstream of adenomatous polyposis coli (APC). *Elife* **6**, (2017).
182. Bao, X. R. *et al.* Mitochondrial dysfunction remodels one-carbon metabolism in human cells. *Elife* **5**, e10575 (2016).
183. Huang, F. *et al.* Inosine Monophosphate Dehydrogenase Dependence in a Subset of Small Cell Lung Cancers. *Cell Metab.* **28**, 369-382.e5 (2018).
184. Kofuji, S. *et al.* IMP dehydrogenase-2 drives aberrant nucleolar activity and promotes tumorigenesis in glioblastoma. *Nat. Cell Biol.* **21**, 1003–1014 (2019).
185. Merrill, B. J., Gat, U., DasGupta, R. & Fuchs, E. Tcf3 and Lef1 regulate lineage differentiation of multipotent stem cells in skin. *Genes Dev.* **15**, 1688–1705 (2001).
186. Birts, C. N. *et al.* p53 is regulated by aerobic glycolysis in cancer cells by the CtBP family

of NADH-dependent transcriptional regulators. *Sci. Signal.* **13**, (2020).
187. Ezhkova, E. *et al.* EZH1 and EZH2 cogovern histone H3K27 trimethylation and are essential for hair follicle homeostasis and wound repair. *Genes Dev.* **25**, 485–498 (2011).
188. Sen, G. L., Reuter, J. A., Webster, D. E., Zhu, L. & Khavari, P. A. DNMT1 maintains progenitor function in self-renewing somatic tissue. *Nature* **463**, 563–567 (2010).
189. Millard, P., Letisse, F., Sokol, S. & Portais, J.-C. IsoCor: correcting MS data in isotope labeling experiments. *Bioinformatics* **28**, 1294–1296 (2012).